Università degli studi di Trieste

Sede Amministrativa del Dottorato di Ricerca

XVIII Ciclo del

Dottorato di Ricerca in Fisica

Properties of Galactic and Extra-Galactic Novae

(Settore scientifico-disciplinare: FIS/05 ASTRONOMIA E ASTROFISICA)

Dottorando

Alessandro Ederoclite

Dipartimento di Astronomia

Università di Trieste

Coordinatore del Collegio dei Docenti

Chiar.mo Prof. Gaetano Senatore

Dipartimento di Fisica Teorica

Università di Trieste

Relatore

Dott. Paolo Mazzali

INAF–Oss.Astron. di Trieste

Max–Planck–Institute for Astrophysics – Garching

Correlatore

Chiar.ma Prof.ssa Francesca Matteucci

Dipartimento di Astronomia

Università di Trieste

Trieste University

Astronomy Department

PhD in Physics – XVIII Cycle

Properties of

Galactic and Extra-Galactic Novae

(Settore scientifico-disciplinare: FIS/05 ASTRONOMIA E ASTROFISICA)

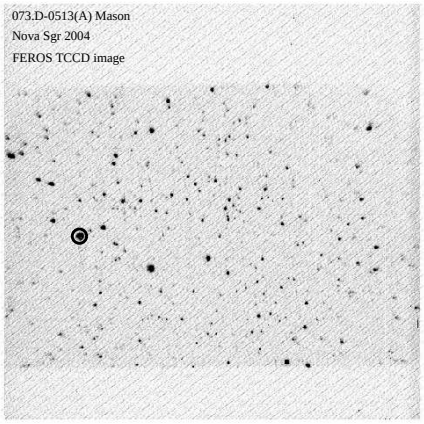

PhD candidate: Alessandro Ederoclite

Tutor: Dr.P.A.Mazzali

(Max Plank Institute for Astrophysics – Garching, INAF – Trieste Observatory)

Co-Tutor: Prof.ssa M.F.Matteucci

(Astronomy Department – Trieste University)

PhD Coordinator: Prof. G.Senatore

(Theoretical Physics Department – Trieste University)

To my family

Abstract

English

Classical nova explosions are thought to be the result of the nuclear reactions on the surface of a white dwarf accreting mass from a secondary companion that is filling its Roche lobe in a close binary system. Classical novae may contribute, to some extent, to the pollution of the interstellar medium, and it is therefore important to study both the number of novae occurring in different types of galaxies and the properties of individual objects. This Thesis is aimed at the study of a wide range of properties of galactic and extra–galactic novae using various techniques and with the most modern instruments available.

It has been proposed by various authors that there is a relation between the number of novae occurring in a galaxy in a year (the nova rate) and the infra-red luminosity (therefore the mass) of the galaxy. Another much debated relation is that between the normalized nova rate (the nova rate divided by the infra-red luminosity of the host galaxy) and the colour of the galaxy (and therefore the morphology). To investigate these relations we measured the nova rate in six spiral galaxies that have been observed for other purposes with the Hubble Space Telescope, and we observed two elliptical galaxies in the Virgo cluster with the ESO Very Large Telescope on Cerro Paranal (Chile).

The elliptical galaxies have also been studied to check a possible correlation between the radio–emission of the galaxy and the classical nova rate. Such a correlation is observed for Type Ia supernovae and, if there is any relation between these two classes of objects, one should expect to find it for classical novae as well. Moreover, a model of the chemical evolution

of elliptical galaxies has been used here which is able to reproduce various observed properties of the galaxies. The parameters regarding the nova–rate are analyzed and discussed.

The knowledge of the number of novae occurring in a galaxy is useless if properties of individual objects are unknown. We carried out observations of Nova Sgr 2004 during outburst and followed it up until the nebular phase. We give a detailed analysis of the dynamical, chemical and physical properties of this object.

A detailed photometric study of the old nova RR Pic (which underwent a classical nova outburst in 1925) is also given. We provided the best light curve ever obtained for this object thus showing that the supposed eclipse is shifted with respect to where it was expected and there are hints for a super-hump.

Finally, old novae can be recovered by their colours. We show here the attempts to recover four ex–novae from pure photometry.

Italiano

Le novae classiche sono considerate il risultato delle reazioni termonucleari sulla superficie di una nana bianca che accresce massa da una stella secondaria che riempie il proprio lobo di Roche in un sistema binario stretto. Le novae classiche possono contribuire in qualche modo all'arricchimento del mezzo interstellare ed è, quindi, importante studiare sia il numero di novae che avvengono in differenti tipi di galassie sia le proprietà dei singoli sistemi. Questa Tesi è mirata a studiare un'ampia gamma di proprietà delle novae galattiche ed extra–galattiche usando diverse tecniche ed usando gli strumenti più moderni.

È stato proposto da diversi autori che c'è una correlazione tra il numero di novae in una galassia ogni anno (il nova rate) e la luminosità infrarossa (quindi la massa) della galassia. Un'altra relazione molto dibattuta è quella tra il nova rate normalizzato (il nova rate diviso per la luminosità infrarossa della galassia) e il colore della galassia (quindi la morfologia). Per investigare queste relazioni noi abbiamo misurato il nova rate in sei galassie a spirale che

erano state osservate per altri scopi con il Telescopio Spaziale Hubble e abbiamo osservato due galassie ellittiche nell'ammasso della Vergine con il Very Large Telescope a Cerro Paranal (Cile).

Le galassie ellittiche sono anche state studiate per verificare una possibile correlazione tra l'emissione radio della galassia e il rate di novae classiche. Simile correlazione è osservata per Supernovae di tipo Ia e, se esiste un qualche tipo di relazione tra queste due classi di oggetti, ci si aspetta di trovarla anche per novae classiche. Inoltre è stato usato un modello di evoluzione chimica delle galassie ellittiche, che è in grado di riprodurre diverse proprietà osservate delle galassie. I parametri che riguardano il nova–rate sono analizzati e discussi.

La conoscenza del numero di novae che avvengono in una galassia è inutile se non sono note le proprietà dei singoli oggetti. Abbiamo condotto osservazioni di Nova Sgr 2004 durante l'esplosione e l'abbiamo continuata ad osservare fino allo stato nebulare. Diamo un'analisi dettagliata delle proprietà dinamiche, chimiche e fisiche di questo oggetto.

Si presenta anche uno studio fotometrico dettagliato della vecchia nova RR Pic (che è esplosa come nova classica nel 1925). Mostro la miglior curva di luce mai ottenuta per questo oggetto che mostra che l'eclisse è spostata rispetto a dove era attesa.

Infine, le novae vecchie possono essere riscoperte grazie ai loro colori. Mostro il tentativo di recuperare quattro vecchie novae nella nostra galassia grazie a pura fotometria.

Contents

Chapter 1

Introduction

1.1 The history of classical novae

Classical novae (CNe) have been known for centuries and, as for supernovae, their understanding is still far from complete.

The presence of variable stars was one of the main challenges to Aristotelian philosophy. The power of this philosophy was such that novae and supernovae passed almost entirely unacknowledged in European and Middle Eastern astronomies until Copernicus. China, Japan and Korea, however, being far from the influence of European philosophy kept detailed records of astronomical events for centuries. Situation for western astronomy did not change with the supernovae of 1572 and 1604, observed by Brahe and Kepler, respectively. Understanding that there are variable stars did not really mean new studies on the topic. The first nova to be studied in Europe was Nova Vulpecula 1670 (CK Vul).

Before the introduction of photography in the late 1800, novae were found mainly as naked eye objects. Novae are still discovered mainly by amateurs.

CNe have been claimed to be good distance indicators since a long time (Zwicky 1936). Despite of this, little interest in CNe out of the Milky Way has been shown by the scientific community (despite the notable exeption of the Padova group: Rosino 1964, 1973, Rosino & Bianchini 1973) until the 80's.

Cecchini & Gratton (1942), Payne-Gaposchkin (1957) and McLaughlin (1960a) wrote important monographies about the phenomenology of Classical Novae. It was already clear that CNe were ejecting large amounts of matter at velocities of hundreds or thousands of kilometers per second, nevertheless the origin of these objects was still debated.

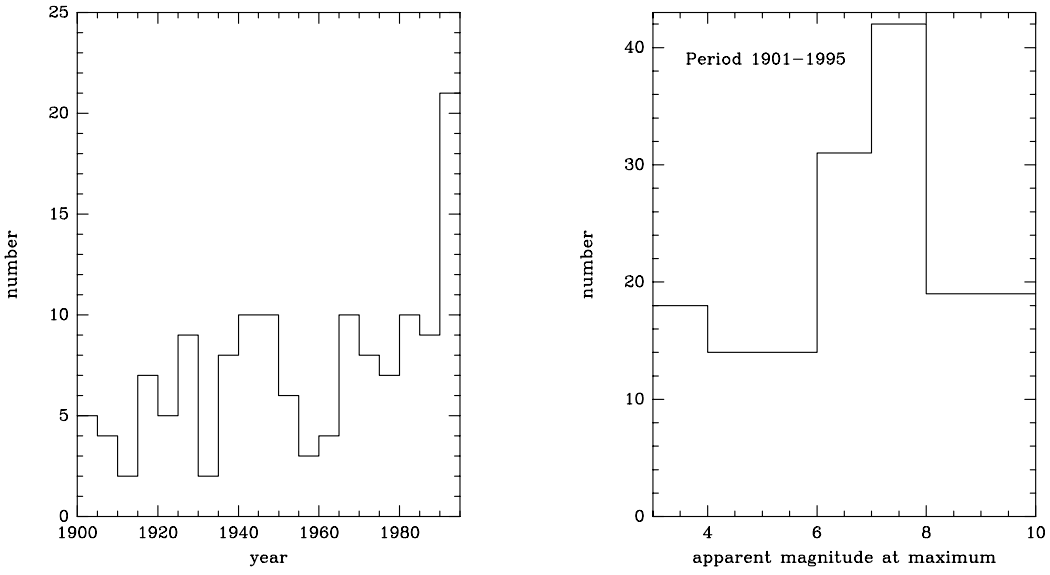

(a) (b)

Figure 1.1: *(a) Number of novae discovered during the last century (period 1901-1995), from Hernanz (2004). (b) Histogram of nova discoveries as a function of the visual apparent magnitude at maximum. (period 1901-1995), from Hernanz (2004)*

Only with observations by Walker (1954) and Kraft (1959, 1964) it was finally understood that novae occur in short-period binary systems.

During the '70s, Starrfield et al. (1972) gave detailed descriptions of the thermonuclear reactions going on in CNe.

The International Ultraviolet Explorer (IUE) had a major role in the understanding of the nova phenomenon since it covered the wavelength range in which novae are brighter.

The introduction of CCDs, finally, gave us the possibility to study with a high signal to noise ratio both emission and absorption features.

It can be seen from Figure 1.1(a) that the discovery rate of CNe is not dramatically related with technological improvements. This can be explained with the fact that novae are mainly discovered by amateurs. The observed increase of the last decade of the 20th century can be related with the relative diffusion of CCDs.

CNe have pushed the work on Cataclysmic Variables (CVs). Today CNe are considered a subclass of CVs.

At the beginning of the '90s the Cerro Tololo Nova Survey gave birth to four fundamental papers (Williams et al. 1991, 1994 and Williams 1992, 1994) that changed both the

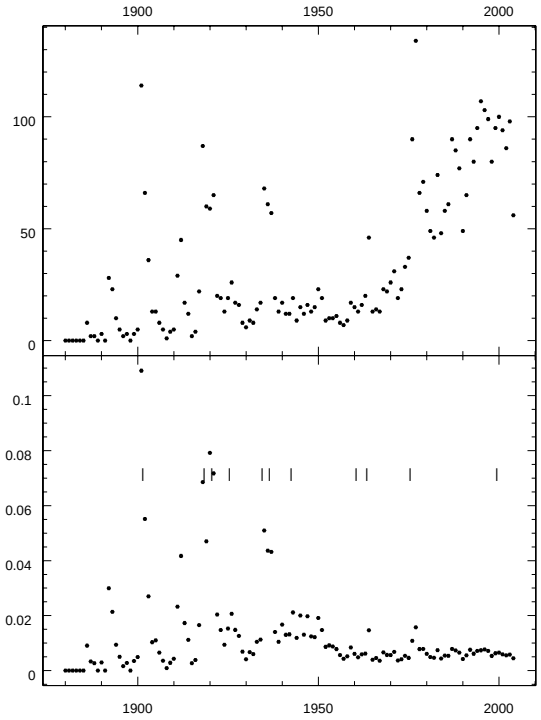

Figure 1.2: Upper panel *shows the number of papers per year with the word "nova" in the title* **Lower panel** *shows the number of papers per year with the word "nova" in the title divided by the total number of refereed articles published in the same year. Ticks show the eleven brightest novae of XX century.*

classification scheme and our understanding of the formation of nova spectra.

Figure 1.2 shows, in the upper panel, the number of refereed articles with the word "nova" in the title. The counts are not affected by supernovae. The obvious increase after 1960 is due to an increase in the total number of papers, not to an increased interest of the scientific community on classical novae. This can be seen looking at the lower panel that shows the number of refereed articles with the word "nova" in the title divided by the total number of refereed papers. the interest of the scientific community for classical novae appears to be roughly constant (about 0.5%) with a tiny increase over the 20th century and a few spikes related with very bright objects.

1.2 Cataclysmic variables

Cataclysmic variables are usually defined as *close binary systems made up of a white dwarf ("the primary") and a late–type companion ("the secondary") which is filling its Roche lobe.*

Warner (1995) defines close binaries as binary systems in which some significant interaction other than simple inverse square law gravitational attraction between point masses takes place.

The effects of tidal interaction on the secondary cause it to rotate synchronously with the orbital revolution and eliminate any initial eccentricity of orbit.

Recalling Kepler's third law, we can write the orbital period of a binary system as

$$P_{orb}^2 = \frac{4\pi^2 a^3}{G[M(1) + M(2)]}$$

where a is the separation between the centres of mass of the binary components and $M(1)$ and $M(2)$ are the masses of the primary and secondary respectively. Calling q the *mass ratio* $M(2)/M(1)$ one can write

$$a(\mathrm{cm}) = 3.53 \times 10^{10} M_1^{1/3}(1)(1+q)^{1/3} P_{orb}^{2/3}(h) \tag{1.1}$$

Taking a set of Cartesian coordinates (x, y, z) rotating with the binary, with origin at the primary, where the x–axis lies along the line of centres, the z–axis is perpendicular to the orbital plane and the y–axis is in the direction of orbital motion of the primary, the total potential at any point, which is the sum of the gravitational potentials of the two stars and the effective potential of the fictitious centrifugal force, is

$$\Phi = -\frac{GM(1)}{(x^2+y^2+z^2)^{1/2}} - \frac{GM(2)}{[(x-a)^2+y^2+z^2]^{1/2}} - \Omega_{orb}^2[(x-\mu a)^2 + y^2] \tag{1.2}$$

where $\mu = M(2)/[M(1)+M(2)]$ and $\Omega_{orb} = 2\pi/P_{orb}$. Pringle (1985) proved that the surface of a synchronously rotating star lies on $\Phi_R = \text{const}$, the equipotentials define the shape of the secondary. If the secondary is large enough, its surface becomes more distorted until it fills the surface which passes through the point where equipotential surfaces cross, called the inner Lagrangian point (sometimes abbreviated "L1"), which is a saddle point of Φ_R. That surface, known as the Roche lobe of the secondary, is the largest closed equipotential that can contain the mass of the secondary. A CV, in which the secondary fills its Roche lobe but the primary lies well within its, is called a semi–detached system.

At L1 gas can escape from the atmosphere of the secondary into the Roche lobe of the primary. In a non–magnetic CV, as the gas carries its own angular momentum, it does not fall directly onto the primary's surface but starts to spiralize thus forming an accretion disc. The fundamental model of accretion disc is due to Shakura & Sunyaev (1973). An example of continuum emitted from the accretion disc is shown in Figure 1.3. The luminosity of the disc is given by

$$L = \frac{GM_1\dot{M}_{disc}}{2R_1} \tag{1.3}$$

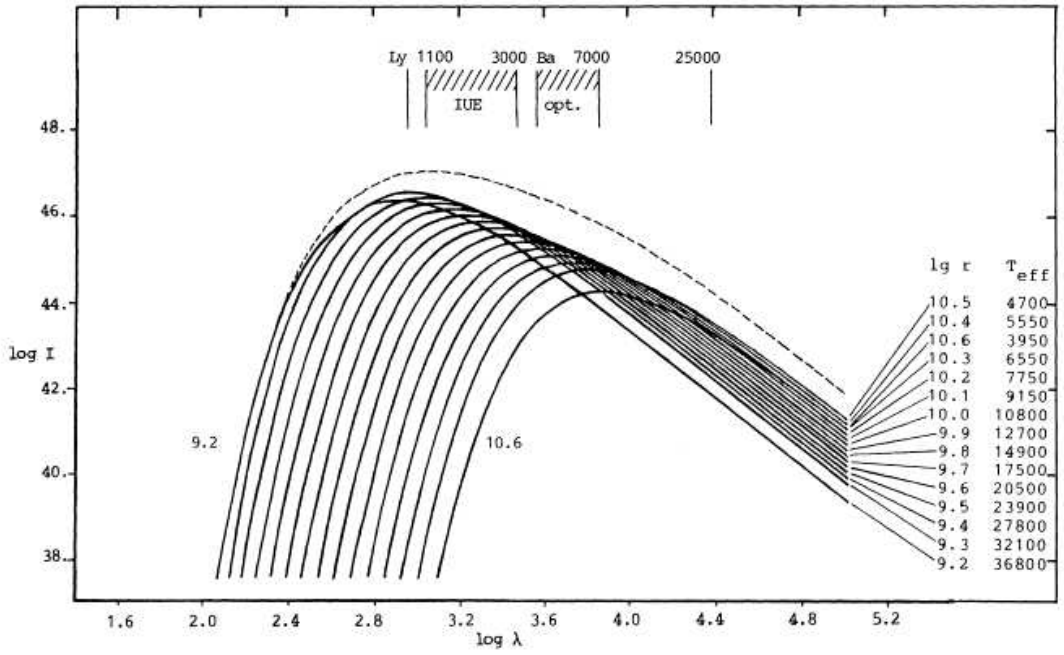

Figure 1.3: *Contribution of blackbody annuli to the total intensity distribution of an accretion disc. Model is computed for* $M(1) = 1$ *and* $\dot{M} = 10^{-9} M_{\odot} y^{-1}$. *The intensity emitted by each annulus is weighted by the area of the annulus. From La Dous (1989)*

that can be expressed as

$$L_{32}(\mathrm{d}) = 6.7 M_1(1) \dot{M}_{16}(1) R_9^{-1}(1)$$

The point where the stream, flowing through the L1, reaches the disc is usually called "hot spot" (or "bright spot").

In magnetic CVs, the magnetic field can be strong enough to partially (Intermediate Polars) or totally (Polars) control the accretion geometry.

The observed light arises from different parts of the system. The accretion disc is usually the brightest in the optical range because of its size and its temperature(depending on $\dot{M}$ it may dominate in the UV as well). The white dwarf (typical temperatures $\sim 10^4$K) and the secondary star (typically resembling a K4 star, see Howell 2004), on the other hand, contribute mainly in the UV and in the IR, respectively.

CV classification is still evolving. It is mainly a taxonomical tool based mainly on photometric observations. A summary of the classification of CVs is given in Table 1.1.

- *Classical novae* have, by definition, one observed historical eruption. The magnitude

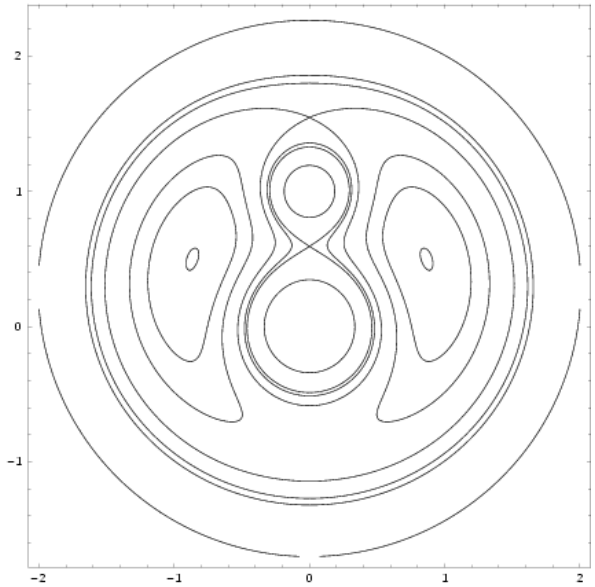

Figure 1.4: *From http://relativity.livingreviews.org/open?pubNo=lrr-2002-2&page=articlesu8.html Cross section of equipotential surfaces in the orbital plane of a binary with $q = 0.4$. The values of the potential surfaces are 5.0, 3.9075, 3.8, 3.559, 3.2, 3.0, and 2.8. The units have been normalized to the orbital separation, so $a = 1$.*

range of the outburst is $\Delta m \sim 12$ mag. Gallagher & Starrfield (1978) define a classical nova as an object which:

- increases its optical brightness by > 9 mag in less than a few days
- goes through significant brightness changes on a time scale of 1000 days or less
- has a spectral development that can be classified in terms of the characteristic nova stages
- has spectra that imply that matter is ejected with velocities greater than 100 km s^{-1} and less than 5000 km s^{-1}
- has no previously observed outburst

- *Dwarf Novae (DNe)* have outbursts of typically 2–5 mag. The interval between outbursts is from ~ 10 d to tens of years with a well–defined time scale for each object. They are believed to be due to release of gravitational energy caused by a temporary large increase in rate of mass transfer through the disc. There are distinct classes of DNe:

Class	Sub-class	Characteristics
Classical Novae (CNe)		only observed in eruption
Dwarf Novae (DNe)		
	Z Cam	protracted standstills 0.7 mag below maximum brightness.
	SU UMa	have superoutbursts that last 5 times the duration of an ordinary outburst
	U Gem	all that are neither Z Cam nor SU Uma
Recurrent Novae (RNe)		prevously recognized CNe that repeat their eruptions
Nova Likes (NLs)		all non eruptive CVs

Table 1.1: *Classification of Cataclysmic Variables*

  - *Z Cam* show protracted standstills about 0.7 mag below maximum brightness during which outbursts cease for intervals of tens of days to years.
  - *SU UMa* stars have occasional superoutbursts in which the star achieves brighter state at maximum and remains in outburst for $\sim$ 5 times the duration of an ordinary outburst
  - *U Gem* include all the stars that are neither Z Cam nor SU UMa

- *Recurrent Novae* are previously recognized CNe that are found to repeat their eruption.
- Nova-Like variables (NLs) include all the 'non–eruptive' CVs. It is believed that this class contains pre–novae, post–novae and Z Cam stars in permanent standstill. Most NLs have emission line spectra, but a subgroup show in addition broad absorption lines. The latter is called UX UMa stars.

The physical parameter of CVs known with the best precision is, usually, the orbital period. It is related to the scale of the system.

Photometric periods can be easily observed from light curves. An example of a light curve of a CV is given in Figure 1.5. This figure shows the average of 17 periods of Z Cha as observed by Wood et al. (1986) from Cerro Tololo Interamerican Observatory (CTIO). The biggest eclipse in the light curve is due to the eclipse of the hot spot. The second deepest dip

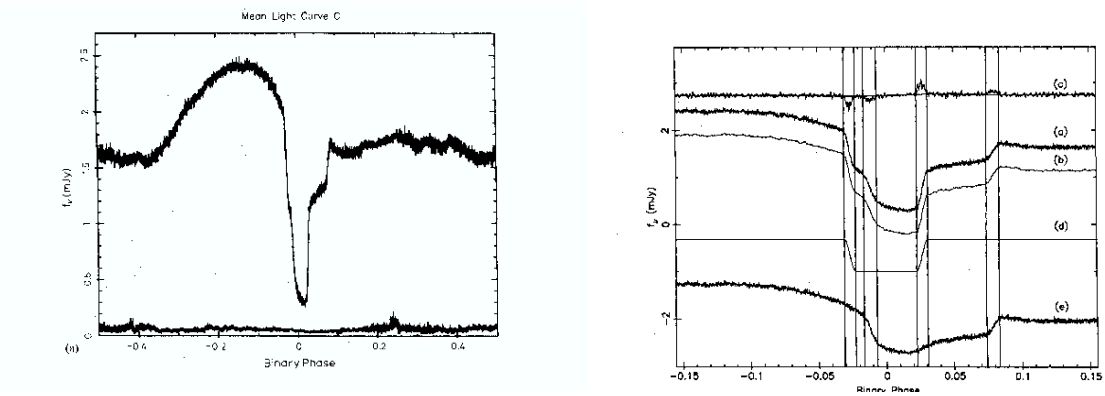

Figure 1.5: Left panel: *Light curve of Z Cha, from Wood et al. (1986).* **Right panel:** *Extraction of the white dwarf eclipse of Z Cha, from Wood et al. (1986). (a) is the original curve (b) is a smoothed light curve arbitrarily shifted downwards (c) is the derivative of the smoothed light curve (d) is the reconstructed white dwarf eclipse (e) si the original light curve minus the white dwarf eclipse. The vertical lines show, from left to right, the white dwarf entering the eclipse, the white dwarf completely behind the secondary star, the hot spot entering the eclipse, the hot spot completely eclipsed, the white dwarf coming out of the eclipse, the white dwarf being completely visible the hot spot coming out of the eclipse and the hot spot completely visible.*

is due to the white dwarf being eclipsed behind the secondary. A detailed decomposition of the ligth curve of Z Cha is given in the right panel of Figure 1.5, from Wood et al. (1986).

An important tool for the study of CV evolution is the histogram of orbital periods (shown in Figure 1.6(b)). The distribution of periods of CVs shows a deficiency for $2.2h < P_{orb} < 2.8h$. This is the so-called "period gap". This distribution also shows that there is a clear minimum at $P_{orb} \sim 75$ min and a steady drop-off in numbers towards longer orbital periods. The 2.8–h upper limit of the gap corresponds to secondary stars which are just becoming fully convective($M(2) \sim 0.3M_{\odot}$) and in which the dynamo mechanism is partially suppressed leading to a drastic decrease of the efficiency of the magnetic braking and, consequently, of the accretion rate (Zangrilli 1997). The secondary then shrinks inside its Roche lobe until gravitational radiation will bring them again in contact, which will happen when the binary has reached $P_{orb} \sim 2h$.

Other important modulations of light curves are called "superhumps" and usually differ by a few percent from the orbital period. Two opposite cases are observed:

- *Positive superhumps* are thought to represent the beat period between the apsidal prograde precession of the eccentric outer edge of the disc and the orbital motion of the

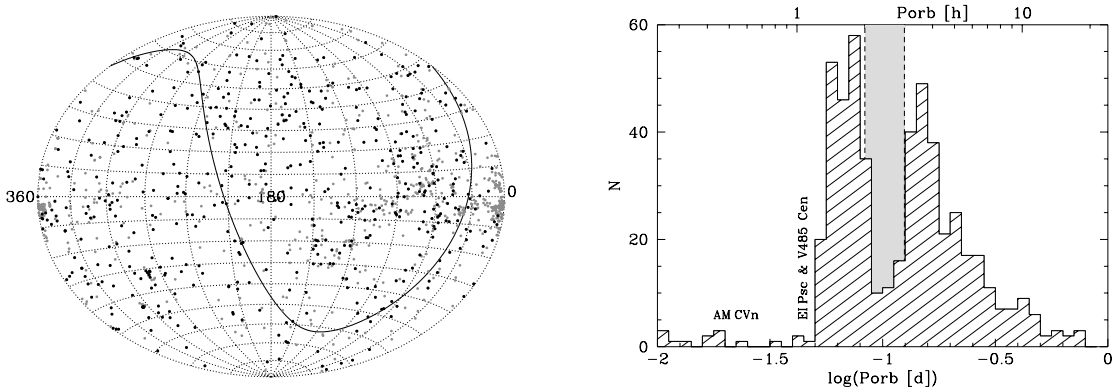

(a) (b)

Figure 1.6: *(a) The distribution of the known CVs from Downes et al. (2001) in galactic coordinates. The galactic centre wraps around at the right/left edge of the plot, the solid line indicates declination $\delta = 0$. CVs with a known orbital period are shown as black dots, those without as grey dots. (b) The period distribution of the 531 CVs listed by Ritter & Kolb (2003) , V7.3. The $2-3\,h$ period gap is indicated in grey.*

secondary. They are thought to be produced at relatively large mass transfer rates, when the outer edge of the disc expands reaching the 3:1 resonance radius. Bianchini et al. (2001) derived a relation between the superhump period (P_{SH}) and the mass ratio:

$$\frac{P_{SH_+}}{P_{orb}} = \frac{1+q}{1+0.74q} \tag{1.4}$$

- *Negative superhumps* are interpreted as the result of a precessing disc. The precession of the outer annulus of a tilted disc in this case is retrograde. Again, from Bianchini et al. (2001),

$$\frac{P_{SH_-}}{P_{orb}} = \left(1 + 0.35\frac{q}{(1+q)^2}\right)^{-1} \tag{1.5}$$

1.3 Properties of light curves of classical novae

The typical behaviour of the light curve of a nova (see Figure 1.7) is described in McLaughlin (1939, 1943), Payne-Gaposchkin (1957), and Duerbeck (1981).

A few important phases can be easily identified. The initial rise usually lasts less than 3 days (notable exceptions being V1500 Cyg and Nova LMC 1991, see Della Valle 1991). Usually a nova climbs about 9 magnitudes in this phase. Many novae show a pre-maximum

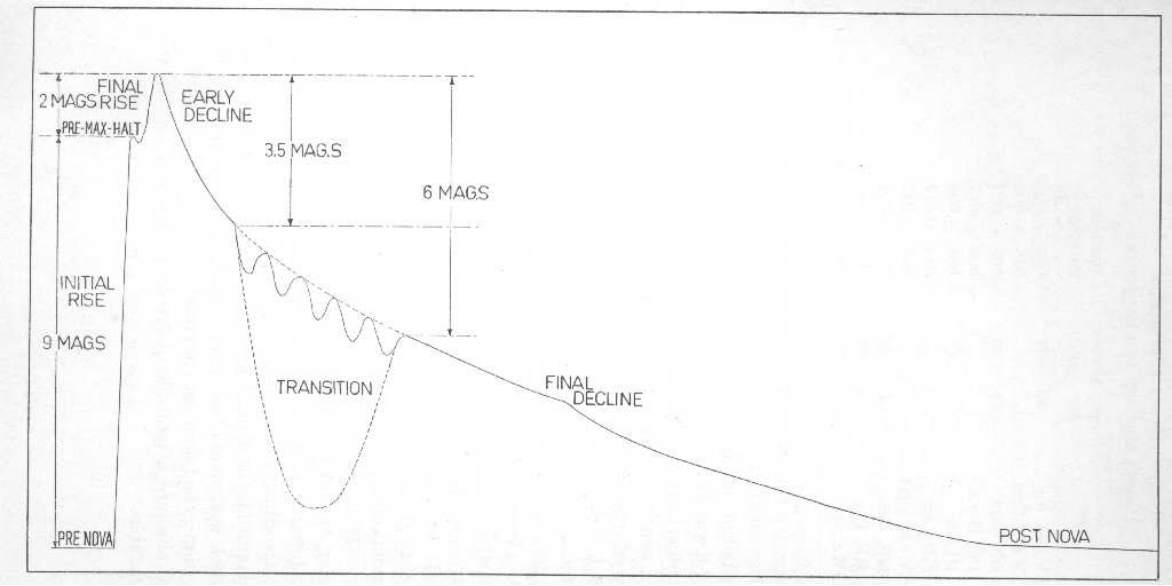

Figure 1.7: *The prototypical light curve of a nova (from McLaughlin 1960a)*

halt, followed by a final rise of the last two magnitudes to maximum. Schmidt (1957) proposed that there is a relation between the rate to final rise to maximum and the decline after maximum:

$$\log t_{r,2} = -0.3 + 0.7 \log t_2 = -0.5 \log t_3 \quad ,$$

where $t_{r,2}$ is the time needed to climb the last two magnitudes and t_2 and t_3 is the time needed to decline 2 and 3 magnitudes from maximum, respectively.

Several relations have been derived concerning the rate of decline. The most important relation is the one between the rate of decline and the absolute magnitude at maximum (MMRD). The first pioneering works have been carried out by Zwicky (1936) and McLaughlin (1939). This relation (shown in Figure 1.8) is usually written in the form:

$$M(\max) = a_n \log t_n + b_n \quad ,$$

where n (is usually 2 or 3 and represents the number of magnitudes faded from maximum).

Pfau (1976), on the basis of 27 extragalactic and 11 galactic novae, suggested the relation

$$M_B = -10.67(\pm 0.30) + 1.80(\pm 0.20) \log t_3 \quad .$$

Cohen (1985) was the first to determine distances from novae using expansion parallaxes. She derived

$$M_V = -10.70(\pm 0.30) + 2.41(\pm 0.23) \log(t_2) \quad .$$

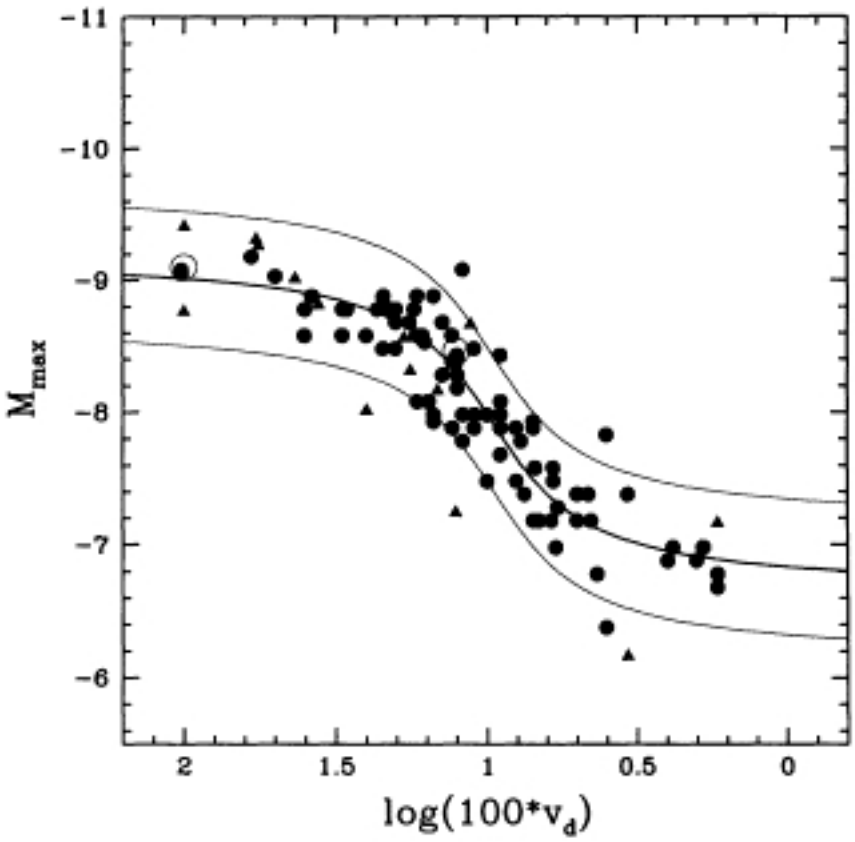

Figure 1.8: *Maxiimum magnitude vs. rate of decline relationship as from Della Valle & Livio (1995)*

On the basis of a survey for novae in M31, Capaccioli et al. (1989) suggested

$$M_{V,max} = -7.89 - 0.81 \arctan[(1.32 - \log t_2)/0.19] \quad .$$

On the basis of both galactic and extragalactic (i.e. M31 and LMC) novae, Della Valle & Livio (1995) derived

$$M_{V,max} = 7.92 - 0.81 \arctan \frac{1.32 - \log t_2}{0.23} \quad .$$

Downes & Duerbeck (2000), using the same novae but refined distances, derived

$$M_{V,max} = -8.02 - 1.23 \arctan \frac{1.32 - \log t_2}{0.23} \quad .$$

Downes & Duerbeck (2000), using distances derived from expansion parallaxes, for a sample of 28 galactic novae, derived:

$$M_V = (-11.32 \pm 0.44) + (2.55 \pm 0.32) \log(t_2/\text{days}) \quad .$$

By a formal fit to their novae in M49, Ferrarese et al. (2003), obtain

$$M_{V,max} = (-8.27 \pm 0.59) - 0.81 \arctan \frac{1.32 - \log t_2}{0.23}$$

$$M_{V,max} = (-8.56 \pm 0.86) - 1.23 \arctan \frac{1.32 - \log t_2}{0.23} \quad ,$$

allowing only the zeropoints of relations by Della Valle & Livio (1995) and Downes & Duerbeck (2000) to vary. Darnley et al. (2006) provided $m_V = (12.98 \pm 0.44 + (2.55 \pm 0.32) \log(t_2/\mathrm{days})$ for novae in M31.

It has been noted by van den Bergh & Younger (1987) that novae get bluer as they decline, therefore:

$$\log t_2(\mathrm{V}) = 0.953(\pm 0.013) \log t_2(\mathrm{B}) \quad .$$

Another fundamental property is that all novae show almost the same absolute magnitude 15 days after maximum light (Buscombe & de Vaucouleurs 1955). Ferrarese et al. (2003), using nine novae observed in M49, provided $M_{15,V} = -6.36 \pm 0.19$ (random) $\pm$ 0.10 (systematic). They note that one should excercise considerable caution when estimating distances with this method because of the large standard deviation shown for $M_{15,V}$ and the rather poor agreement between the different calibration of it based on samples of Galactic novae. Darnley et al. (2006) obtained $M_{15,r'} = -6.3 \pm 0.9$ mag and $M_{15,i'} = -6.3 \pm 1.0$ mag. Jacobi et al. (1992) showed that several "exceptional" novae in M31 offered clear counterexamples to the universality of this relation.

Relations like the MMRD and the Buscombe - de Vaucouleurs relations are of extreme importance to use novae as distance indicators in the first step of the cosmological ladder and as a calibration for SNeIa independent from Cepheids.

About 3–4 magnitudes below maximum light, a few novae show a deep mimimum 7 – 10 mag deep, lasting 2 – 3 months, after which the nova brightens and follows the extrapolated early decline (e.g. DQ Her, T Aur, LW Ser) while others start large scale quasi periodic brightness oscillations with amplitudes 1 – 1.5 mag (e.g. V603 Aql, GK Per, DK Lac).

Colors of novae have been studied in an outstanding work by van den Bergh & Younger (1987). They analyzed UBV photometry of 14 CNe. They derived two fundamental relations (used to give a first guess of interstellar extinction in the direction of a nova):

$$(B-V)_{\max} = 0.23 \pm 0.06 \tag{1.6}$$

$$(B-V)_{t_2} = -0.02 \pm 0.04 \quad . \tag{1.7}$$

The above relations have $\sigma =$ 0.16 and 0.12 mag, respectively.

1.4 Properties of spectra of Classical Novae

Nova spectra have been studied for almost the whole second half of the 20th century on the basis of McLaughlin's (1943) work. This description is completely taxonomical and independent of speed class. Just an outline of this description is given here only for historical reasons.

Novae usually show four absorption line systems:

- **pre-maximum spectra** this is a set of lines that is first observed two magnitudes *before* maximum light. It usually consists of weak diffuse lines with large negative displacements.

- **principal spectrum** this lines appear after the lines belonging to the pre-maximum spectrum have disappeared. It reaches its maximum about 3mags *after* maximum. This spectrum resembles closely the one of an A or F class supergiant.

- **diffuse enhanced spectrum** This is a set of wide and diffuse lines whose displacement in the blue is approximately twice as much as the principal absorption.

- **Orion spectrum** This spectrum, made up of O II, N II and He I lines, is the last one to appear. Its lines are broad and diffuse and velocities are nearly the same as those of the diffuse enhanced spectrum.

McLaughlin (1943) proposed this description on the basis of **seven** galactic novae.

McLaughlin (1960b) discovered strong Ne I absorption lines in the Orion spectrum of V528 Aql.

A new classification based on emission lines has been proposed by Williams (1992) after observation of a dozen of galactic novae.

Most novae are observed to fall into two classes: 'Fe II' and 'He/N'. 'Fe II' spectra are formed in optically thick winds and show expansion velocities between 1000 and 3500 km s^{-1}. 'He/N' spectra originate in a discrete shell of gas expelled at the time of outburst and usually have expansion velocities exceeding 2500 km s^{-1} (see Table 1.2).

Fe II	He/N
FWHM < 2000 km s^{-1}	2000 km s^{-1} $<$ FWHM < 50000 km s^{-1}
P Cygni profiles	Flat-topped line peaks with little absorption
slow evolution	fast evolution
Initial forbidden lines:	Initial forbidden lines:
N and O auroral transitions	[FeX]λ6375 and [FeVII]6087
[O I]λ 6300	[NeIII] or [Ne V]
Low ionization fluorescence lines in red	...or no forbidden lines at all
	F(He II λ4686) $>$ F(Hβ), eventually
	Flat, bluish continuum

Table 1.2: *Classification from Williams (1992)*

A classification of different phases has been given in Williams et al. (1991). Every spectrum is classified as belonging to either phase C, P, A,or N depending on the following criteria:

- Phase C. If [Fe X]λ6375 emission is clearly present and stronger than [Fe VII]6087, the nova spectrum is considered to be in the **coronal phase**, regardless of any other line strngths

- Phase P. If not in phase C, the spectrum is considered to be in the **permitted-line phase** when the strongest non-Balmer line is a permitted transition

- Phase A. If not in phase C, the spectrum is considered to be in the **auroral line phase** whenever any forbidden auroral transition has a flux greater than that of the strongest non-Balmer permitted line, regardless of any nebular line strengths

- Phase N. If not in phases C or A, the spectrum is considered to be in the **nebular-line phase** when the strongest non–Balmer line is a forbidden nebular transition.

Nova ejecta have very high densities therefore showing mainly permitted lines (phase 'P'). When density drops, first 'auroral' (phase 'A') transitions (such as, [NII] λ 5755, [OIII] λ4363, [OII]$\lambda\lambda$7319,7330) appear and then 'nebular' (phase 'N') transitions (such as [OIII]λ5007, [NII]λ6584,[NeIII]λ3869,[FeVII]λ6087). Coronal emission may appear at the end of the evolution (phase 'C'). Each class has several sub-classes plus two 'options' (if [OIII]λ8446 line is

stronger than Hβ and if the spectrum of the secondary star is clearly visible).

1.5 A modern understanding of the nova phenomenon

The commonly accepted model for a Classical Nova explosion is the violent thermonuclear runaway on the surface of a white dwarf accreting mass from a red dwarf star.

This scenario was first proposed by Kraft (1962), based on a work by Mestel (1952).

The most important thing to be kept in mind is the equation of state for degenerate matter ($P \propto \rho^{\gamma}$), therefore independent of the temperature. If temperature and density, because of accretion, are high enough to start nuclear reactions, any increase in temperature will lead to an enhanced generation of energy without any increase of pressure, thus to an exponential runaway in the nuclear reactions. This process goes on as far as the Fermi temperature T_F is reached. At this point the equation of state becomes the one of a perfect gas and violent expansion starts.

The pressure at the base of the accreted envelope is:

$$P_b = \frac{GM(1)M_{env}}{R^2(1)} \frac{1}{4\pi R^2(1)} \quad , \tag{1.8}$$

where M_{env} is the mass of the envelope. If $P_b > P_b(crit) = 1 \times 10^{20}$dyn for solar abundance of CNO then the expansion reaches escape velocity and the envelope is ejected (see Warner 1995). The envelope mass required to produce $P_b(crit)$ has been computed by Livio (1993)

$$M_{env}(crit) = 1.7 \times 10^{-4} R_9^{2.8}(1) M_1^{-0.7}(1) \quad . \tag{1.9}$$

This leads us to note that if, after the outburst, accretion is restored, the binary system would go through a new CN outburst after a time

$$T_R = M_{env}(crit) / < \dot{M}(1) > \tag{1.10}$$

T_R is usually referred to as "recurrence time".

The fundamental parameters which determine the speed class of a nova are M_{WD}, L_{WD} and $\dot{M}$.

José & Hernanz (1998) noted that the dominant nuclear reaction at the beginning of the TNR in a nova outburst is typically $^{12}\mathrm{C}(p,\gamma)^{13}\mathrm{N}$, which is followed by a combination of β^+ decays, or (p,γ) and (p,α) reactions, as a function of the local temperature (a scheme of the CNO sycle is shown in Figure 1.9). As pointed out by Starrfield et al. (1972), some of

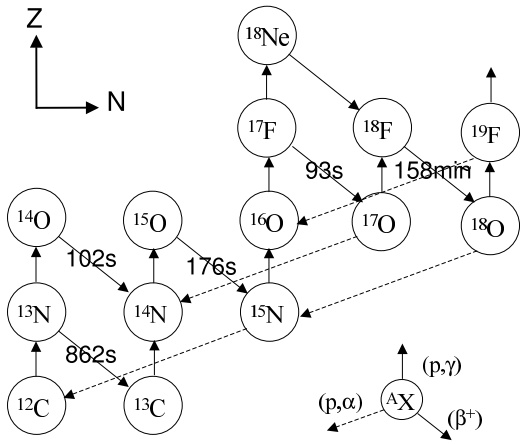

Figure 1.9: *Scheme of the CNO cycle from Hernanz (2004)*

the most overabundant species at peak temperature, except hydrogen and helium, are the short-lived β^+-unstable nuclei ^{13}N, ^{14}O, ^{15}O and ^{17}F, which decay releasing enough energy to account for the ejection of a fraction of the envelope. Therefore, their daughter nuclei ^{13}C, ^{14,15}N, and ^{17}O are among the main products in the ejecta of classical novae.

The main model of the ejecta has been proposed by Bath & Shaviv (1976). All novae at maximum light have the Eddington luminosity of a $\sim$1– 2 $M_\odot$ object. Radiation pressure in the optically thick continuum of the envelope is assumed to accelerate the ejecta. Electron scattering is supposed to be the dominant opacity mechanism. Bath & Shaviv (1976) showed that the optical decline is due to an increasing bolometric correction as the wind thins out and the photosphere receds to deeper (and therefore hotter) layers. They also showed mass outflow at maximum light to be of the order of $\sim 10^{21}$– 10^{22}gm s^{-1}.

A consequence of the receding photosphere is the fact that novae get bluer during their evolution, as already mentioned in Section 1.3.

Williams (1992) proposed that the changing in line emission is interpreted in terms of photoionization of the expanding shell by an evolving radiation source associated with the central remnant.

Williams et al. (1991) noted that:

1. immediately after outburst, the emission lines are first produced in conditions in which they are all permitted transitions. Forbidden lines appear later within a time scale of a few days to months.

2. Within 1 month of the outburst, recurrent novae enter a high ionization phase, marked

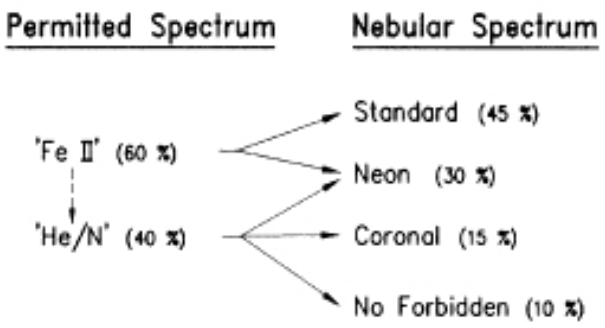

Figure 1.10: *Evolution and relative frequencies of nova spectra, from Williams (1992)*

either by strong coronal [Fe X] emission (V745 Sco, V3890 Sgr) or very strong He II (V394 CrA, LMC 1990 No.2).

3. The so-called neon novae, which all have strong [Ne III] or [Ne V] lines and therefore pass through the phase N_{ne}, appear to evolve directly from the permitted to the nebular phase, without passing through a coronal or auroral phase.

Williams (1992) noted that observationally emission lines become narrower as they evolve. This is expected for ejected gas which is not expanding uniformly or for a wind with a monotonically outwardly increasing velocity for which the mass–loss rate $\dot{M}$ steadily decreases with time. Williams (1992) recalls that one of the central results of both radiatively and thermally driven winds is that the terminal velocity is directly related to the escape velocity of the gas at the critical, or sonic, point which is usually very near the base of the wind, i.e. near the photosphere. If this pertains in a general way to the gas ejected by novae, it suggests that the highest velocity gas has been ejected from closer to the white dwarf surface than the lower velocity gas. This is consistent with the broader lines of the "He/N" emission spectrum originating in the discrete shell, which is ejected at high velocities from the white dwarf surface at the peak of the outburst. The inward migration of the photosphere toward the white dwarf surface from very large values out in the wind may explain the steady increase in the outflow velocity in the principal absorption system with time.

Emission lines arise both from the discrete ejected shell and the wind. Depending upon M_{sh}, $\dot{M}_w$, v_{ej}, v_w and the lifetime of the wind, an individual nova will have emission from either the shell or the wind.

1.6 The hibernation scenario

Novae are considered recurrent objects, i.e. several classical nova outbursts occur in the same binary system (the difference with "recurrent novae" is in the fact that RNe have more than one *observed* outburst while CNe have only one *observed* outburst). The recurrence time is related with the accretion rate and the mass of the white dwarf (as shown in Equation 1.10). On the other hand the number of novae that are observed in a galaxy is related to the recurrence time. The space density ($D_{CV} \approx 10^{-6}$ pc^{-3}, Patterson 1984) of CVs found in Galactic surveys implies recurrence times $\tau_{rec} \approx 10^3$ yr and high mass accretion rates $\dot{M}_{av} \gtrsim 10^{-8} M_\odot$ yr^{-1}. Simulations show that $\dot{M} \gtrsim 10^{-9} M_\odot$ yr^{-1} onto a white dwarf results in a steady nuclear burning or weak flashes and not thermonuclear runaways and nova explosions (unless the white dwarf is very close to the Chandrasekhar limit e.g. Starrfield et al. 1985). Shara et al. (1986) solved this inconsistency proposing the so-called "hibernation model". In the hibernation model, the mass transfer stops (for 90–99% of the recurrence time) because the secondary star loses contact with its Roche lobe. This is due to the fact that, during the explosion, the binary system loses mass (the ejected shell). Thus, the secondary shifts further from the white dwarf, but keeps contact with its Roche lobe because it is heated by the white dwarf. When the system cools down, the secondary loses contact with its Roche lobe and accretion stops. The system starts losing angular momentum via magnetic braking and/or gravitational waves, the system shrinks, the secondary comes again in touch with its Roche lobe and accretion starts again.

1.7 Nova populations

The concept of stellar population was introduced by Baade (1944, 1957) .

Kukarkin (1949), Kopylov (1955) and Plaut (1965) pointed out the existence of a concentration of novae towards the galactic plane and the galactic center and classified them as belonging to the 'disk population'. Minkowski (1948, 1950) and Payne-Gaposchkin (1957) showed that the galactic longitudes of novae and planetary nebulae (PNe) have similar distributions and therefore novae, like PNe, belong to Pop II stellar population. Baade (1958) assigned novae to Pop II stellar population because of the occurrence of a few ones (e.g. T Sco 1860) in very old stellar population systems, such as the Globular Clusters. Iwanowska & Burnicki (1962) suggested that novae are a mixture of Pop I and Pop II objects, and Patterson

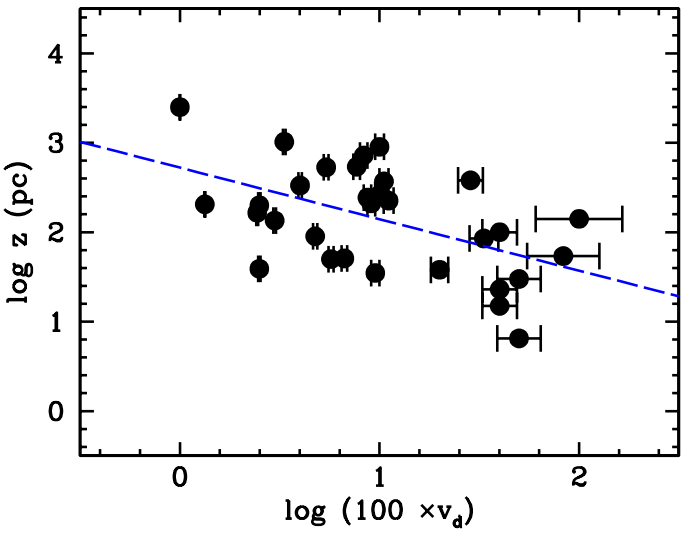

Figure 1.11: *The relationship between height above the galactic plane vs. rate of decline, $v_d = 2/t2$. The sizes of the errorbars in log z axis are comparable to the sizes of the dots.*

(1984) proposed that novae belong to an 'old disk' population. Tomaney & Shafter (1992) found that novae belonging to the bulge of M31 are spectroscopically different from novae observed in the neighborhood of the Sun and deduced that galactic novae are mainly 'disk' objects. Different conclusions were drawn by Della Valle & Duerbeck (1993) who compared the cumulative distributions of the rates of decline for M31, LMC and Milky Way nova populations and found that galactic and M31 distributions are indistinguishable, whereas M31 and LMC distributions are different at $\gtrsim 99\%$ significance level.

Duerbeck (1990) showed that nova counts in the Milky Way do not follow a unique distribution. DellaValle & Livio (1998) showed that the rate of decline correlates with the spatial distribution of novae in the Milky Way.

Della Valle (2002) showed that there is a relation between the rate of decline and the height above the galactic plane (see Figure 1.7):

$$\log z = (-0.58 \pm 0.18) \times \log(100 \times v_d) + (2.7 \pm 0.2)$$

which means

$$\log z = (-1.9 \pm 0.5) M_{WD}/M_{\odot} + (3.7 \pm 0.6) \quad .$$

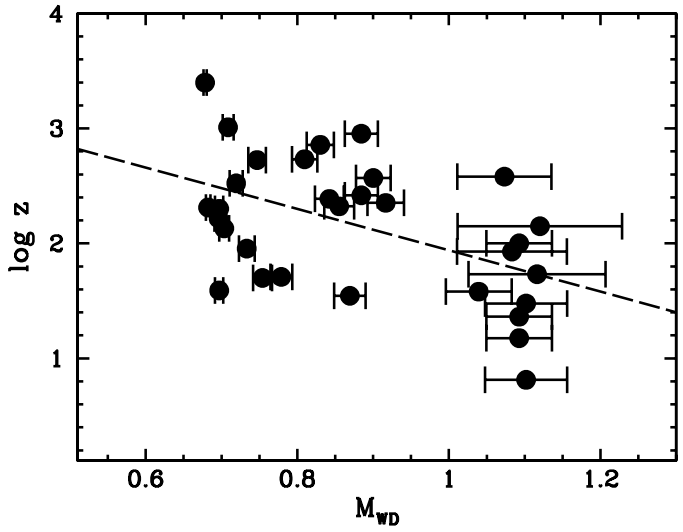

Figure 1.12: *The relationship between height above the galactic plane vs. mass of the underlying WD (in solar masses). The sizes of the errorbars in log z axis are comparable to the sizes of the dots.*

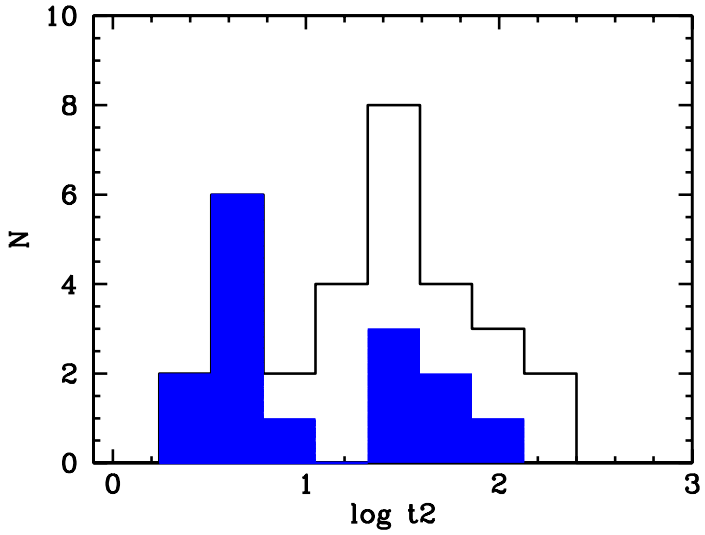

Figure 1.13: *Frequency distribution of the rates of decline for the novae of the fiducial sample. The shaded region represents novae with* $z \lesssim 150pc$.

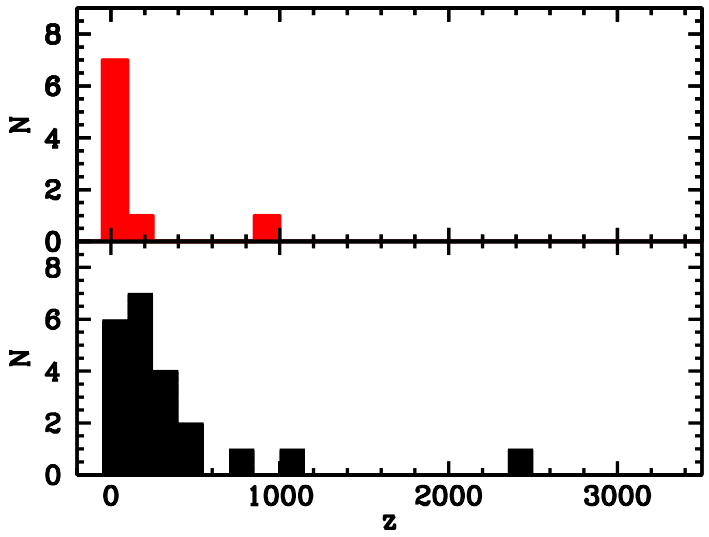

Figure 1.14: *Frequency distribution of the height above the galactic plane for He/N (and FeII-b) novae (top panel) and FeII novae (bottom panel). From Della Valle (2002).*

Analyzing a fiducial sample of galactic novae, DellaValle & Livio (1998) showed that disk novae (objects with $z < 150$ pc) are mostly 'fast' novae whereas 'bulge' novae are mostly 'slow'. The same authors also showed that He/N novae tend to concentrate close to the Galactic plane while FeII novae can be found at higher galactic latitudes. To explain this behaviour it has to be noted that the more massive the white dwarf (for a given $\dot{M}$ and T_{WD}) the smaller is the mass of the accreted envelope and more violent is the outburst.

Ferrarese et al. (2003) on the other hand showed that M49 (a giant elliptical galaxy, therefore dominated by population II stars) novae behave like LMC (a barred spiral, therefore dominated by population I stars) novae. Their survey provides no clear support for a classification of novae into a disk and bulge populations.

1.8 The nova rate and the evolution of the Universe

José & Hernanz (1998) showed that classical novae can produce ^{7}Li, ^{13}C, ^{15}N, and ^{17}O (see Figure 1.15)

This result has been used by Romano & Matteucci (2003) to prove that novae are needed to reproduce evolution of various elements.

Novae are expecially required to reproduce the evolution of ^{7}Li. Li is supposed to be

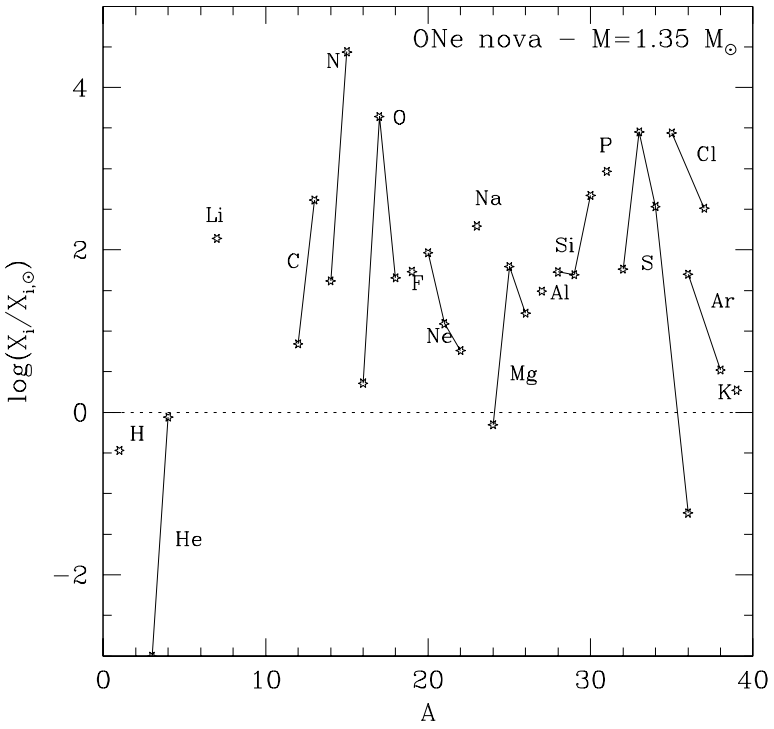

Figure 1.15: *Abundances for an ONe nova from a 1.35 $M_\odot$ (from José & Hernanz 1998)*

produced partly during the Big Bang, in massive stars, type II supernovae, AGB stars, red giant stars and by cosmic ray spallation. Figure 1.16 shows the evolution of ^{7}Li[1]. Points are data from observations of galactic stars. Data with [Fe/H] ≤ -1 were observed for the first time by Spite & Spite (1982). This is usually referred as the "Spite plateau". Curves refer to different models computed by Romano et al. (2001). Model "A" refers to a model without contribution of novae to the chemical enrichment. Model "B", refers to a model considering both SNeII and novae and model "C" refers to a model without C-stars. These authors conclude that one single stellar category of ^{7}Li producers could never explain all the observed features of this plot. For the present discussion, it is worth noting that it is impossible to reproduce present-time abundances of ^{7}Li without CNe even though CNe cannot justify the rise off the Spite plateau.

Absolute abundances in CN ejecta alone are not enough to study the role of CNe in the chemical evolution of the universe. It is crucial to know how many novae occur in a galaxy in a year. This is what is usually called "nova rate". Our knowledge on observed nova rates can be summarized from Table 1.3.

[1] $A(Li) = \log_{10}(N_{Li}/N_H) + 12$

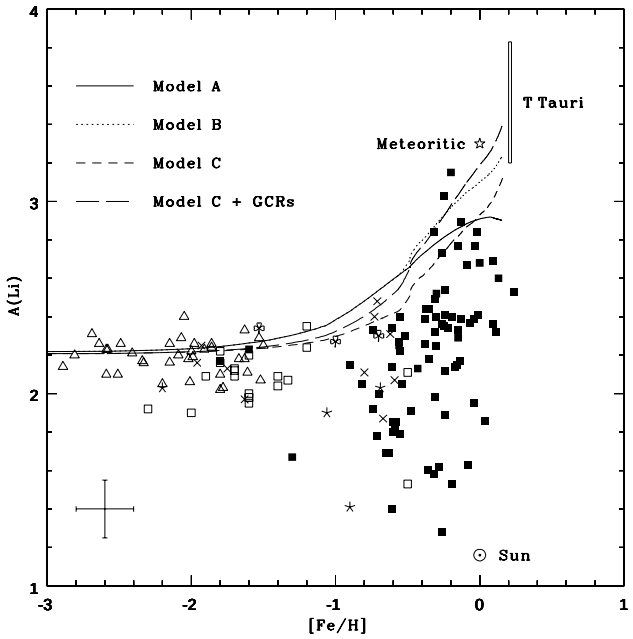

Figure 1.16: A(Li) *versus* [Fe/H] *theoretical predictions for the solar neighborhood from models by Romano et al. (2001) , compared with the observational diagram coming out from our data analysis. The upper limits have been removed from the sample. Filled symbols: disk stars; empty symbols: non-disk stars. Crosses and asterisks identify stars without kinematical membership determination; clovers are objects with multiple* ^{7}Li *determination in the literature for which the average value has been taken. Solar, meteoritic* ^{7}Li *abundances are also shown. (Figure from Romano et al. 2001)*

Galaxy	Novae/yr	B_{tot}	(B–K)	(m–M)	ν_K	T
LMC	2.5 ± 0.5	0.57	2.74	18.58 ± 0.1	5.1 ± 1	9
SMC	0.7 ± 0.2	2.28	2.71	19.00 ± 0.1	4.8 ± 1.5	9
M33	4.6 ± 0.9	5.75	2.87	24.64 ± 0.2	3.7 ± 0.9	6
M101	12 ± 4	8.26	3.24	29.35 ± 0.2	0.9 ± 0.3	6
M51	18 ± 7	8.41	3.43	29.60 ± 0.2	1 ± 0.4	4
M31	29 ± 4	3.51	3.85	24.42 ± 0.2	1.5 ± 0.2	3
M81	24 ± 8	7.39	3.99	27.80 ± 0.2	1.7 ± 0.6	2
N5128	28 ± 7	6.32	3.38	27.80 ± 0.2	3.3 ± 0.8	–2
N1316	130 ± 40	9.20	4.15	31.50 ± 0.3	1.7 ± 0.5	–2
M87	91 ± 34	9.49	4.17	30.90 ± 0.2	2.1 ± 0.8	–4
VirgoEs	160 ± 57	9.46	4.26	31.35 ± 0.2	2.2 ± 0.8	–4

Table 1.3: *Absolute and normalized nova rates (from Della Valle 2002)*

It easily follows that the bigger the galaxy, the higher the nova rate. More interesting is to look at the so-called "normalized nova rate" (i.e. the nova rate divided by the K-band luminosity of the host galaxy).

The lower panel of Figure 1.17 has been obtained using the K-band luminosity from $B-K$ and B-magnitudes (as from Table 1.3). The upper panel of Figure 1.17 comes from K-band luminosities from the Two Micron All Sky Survey (2MASS). The point that is shown twice is M33 for which two estimates of the nova rate are available. Excluding this galaxy, the weighted average nova rate is $\langle \nu_K \rangle = 1.58 \pm 0.16 \quad \mathrm{yr}^{-1}\ 10^{-10} L_{K\odot}$ for the lower panel and $\langle \nu_K \rangle = 2.41 \pm 0.27 \quad \mathrm{yr}^{-1}\ 10^{-10} L_{K\odot}$ if 2MASS data are used. The ~ 35 % increase in the normalized nova rate is a consequence of the 0.2 mag systematic difference between the two estimates of K-band magnitudes, with the 2MASS magnitudes being fainter. It is unclear which magnitude estimate is more reliable. Either case, with the possible exception of the LMC, every galaxy, for which a reliable measurement of $\langle \nu_K \rangle$ exists, appears to be consistent with a "universal" value of $\approx 1.6 - 2.4$ year^{-1} $10^{-10} L_{\mathrm{K}\odot}$.

Theoretical nova rates have been computed by Yungelson & et al. (1997) and Matteucci et al. (2003). Yungelson & et al. (1997) combined a model of the Zero Age Cataclysmic Variables (ZACV) population and its formation rate (obtained by a population code) with an algorithm for the evolution of cataclysmic variables and use the grid of nova models of Prialnik & Kovetz (1995) to derive the nova rate. In this framework, a crucial role is played by the star formation period T_f, the efficiency of energy deposition into the common envelope α_{ce}, and the distribution of the initial mass ratio of the components of the CV ($f(q) \propto q^{\alpha}$). Yungelson & et al. (1997) computed several models for various values of T_f, α_{ce} and α. Their main conclusions are:

- observed nova rates in disc galaxies are mainly dominated by the star formation rates in the past $(1-2) \times 10^9$ yr
- normalized nova rate is higher for galaxies of low mass ($M \lesssim 2 \times 10^{10} M_{\odot}$) than for high-mass galaxies. This is a consequence of the previous point in combination with the dependence of the K luminosity on the star formation history
- differences between "disk" and "bulge" novae are probably a consequence of the fact that "bulge" novae belong to a relatively old parent population, having, typically, lower white dwarf masses

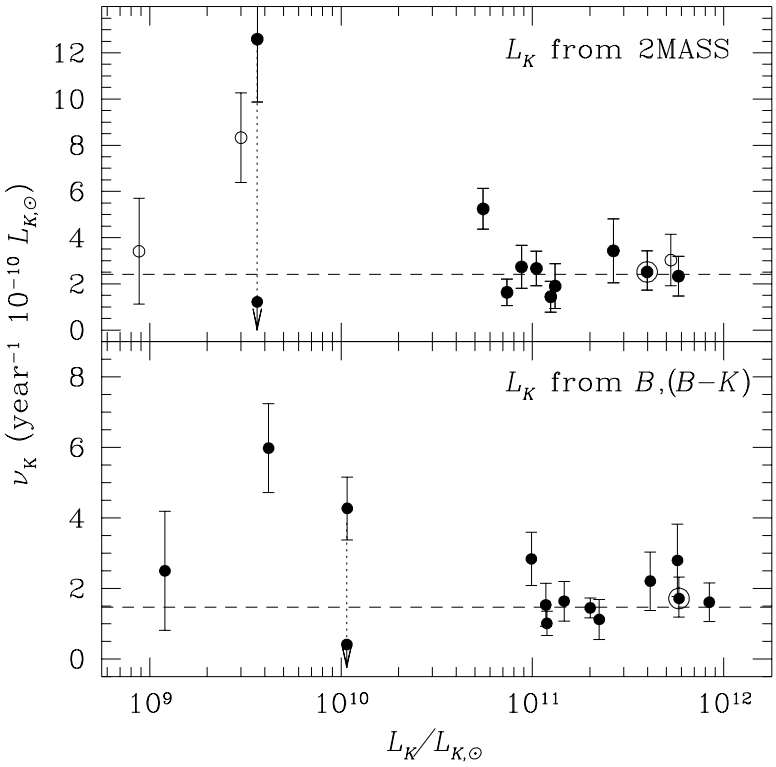

Figure 1.17: *Luminosity-specific nova rates, ν_K, for all galaxies with measured global nova rates. The global nova rates have been normalized by the total K-band luminosity of each galaxy, derived from 2MASS (upper panel - the open circles denote galaxies for which 2MASS magnitudes are not available, and K-band magnitudes were derived from the RC3 B-band magnitudes as in the lower panel) or inferred from the RC3 B-band magnitudes via a color correction (lower panel – see text for further details). M49 is indicated by the circled point. For M33, two different — and inconsistent — estimates of the nova rate are available (see text for details). The dashed line shows the weighted mean, exluding M33: $\bar{\nu_K} = 1.58 \pm 0.16$ year^{-1} $10^{-10} L_{K,\odot}$ in the lower panel, $\bar{\nu_K} = 2.41 \pm 0.27$ year^{-1} $10^{-10} L_{K,\odot}$ in the upper panel (from Ferrarese et al. 2003).*

- determination of the nova rate can, in principle at least, be used to place meaningful constraints on the initial distribution of binary systems over mass ratios.

Matteucci et al. (2003) use the chemical evolution models elaborated by Chiappini et al. (2001), Matteucci et al. (1998) and Calura et al. (2003) for the Milky Way, ellipticals and late spirals, respectively. Details on this model are given in Section 2.3. They summarize their results as follows:

- nova rates in ellipticals reach a maximum after $\sim 10^9$ years since the beginning of star formation. The same behaviour is shared by type Ia SNe although they reach a maximum only after a few 10^8 years. The delayed maximum in the nova rate relative to the SN Ia rate is due to the longer time delay assumed for novae to appear relative to SNe Ia.

- a model for ellipticals which assumes a strong burst of star formation occurring at early cosmic times can reproduce the majority of the observational constraints in ellipticals

- the nova rate in ellipticals is rather independent from the adopted IMF but it depends on the assumption that the efficiency of star formation is an increasing function of the luminous galactic mass (inverse wind model of Matteucci 1994).

1.9 Old Novae: a subclass of CVs?

CNe, a long time after the outburst, are sometimes referred to as "old novae". They are also called "Nova Remnants". The subclass of novalikes known as SW Sex stars has been also called 'quiescent novae' (Vogt 1989). Warner (1995) recalls that the identification of SW Sex stars with 'quiescent novae' is incorrect.

The study of old nova systems is deeply related with evolution of CVs.

Spectroscopic surveys of novae at minimum light (Humason 1938, Greenstein 1960, Kraft 1964) showed that old novae either show UX UMa type spectra or RW Tri type. The UX UMa stars have persistent broad band Balmer absorption–line spectra. RW Tri have pure emission line spectra (albeit occasionally with sharp absorption cores). The difference between the two classes can be explained in terms of inclination effects.

In recent novae, emission lines from the ejected shell are often superimposed on the lines from the central binary.

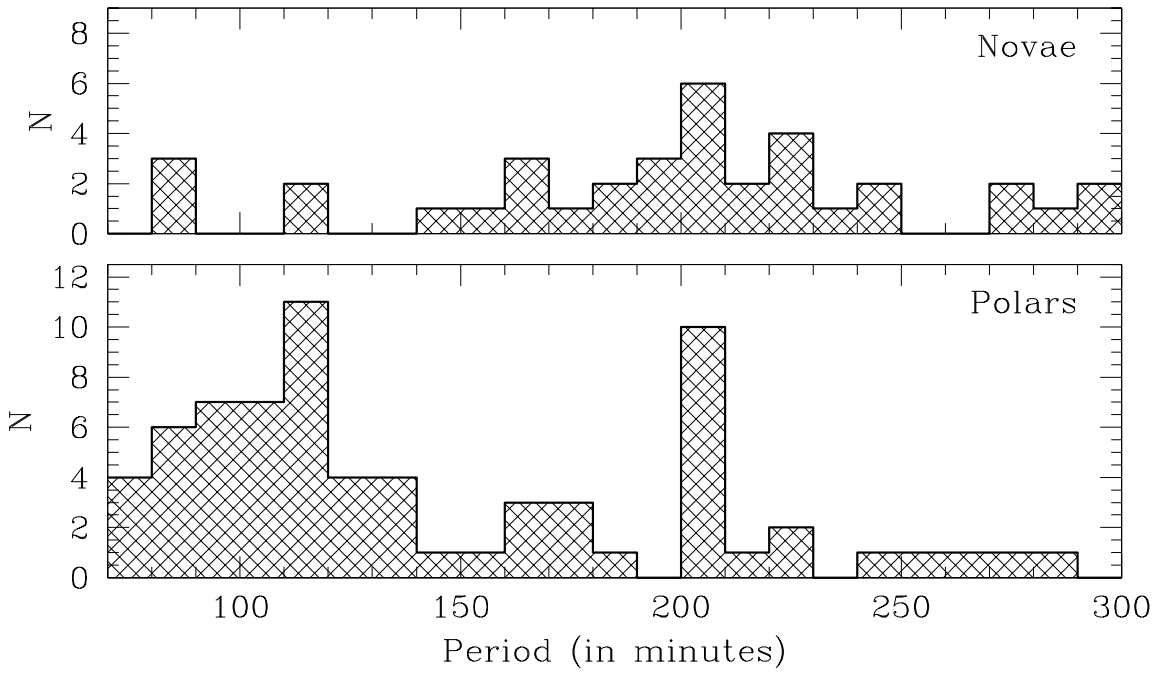

Figure 1.18: *Orbital periods for Nova Remnants (upper panel) and Polars (lower panel)*

Comparison of magnitudes of novae pre– and post–outburst are important to constrain the evolution of CN systems (i.e. whether the white dwarf loses or gains mass). McLaughlin (1939, 1941, 1960b) concluded that pre– and post–nova are essentially identical. This remains true even if three very fast novae (GQ Mus, CP Pup and V1500 Cyg) have higher post–outburst magnitude.

Warner (1995) reports that absolute magnitude of old novae is in the range V = 3.4 – 4.4 mag (after referring to a standard inclination, Warner 1986).

Warner (2002) shows that nova remnants do not show an obvious period gap (see Figure 1.18) but there is a concentration in the range 2.8 – 4.1 h. Warner (2002) notices that both nova remnants and polars have peaks around 114min (1.9h) and 202min (3.37h). This leads him to assume that a non–negligible amount of CNe may arise from magnetic systems.

According to the "hibernation scenario" (see Section 1.5), all classical novae pass through a dwarf nova phase. If this is the case, all dwarf nova systems are classical nova candidates. Shara (1989) did not find any remnant of the bright novae noted in Oriental records of one or two millennia ago. In case of no hibernation, these objects should have magnitudes $\sim$ 12 – 15.

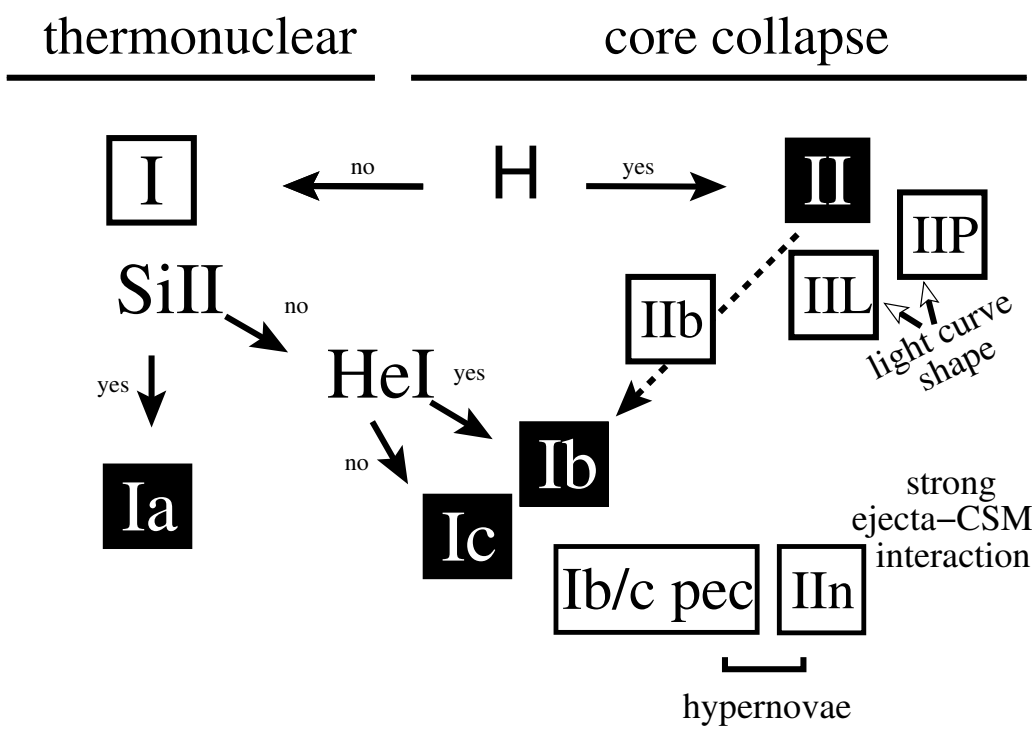

Figure 1.19: *The current classification scheme of supernovae. Type Ia SNe are associated with the thermonuclear explosion of accreting white dwarfs. Other SN types are associated with the core collapse of massive stars. Some type Ib/c and IIn SNe with explosion energies $E > 10^{52}$ erg are often called hypernovae.(from Turatto 2003)*

In the framework of the evolutionary scenario of CVs, the question about how Nova Remnants are related to other types of CV remains unanswered.

1.10 Type Ia Supernovae: related objects?

Supernovae (SNe) are the second brightest explosion in the universe (only Gamma Ray Bursts, GRBs, are brighter).

SNe are classified according to their spectra. Those which show hydrogen lines are classified as type II, while those which don't show hydrogen lines are classified as type I. SNe type II can be subdivided, according to their light curve, in type IIP and type IIL according to the presence (IIP) or the absence (IIL) of a plateau in the light curve. SNe type I are further subdivided into the SNe Ia that show prominent silicon lines, the SNe Ib that show no Si lines and the SNe Ic that show neither Si nor helium lines.

Different types of SNe have been finally understood to be produced by different types of

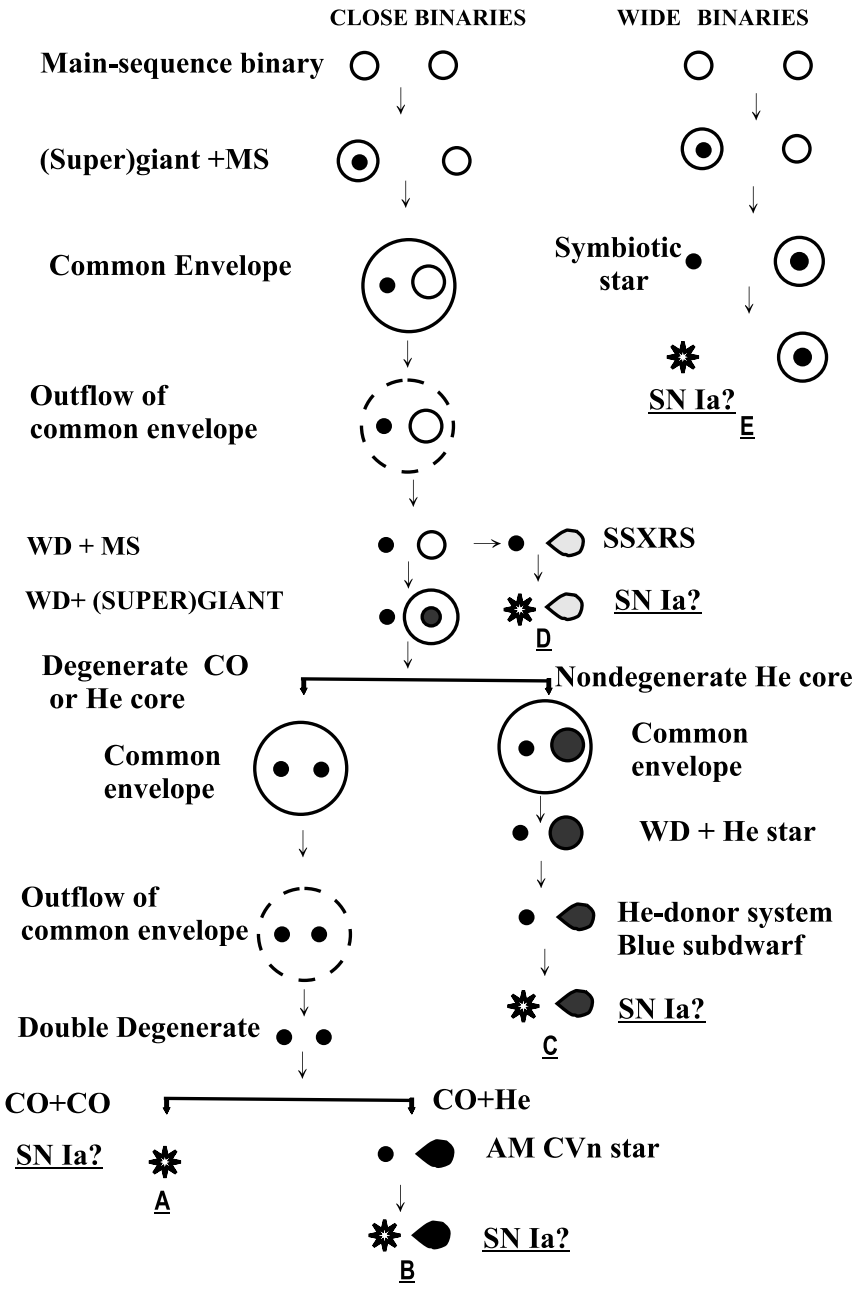

Figure 1.20: *Type Ia SN progenitors (from Yungelson 2003)*

progenitors.

Today we can make a classification on the basics of just the physical process that powers the explosion: thermonuclear SNe (i.e. type Ia) and core-collapse SNe (i.e. all the others).

Core collapse SNe are due, as the name suggests, to the collapse of massive stars. SNe II are believed are supposed to be deaths of massive stars whose degenerate cores have exceeded the Chandrasekhar mass. SNe Ib/c are believed to represent the deaths of massive stars that have lost their hydrogen envelopes during a mass-loss phase.

Two distinct scenarios for thermonuclear SNe have been proposed: "single degenerate" and "double degenerate", both invoking the presence of a massive white dwarf (they are sketched in Figure 1.20).

According to the "single degenerate" scenario (Kenyon et al. 1997, Munari & Renzini 1997, Whelan & Iben 1973) a SNIa comes from the deflagration of a massive white dwarf that accretes matter from a red giant. When the mass of the WD reaches the Chandrasekhar mass, the explosion occurs.

According to the "double degenerate" scenario (Iben & Tutukov 1984) a SNIa comes from the merging of two WDs (not necessarily massive).

The progenitor of a SN Ia in the single degenerate scenario is pretty similar to a nova system (differences being the masses of the components).

Type Ia supernovae have been shown to be standardizable candles. The meaning of the word "standardizable" can be explained in the following way: maximum magnitude relates with the rate of decline (Phillips 1993, Phillips et al. 1999). Even if this relation could remind of the same relation for CNe, this points in the other direction: the brighter the SNa, the slower its rate of decline.

SNeIa are also found to occur in any type of galaxy, also in ellipticals, and are not associated with the arms of spirals.

Being bright, standardizable and almost obiquitous, SNeIa have been largely used as distance indicators. It has been with SNe Ia that Perlmutter et al. (1997) measured cosmological parameters and Riess et al. (1998) gave observational evidence for an accelerating universe.

SNeIa are supposed to be related to CNe since it has been proposed that some CNe (i.e. Recurrent Novae occurring on massive white dwarfs, e.g. U Sco, Sarna et al. 2006) can evolve and eventually end their existence as SNeIa (Hachisu 2003 and Yaron et al. 2005). This is based on the hypothesis that the underlying WD is not eroded during an outburst but rather

increases its mass toward the Chandrasekhar limit.

Chapter 2

The nova rate

2.1 The nova rate in spirals

2.1.1 Observations and data reduction

The Hubble Space Telescope (hereafter HST) has been used for a large project to measure the distances to various galaxies via the period – luminosity relation for Cepheids. This data set has not been used yet for an extensive search of variables other than Cepheids, even if Ferrarese et al. (1996) showed that it is possible to use this data set to detect classical novae. I took advantage of the public availability of the data through the STScI archive (`archive.stsci.edu`).

Images have been obtained with WFPC2. This instrument is made up of four 800 × 800 pixels detectors: three Wide Field Camera (WFC) chips, with a pixels size of 0".10 and a field of view of 1'.3 × 1'.3 per chip and one high-resolution Planetary Camera (PC1), with a pixel size of 0".046 and a field of view of 36" × 36". The gain and readout noise are about 7 e^-/DN and 5e^-, respectively. Further details about the instrument can be found in the HST WFPC2 Instrument Handbook (Biretta et al. 2001).

Data retrieved from the archive are already pipeline reduced (bias and flat field). Each epoch in each filter consists of two one-orbit duration exposures taken on successive orbits of the spacecraft. This allows the removal of cosmic rays by an anti-coincidence technique described by Saha et al. (1996a). I applied the geometric distortion correction using a pixel area map following Stetson et al. (1998).

I have applied two different (and independent) techniques to find novae in my data sets.

Either I produced light curve for each star in the frames (analogously to Ferrarese et al. 2003), or single out just the variables (following Della Valle & Gilmozzi 2002). Both methods required psf-photometry which I carried out with `IRAF-DAOPHOT`. An important challenge to my study was to be able to find stars to model the point spread function (PSF). At the distance of these galaxies, globular clusters look like bright stars, therefore any automatic identification of PSF stars would pick wrong objects. For each analyzed frame, I carefully selected at least 15 stars, trying to cover the widest range of magnitudes and trying to cover the whole area of the chip. Measured magnitudes had to be corrected for aperture (standard magnitudes are measured with an aperture of 0.5").

The WFPC2 was found, shortly after launch, to have a charge transfer efficiency (CTE) problem; objects appeared about 10% fainter at the top of the chip when compared to the bottom of the chip. The equations for CTE correction can be found on Andrew Dolphin's webpage `http://www.noao.edu/staff/dolphin/wfpc2_calib/` First, it is required to compute the following variable values:

```
lct0 = ln(counts/electrons) - 7
bg = sqrt(background/electrons^2 + 1) - 10
lbg = ln(sqrt(background/electrons^2 + 1)) - 1
yr = (MJD - 50193) / 365.25
```

Second, correct for the CTE loss in X readout

```
XCTE(mags)=0.0021*exp(-0.234*bg)*x/800
```

third, recalculate `lct` using

```
lct = lct0 + 0.921*XCTE
```

Finally, correct for the CTE loss in Y readout:

```
c1 =
0.0114*(0.670*exp(-0.246*lbg)+0.330*exp(-0.0359*bg))*(1.+0.335*yr-0.0074*yr*yr)y/800
c2=3.55*exp(-0.474*lct)
YCTE(mags)=ln(exp(c1)*(1+c2)-c2)/0.436
```

The correct magnitude is

$$m_{corrected} = m_{measured} + \mathrm{XCTE} + \mathrm{YCTE}$$

Moreover, contaminants accumulate on the CCD windows over time, producing a time-dependent loss of throughput. The WFPC2 is warmed to about +22°C for about 6hours to remove the buildup of contaminants. This used to be done every 28 days. Decontamination dates are available on the webpage
`http://www.stsci.edu/instruments/wfpc2/Wfpc2_memos/wfpc2_decon_dates.html`
The corrected flux is:

```
corrected flux = flux * (1 + (% decline per day / 100)*(Days since
decontamination)
```

A `FORTRAN77` program applied corrections for the difference of the F555W filter from the standard Johnson V, the correction for the contamination and the aperture correction. The same program also computes light curves of any object that is detected and rejects non-variable objects by the simple assumption that the scatter of the light curve is greater than a given threshold. For each galaxy the cepheids reported in the literature have been used as a cross check.

The second method is manual in the sense that it requires blinking of pair of frames in order to detect the variable stars. Blinking is performed after the subtraction of the background obtained applying a median filter to the images. CNe are identified again by inspection of the light curves.

As a cross check, both methods have been successfully applied on M49 where I managed to find the same novae than in Ferrarese et al. (2003). I also tested the influence of the time distribution of the frames on the possibility to discover novae (the time spacing of the HST key project is such to maximize the detection of Cepheids). Re-sampling (after interpolation by a spline) the light curve in Ferrarese et al. (2003), I find that I miss one nova out of nine (see fig.2.1).

To infer the nova rate from the counts I use the "time coverage technique" , originally proposed for SNe by Zwicky (1942) and subsequently revised for novae by Capaccioli et al. (1989) and Shafter et al. (2000). Let m_M be the average maximum magnitude of the novae observed in the data set, m_l the limiting magnitude of the images and v_d the average rate of decline of the novae of the data set. The "single frame control time" (also called "mean nova lifetime", Shafter et al. 2000) is defined as $\tau = \frac{m_l - m_M}{v_d}$ (which is the time interval during which it is possible to detect a nova). The "global control time" (the time covered by the

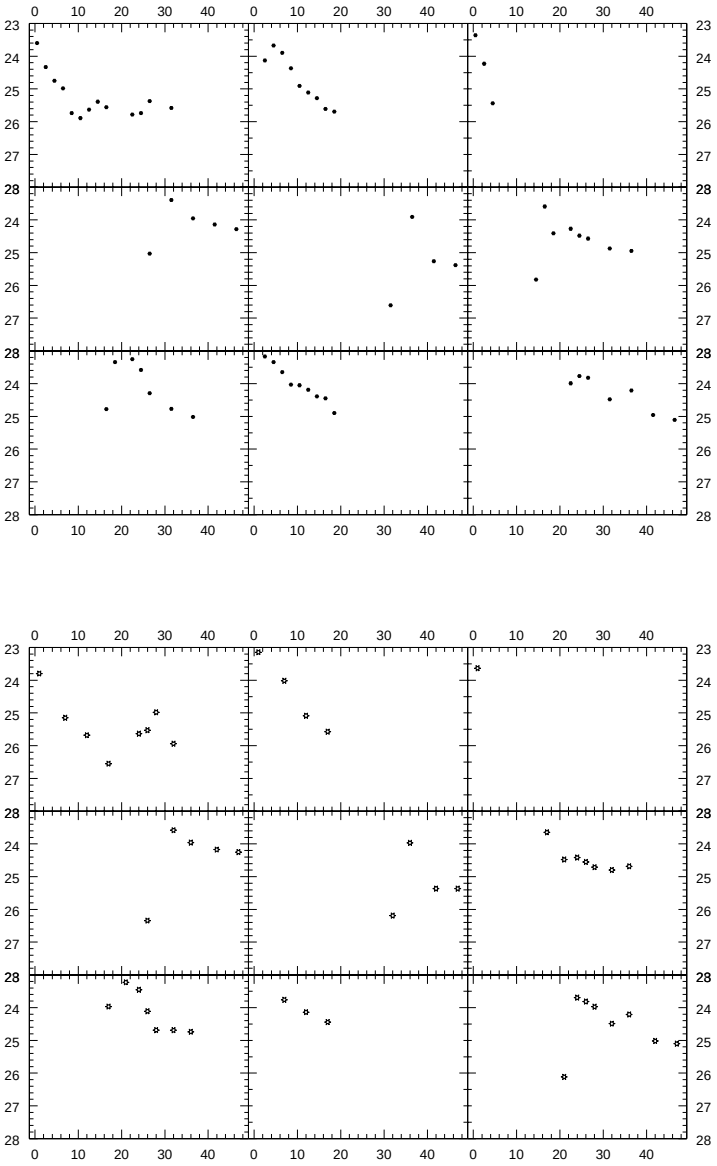

Figure 2.1: ***Upper panel:*** *Light curves as from Ferrarese et al. (2003)* ***Lower panel:*** *Same light curves with the sampling from the HST key project. The nova in the upper right panel cannot be identified from the light curve.*

whole data set) is given by:

$$T = \tau \times (1 + \sum_{i=2}^{n} \beta_i)$$

where

$$\beta_i = \begin{cases} \frac{t_i - t_{i-1}}{\tau} & \text{if } (t_i - t_{i-1}) < \tau \\ 1 & \text{if } (t_i - t_{i-1}) > \tau \end{cases}$$

and t_i is the epoch of the i^{th} observation. The nova rate is the number of novae observed divided by the global control time.

2.1.2 Results

I have analyzed data for 6 spiral galaxies. In the following I present results for individual galaxies. Results are summarized in Figure 2.5.

NGC3982

NGC3982 has been the first galaxy of the sample to be analyzed. This was a natural choice since the galaxy is seen face-on and the whole galaxy is visible in the images. I checked the quality of my photometry with the magnitudes of cepheids observed by Saha et al. (2001).

I took advantage of 11 epochs of observation out of 12. The very first one has been excluded since it was relatively largely displaced with respect to the other images. Therefore I take advantage of 40 out of the 53 days of the observation interval.

No novae have been found. I took 3 as an upper-limit at a 95% confidence level. Therefore, given the observation spacing (see Table 2.1), a limiting magnitude of ~ 29 mag, and an average absolute magnitude at maximum of ~ -8 mag (corresponding to a rate of decline of ~ 0.1 mag day^{-1}), one finds a GCT of 40. The upper limit on the nova rate is 88.97 novae yr^{-1}.

NGC3627

NGC3627 is a barred spiral galaxy which hosted SN 1989B. It is too big for the field of view of WFPC2. It has been observed over an interval of 58 days. Saha et al. (1999) discovered 68 cepheids and derived a distance modulus of 30.22 ± 0.12.

No novae have been discovered. Considering the log of the observations (available in Table 2.2), the limiting magnitude (~ 29 mag), the average absolute magnitude at maximum of a nova (~ -8 mag, leading to a rate of decline of ~ 0.1 mag day^{-1}), one infers a GCT of 59 days. This implies an upper limit on the nova rate, at a 95% confidence level, of 60.32 novae yr^{-1}.

FILE	DATE-OBS	TIME-OBS
u5ky0101r_c0f.fits	2000-03-20	11:19:14
u5ky0102r_c0f.fits	2000-03-20	12:53:14
u5ky0201r_c0f.fits	2000-04-02	08:11:14
u5ky0202r_c0f.fits	2000-04-02	09:47:14
u5ky0301r_c0f.fits	2000-04-08	09:05:14
u5ky0302r_c0f.fits	2000-04-08	10:32:14
u5ky0401r_c0f.fits	2000-04-13	09:58:14
u5ky0402r_c0f.fits	2000-04-13	11:10:14
u5ky0501r_c0f.fits	2000-04-16	16:59:14
u5ky0502r_c0f.fits	2000-04-16	18:34:14
u5ky0601r_c0f.fits	2000-04-19	15:52:14
u5ky0602r_c0f.fits	2000-04-19	17:18:14
u5ky0701r_c0f.fits	2000-04-21	12:55:14
u5ky0702r_c0f.fits	2000-04-21	14:22:14
u5ky0801r_c0f.fits	2000-04-23	17:58:14
u5ky0802r_c0f.fits	2000-04-23	19:35:14
u5ky0901r_c0f.fits	2000-04-27	12:03:14
u5ky0902r_c0f.fits	2000-04-27	13:35:14
u5ky1001r_c0f.fits	2000-05-01	12:33:14
u5ky1002r_c0f.fits	2000-05-01	14:05:14
u5ky1101r_c0f.fits	2000-05-07	11:41:14
u5ky1102r_c0f.fits	2000-05-07	13:14:14
u5ky1201r_c0f.fits	2000-05-12	12:21:14
u5ky1202r_c0f.fits	2000-05-12	13:51:14

Table 2.1: *Log of observations of NGC3982*

FILE	DATE-OBS	TIME-OBS
u35i0101r_c0f.fits	1997-11-12	12:36:13
u35i0102r_c0f.fits	1997-11-12	14:07:13
u35i0201r_c0f.fits	1997-11-20	23:50:13
u35i0202r_c0f.fits	1997-11-21	01:24:13
u35i0301r_c0f.fits	1997-11-28	01:14:13
u35i0302r_c0f.fits	1997-11-28	02:45:13
u35i0401r_c0f.fits	1997-12-03	19:58:13
u35i0402r_c0f.fits	1997-12-03	21:30:13
u35i0501r_c0f.fits	1997-12-08	17:42:13
u35i0502r_c0f.fits	1997-12-08	19:15:13
u35i0601r_c0f.fits	1997-12-14	02:45:13
u35i0602r_c0f.fits	1997-12-14	04:17:13
u35i0701r_c0f.fits	1997-12-18	16:23:13
u35i0702r_c0f.fits	1997-12-18	17:58:13
u35i0801r_c0f.fits	1997-12-21	20:18:13
u35i0802r_c0f.fits	1997-12-21	21:48:13
u35i0901r_c0f.fits	1997-12-27	13:28:13
u35i0902r_c0f.fits	1997-12-27	14:58:13
u35i1001r_c0f.fits	1998-01-03	11:39:13
u35i1002m_c0f.fits	1998-01-03	13:10:13
u35i1101o_c0f.fits	1998-01-10	08:11:13
u35i1102r_c0f.fits	1998-01-10	09:42:13
u35i1201r_c0f.fits	1997-11-16	10:09:13
u35i1202r_c0f.fits	1997-11-16	11:40:13

Table 2.2: *Log of observations of NGC3627*

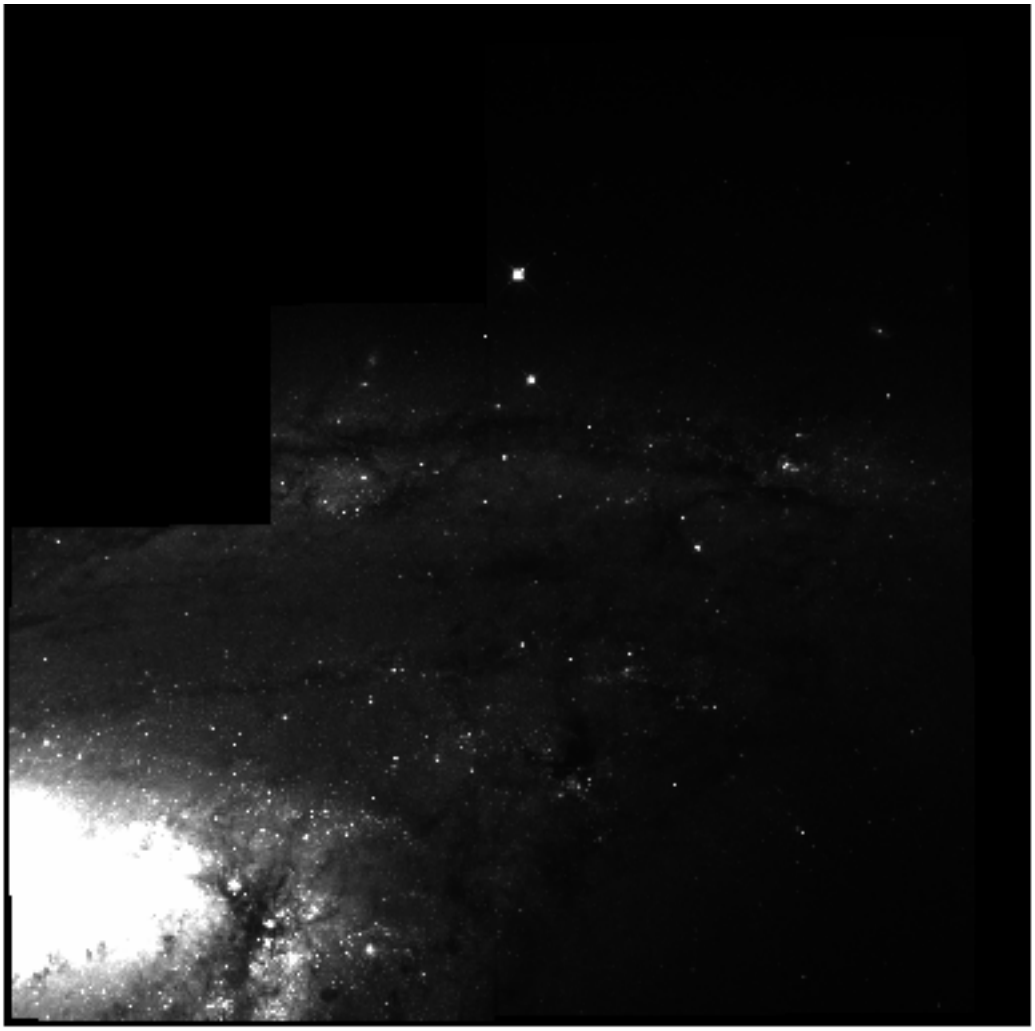

Figure 2.2: *HST image in filter 814W of NGC3627*

NGC4496A

NGC4496A (see Figure 2.3) is a big spiral galaxy that is interacting with a smaller one. The interaction region is clearly visible in these images. The galaxy is also completely visible in the images, while the accreted galaxy lies at the edge of the field of view of WFPC2. NGC4496A is the host galaxy of SN 1960F. Images have been taken over a 70 days period. Saha et al. (1996b) found 95 cepheids and derived a distance modulus of 31.03 ± 0.14.

There have been a few claims that galaxy interaction could enhance the nova rate. Unfortunately, given the small number of novae produced in a spiral galaxy, it is extremely difficult to detect this enhancement.

No nova has been observed in this galaxy. From the log of the observation (see Table

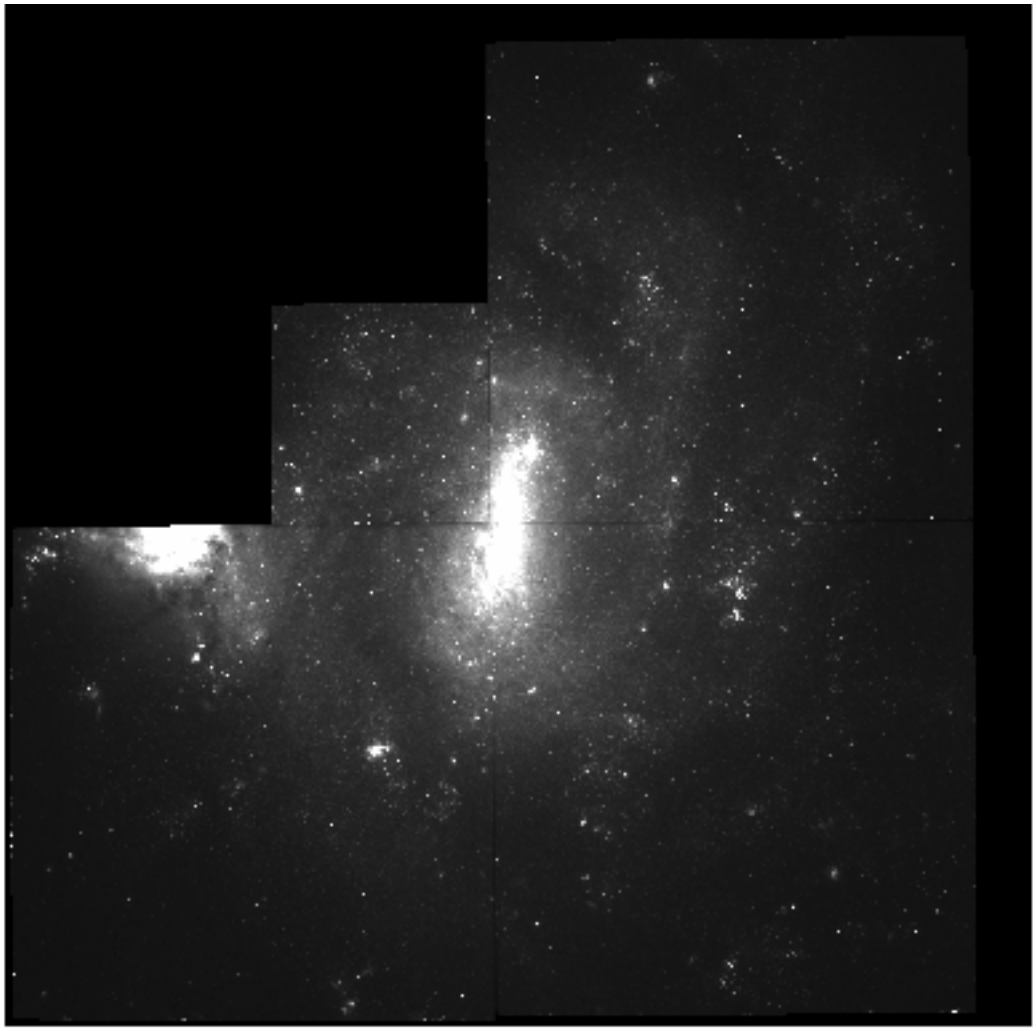

Figure 2.3: *HST image in filter 814W of NGC4496*

2.3), a limiting magnitude of ~ 29 mag and an average absolute magnitude at maximum of a nova of ~ -8 mag (therefore a speed of decline of ~ 0.1 mag day^{-1}), one obtains a GCT of 72 days and, considering an upper limit to a 95% confidence level of 3 novae, one obtain that the upper limit for the nova rate of this galaxy must be 49.43 novae yr^{-1}.

NGC4527

NGC4527 is seen almost edge-on and is too big for the field of view of WFPC2. It was the host galaxy of SN 1991T. It has been observed over an interval of 69 days. Saha et al. (2001) discovered 86 cepheids and derived a distance modulus of $30.74 \pm 0.12 \pm 0.12$.

No novae have been observed in this galaxy. Considering the log of the observations (see Table 2.4), the limiting magnitude (~ 29 mag) and an average absolute magnitude at

FILE	DATE-OBS	TIME-OBS
u2690101t_c0f.fits	1994-05-27	08:30:17
u2690102t_c0f.fits	1994-05-27	09:59:17
u2690201t_c0f.fits	1994-06-06	06:34:17
u2690202t_c0f.fits	1994-06-06	08:05:17
u2690301p_c0f.fits	1994-06-11	08:55:17
u2690302p_c0f.fits	1994-06-11	10:22:17
u2690401t_c0f.fits	1994-06-16	04:47:17
u2690402t_c0f.fits	1994-06-16	06:14:17
u2690501t_c0f.fits	1994-06-18	06:40:17
u2690502t_c0f.fits	1994-06-18	08:06:17
u2690601t_c0f.fits	1994-06-21	00:37:17
u2690602t_c0f.fits	1994-06-21	02:04:17
u2690701t_c0f.fits	1994-06-22	23:16:17
u2690702t_c0f.fits	1994-06-23	00:43:17
u2690801t_c0f.fits	1994-06-26	01:16:17
u2690802t_c0f.fits	1994-06-26	02:43:17
u2690901t_c0f.fits	1994-06-29	01:39:17
u2690902t_c0f.fits	1994-06-29	03:06:17
u2690a01t_c0f.fits	1994-07-01	00:18:16
u2690a02t_c0f.fits	1994-07-01	01:45:16
u2690b01t_c0f.fits	1994-07-03	21:29:16
u2690b02t_c0f.fits	1994-07-03	22:56:16
u2690d01t_c0f.fits	1994-08-07	02:01:16
u2690d02t_c0f.fits	1994-08-07	03:27:16
u2690e01p_c0f.fits	1994-07-16	05:32:16
u2690e02t_c0f.fits	1994-07-16	06:59:16
u2690f01t_c0f.fits	1994-07-20	04:24:16
u2690f02t_c0f.fits	1994-07-20	05:54:16
u2690g01t_c0f.fits	1994-07-26	05:13:16
u2690g02t_c0f.fits	1994-07-26	06:40:16
u2690h01t_c0f.fits	1994-08-02	06:09:16
u2690h02t_c0f.fits	1994-08-02	07:36:16
u2695c01t_c0f.fits	1994-08-06	01:53:16
u2695c02t_c0f.fits	1994-08-06	03:19:16

Table 2.3: *Log of observations of NGC4496*

FILE	DATE-OBS	TIME-OBS
u42g0101r_c0f.fits	1999-04-11	07:03:13
u42g0102r_c0f.fits	1999-04-11	08:36:13
u42g0201r_c0f.fits	1999-04-19	15:00:13
u42g0202r_c0f.fits	1999-04-19	16:31:13
u42g0301r_c0f.fits	1999-04-26	17:52:13
u42g0302r_c0f.fits	1999-04-26	19:23:13
u42g0401r_c0f.fits	1999-05-02	15:43:13
u42g0402r_c0f.fits	1999-05-02	17:13:13
u42g0501r_c0f.fits	1999-06-12	06:53:13
u42g0502r_c0f.fits	1999-06-12	08:27:13
u42g0601r_c0f.fits	1999-05-12	11:05:13
u42g0602r_c0f.fits	1999-05-12	12:34:13
u42g0701r_c0f.fits	1999-05-16	11:49:13
u42g0702r_c0f.fits	1999-05-16	13:19:13
u42g0801r_c0f.fits	1999-05-21	03:02:13
u42g0802r_c0f.fits	1999-05-21	04:33:13
u42g0901r_c0f.fits	1999-05-26	13:35:13
u42g0902r_c0f.fits	1999-05-26	15:11:13
u42g1001r_c0f.fits	1999-06-02	09:59:13
u42g1002r_c0f.fits	1999-06-02	11:29:13
u42g1101r_c0f.fits	1999-06-10	06:31:13
u42g1102r_c0f.fits	1999-06-10	08:05:13
u42g1201r_c0f.fits	1999-06-19	06:29:13
u42g1202m_c0f.fits	1999-06-19	08:05:13

Table 2.4: *Log of observations of NGC4527*

FILE	DATE-OBS	TIME-OBS
u2690i01t_c0f.fits	1994-06-03	06:04:17
u2690i02t_c0f.fits	1994-06-03	07:41:17
u2690j01t_c0f.fits	1994-06-17	03:19:17
u2690j02t_c0f.fits	1994-06-17	04:45:17
u2690k01t_c0f.fits	1994-06-18	09:52:17
u2690k02t_c0f.fits	1994-06-18	11:20:17
u2690l01t_c0f.fits	1994-06-23	02:28:17
u2690l02t_c0f.fits	1994-06-23	03:56:17
u2690m01t_c0f.fits	1994-06-25	02:44:17
u2690m02t_c0f.fits	1994-06-25	04:12:17
u2690n01p_c0f.fits	1994-06-28	07:57:17
u2690n02p_c0f.fits	1994-06-28	09:24:17
u2690o01t_c0f.fits	1994-06-29	20:57:17
u2690o02t_c0f.fits	1994-06-29	22:24:17
u2690p01t_c0f.fits	1994-07-03	05:24:16
u2690p02t_c0f.fits	1994-07-03	06:51:16
u2690q01t_c0f.fits	1994-07-29	10:27:16
u2690q02t_c0f.fits	1994-07-29	11:54:16
u2690r01t_c0f.fits	1994-08-07	05:13:16
u2690r02t_c0f.fits	1994-08-07	06:40:16
u2690s01t_c0f.fits	1994-08-05	01:45:16
u2690s02t_c0f.fits	1994-08-05	03:11:16
u2690t01t_c0f.fits	1994-07-12	09:50:16
u2690t02t_c0f.fits	1994-07-12	11:17:16
u2690u01t_c0f.fits	1994-07-17	10:30:16
u2690u02t_c0f.fits	1994-07-17	11:57:16
u2690v01t_c0f.fits	1994-07-31	02:30:16
u2690v02t_c0f.fits	1994-07-31	04:07:16
u2690w01t_c0f.fits	1994-07-26	08:26:16
u2690w02t_c0f.fits	1994-07-26	09:54:16
u2690x01t_c0f.fits	1994-08-02	02:57:16
u2690x02t_c0f.fits	1994-08-02	04:23:16
u2690y01t_c0f.fits	1994-08-09	03:53:16
u2690y02t_c0f.fits	1994-08-09	05:20:16

Table 2.5: *Log of observations of NGC4536*

maximum of ~ -8 mag (corresponding to a rate of decline of ~ 0.1 mag day^{-1}), one finds a GCT of 69 days. The upper limit on the nova rate is 51.58 novae yr^{-1} at a 95% confidence level.

NGC4536

NGC4536 is a spiral galaxy which hosted SN 1981B. Only one arm of the spiral could be observed with the field of view of WFPC2. This galaxy has been observed over a 67 day interval. Saha et al. (1996a) discovered 73 cepheids and derived a distance modulus of 31.10 ± 0.13.

No nova was discovered in this galaxy. Considering a limiting magnitude of ~ 29 mag, an average absolute magnitude at maximum of novae ~ -8 mag (corresponding to a rate of decline of ~ 0.1 mag day^{-1}) and an upper limit at a confidence level of 95% of 3, one obtains that GCT is 67 days and the upper limits on the nova rate is 53.12 novae yr^{-1}. Note that here I am not considering the incompleteness of not observing the whole galaxy.

NGC4639

NGC4639 is a barred spiral galaxy, observed face-on and fully observable in the WFPC2 field of view. This was the host galaxy of SN1990N. It has been observed over an interval of 71 days. Saha et al. (1997) discovered 18 definite and 6 likely cepheids and derived a distance modulus of 32.03 ± 0.22

No novae have been discovered in this galaxy. Considering the log of observations (see Table 2.6), the limiting magnitude (~ 29 mag), an average absolute magnitude at maximum of ~ -8 mag (corresponding to a rate of decline of ~ 0.1 mag day^{-1}), one obtains a GCT of 70 days. This leads to an upper limit on the nova rate of 50.84 novae yr^{-1}.

2.1.3 Summary and conclusions

The lack of detection is not detection of lack. As it is visible from Figure 2.5, the sample is just at the detection limit.

If the nova population was the same as in M47 (the galaxy studied by Ferrarese et al. 2003), I have shown to be able to identify $\sim$90% of novae. It is likely that nova populations are different. If the nova population is dominated by fast novae, objects may be gone undetected because of the large time spacing between most of the frames.

FILE	DATE-OBS	TIME-OBS
u2nu0101t_c0f.fits	1995-04-24	18:16:17
u2nu0102t_c0f.fits	1995-04-24	19:44:17
u2nu0201p_c0f.fits	1995-05-03	09:40:17
u2nu0202p_c0f.fits	1995-05-03	11:12:17
u2nu0301t_c0f.fits	1995-05-10	09:05:17
u2nu0302t_c0f.fits	1995-05-10	10:31:17
u2nu0401t_c0f.fits	1995-05-17	05:11:17
u2nu0402t_c0f.fits	1995-05-17	06:39:17
u2nu0501t_c0f.fits	1995-05-21	04:05:17
u2nu0502t_c0f.fits	1995-05-21	05:34:17
u2nu0601t_c0f.fits	1995-05-26	06:21:17
u2nu0602t_c0f.fits	1995-05-26	07:49:17
u2nu0701p_c0f.fits	1995-05-30	13:16:17
u2nu0702p_c0f.fits	1995-05-30	14:47:17
u2nu0801t_c0f.fits	1995-06-03	02:30:17
u2nu0802t_c0f.fits	1995-06-03	03:59:17
u2nu0901t_c0f.fits	1995-06-09	06:25:17
u2nu0902t_c0f.fits	1995-06-09	07:58:17
u2nu1001t_c0f.fits	1995-06-15	07:13:17
u2nu1002t_c0f.fits	1995-06-15	08:44:17
u2nu1101t_c0f.fits	1995-06-23	06:37:17
u2nu1102t_c0f.fits	1995-06-23	08:08:17
u2nu1201t_c0f.fits	1995-07-03	06:22:17
u2nu1202t_c0f.fits	1995-07-03	07:48:17

Table 2.6: *Log of observations of NGC4639*

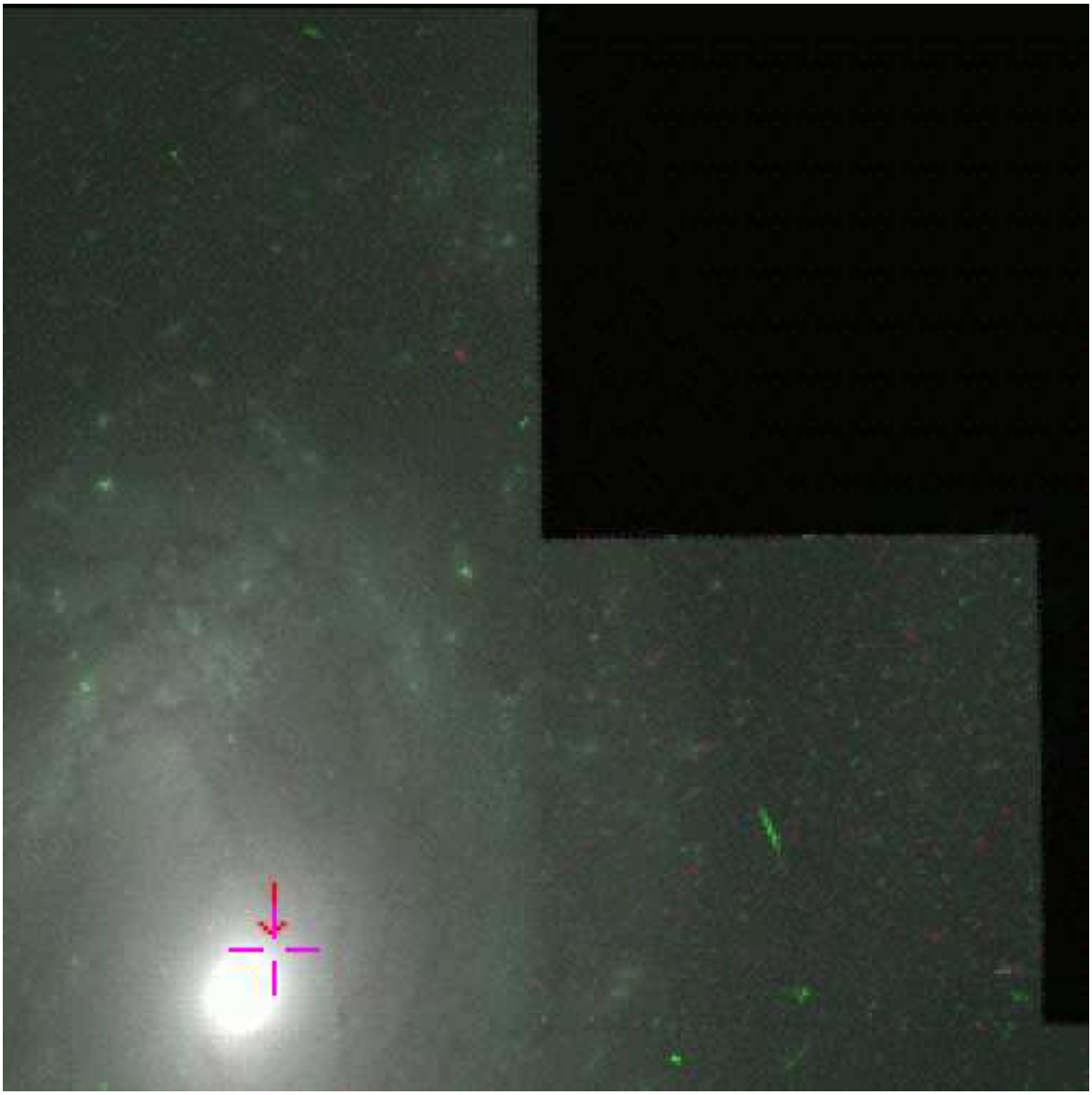

Figure 2.4: *HST image of NGC4639 obtained combining 555W and 814W frames*

2.2 The role of the environment on the nova rate in ellipticals

2.2.1 Introduction

Nobody has ever related novae and the radio emission of host galaxy, even though a few radio loud and radio quiet galaxies have already been studied. It has been shown by Della Valle et al. (2005) that the normalized Type Ia supernova rate for radio loud galaxies is higher than in radio quiet ones. Since the CN systems resemble the progenitors of SNe Ia in the so-called "single–degenerate scenario", it has been natural to observe two elliptical galaxies (a radio

loud and a radio quite) to try to increase the statistics in order to derive a hint whether there is some connection between the normalized nova rate and the radio emission of a galaxy or not.

2.2.2 Observations and data reduction

I observed two elliptical galaxies (NGC 4374 and NGC 4621) in the Virgo Cluster with FORS2 at the Very Large Telescope (VLT) at Cerro Paranal (Chile). Observations were possible because of the approval of the "service mode" proposal *"The influence of the environment on the rate of novae in early type galaxies"* (P.I. A.Ederoclite). The proposers asked to observe for 10 hours with the FORS2@UT2 (one of the four 8–m telescopes of the Very Large Telescope – VLT, at Cerro Paranal, Chile). This proposal was ranked B–queue and completely executed.[1] Observations were carried out in Bessell B, Bessell V and FORS2 Special R filter. Logs of the observations are given in Tab.2.9. Standard reduction was performed by the ESO Quality Control Group in Garching. Aperture photometry was carried out with the `DAOPHOT` package in `IRAF` [2]. Matching of photometric calatalogs and comparisons were performed in `IRAF` with `TTOOLS` in the `TABLES` package.

For a nova to be observed this far (my limiting magnitude on the best frames is $\sim$27), an absolute magnitude at maximum < -4 is required. According to Warner (1995), a very slow nova has a rate of decline of $\sim$0.013–0.008 mag d^{-1}. I used this extreme value to have a first rough way to discriminate between novae and other variables.

CNe have been identified by blinking by eye the images subtracted of the background obtained by application of a median filter (like in Della Valle & Gilmozzi 2002). The same technique has been extensively applied by Neill & Shara (2003) on novae in M81.

The nova rate has been derived via the "control time technique", first proposed by Zwicky (1942) and then adapted to the nova case by Capaccioli et al. (1989) and Shafter et al. (2000) (already reviewed in Section 2.1)

Given the time separation between observations, it is not possible to eliminate the effects

[1] "Service mode" observations are observations made by the Observatory which are executed following the instructions of the observer but without his/her physical presence at the telescope. Accepted proposals are ranked "A","B" or "C" with "A" being the highest priority.

[2] IRAF (Image Reduction Analysis Facility) is distributed by the National Optical Astronomy Observatories, which are operated by the Association of Universities for Research in Astronomy, Inc., under cooperative agreement with the National Science Foundation.

Nova	R.A.	δ
NGC 4374 #1	12:25:00.229	12:53:17.13
NGC 4374 #2	12:25:00.032	12:53:12.93
NGC 4374 #3	12:25:05.334	12:53:02.75
NGC 4621 #1	12:42:01.996	11:37:32.61
NGC 4621 #2	12:42:02.096	11:38:19.93

Table 2.7: *Coordinates of observed novae*

of short-time variables (such as flaring stars). Therefore my values for the nova rate can certainly be seen at least as upper-limits.

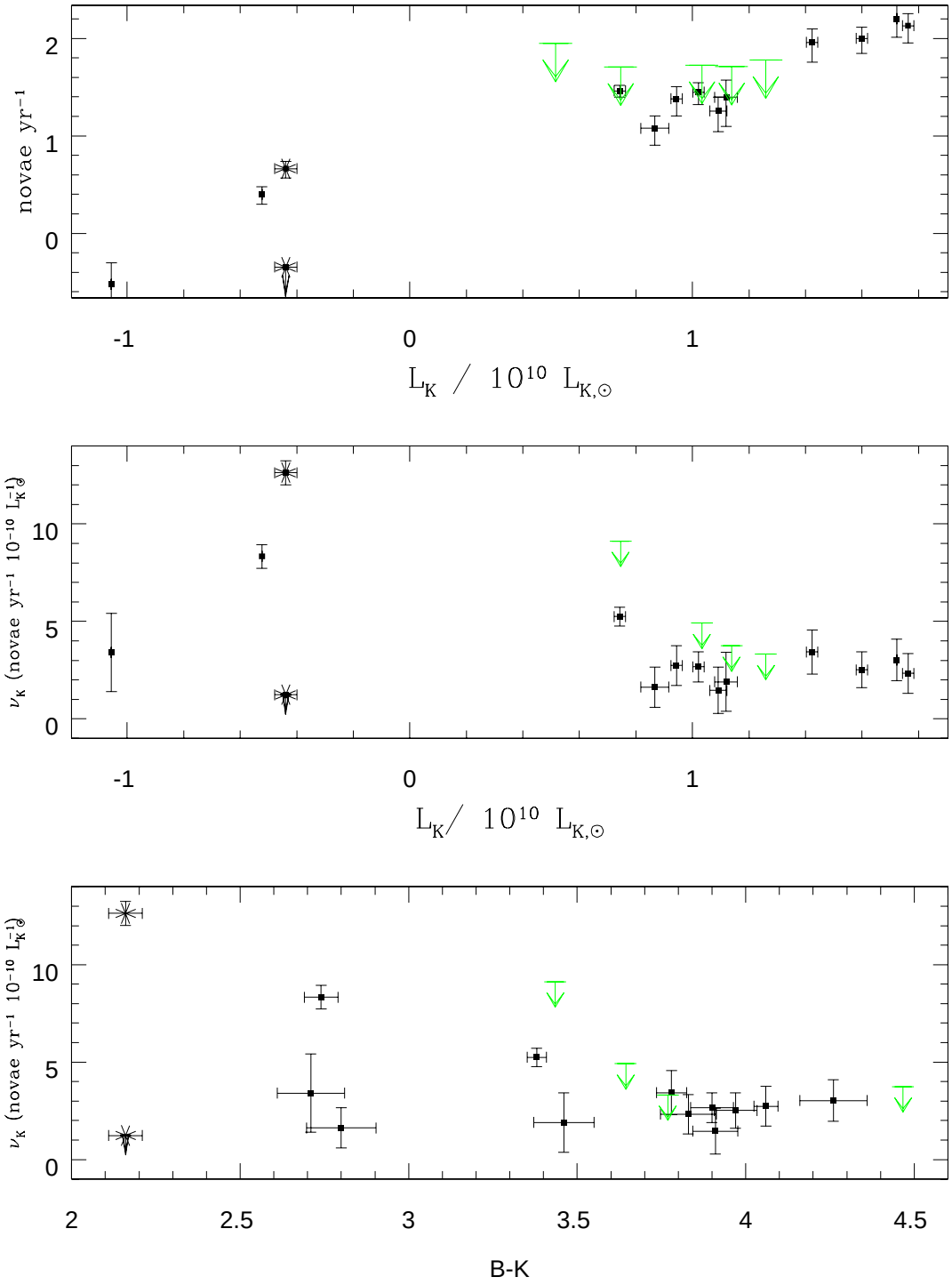

Figure 2.5: *Relations between the nova rate and photometric properties of the galaxy. Upper limits for the galaxies discussed in Section 2.1 are in green.* ***Upper panel*** *shows absolute nova rates vs K-band luminosity of the galaxy,* ***middle panel*** *shows specific nova rates vs k-band luminosity of the galaxy, and* ***lower panel*** *shows specific nova rates vs B-K color of the galaxy.*

Table 2.8: *Nova rates in galaxies from the literature. Galaxy type as from RC3 catalog. A_i and A_G are internal and galactic extinctions from RC3 catalog. Note that, for M33, I include both the value from Della Valle et al. (1994) and the upper limit from Sharov (1993) (points are marked with an asterisk)*

Name	Type	rate [a] (yr^{-1})	B [b] (mag)	K [c] (mag)	Radio Power (10^{29} ergs s^{-1} Hz^{-1})	A_i(mag)	A_g(mag)	m-M [d] (mag)
LMC	9	2.5 ± 0.5	0.91 ± 0.05	-1.83 ± 0.11	0.00	0.07	0.32	18.50 ± 0.13
SMC	9	0.3 ± 0.2	2.70 ± 0.10	-0.01 ± 0.10	0.00	0.24	0.13	18.99 ± 0.05
M33	6	4.6 ± 0.9	6.27 ± 0.03	4.11 ± 0.04	0.00	0.33	0.18	24.64 ± 0.09
		¡0.45						
M101	6	12 ± 4	8.31 ± 0.09	5.51 ± 0.05	0.53	0.05	0.04	29.34 ± 0.10
M51	4	18 ± 7	8.96 ± 0.06	5.05 ± 0.03	0.00	0.30	0.04	29.42 ± 0.27
M100	4	25 ± 12.5	10.05 ± 0.08	6.59 ± 0.04	1.01	0.1	0.11	31.04 ± 0.09
NGC3982	3	¡3	11.78 ± 0.16	8.85 ± 0.02	131.44	0.00	0.10	31.72 ± 0.14
M31	3	29 ± 4	4.36 ± 0.02	0.98 ± 0.02	0.00	0.67	0.35	24.42 ± 0.10
M81	2	24 ± 8	7.89 ± 0.03	3.83 ± 0.02	0.10	0.34	0.35	27.80 ± 0.08
NGC5128	-2	28 ± 7	7.84 ± 0.06	3.94 ± 0.02	0.00	0.00	0.50	28.12 ± 0.14
NGC1316	-2	135 ± 45	9.42 ± 0.08	5.59 ± 0.02	0.00	0.00	0.09	31.66 ± 0.17
M87	-4	91 ± 34	9.59 ± 0.04	5.81 ± 0.02	664.08	0.00	0.10	31.03 ± 0.16
VirgoEl	-4	160 ± 57	9.46 ± 0.10	5.20 ± 0.15	0.00	0.00	0.09	31.17 ± 0.09
M49	-5	100^{+35}_{-30}	9.37 ± 0.06	5.40 ± 0.03	0.95	0.00	0.09	31.06 ± 0.10
NGC 4374	-5	46 ± 27	10.09 ± 0.05	6.22 ± 0.02	18.08	0.00	0.013	31.72
NGC 4621	-5	39 ± 27	10.57 ± 0.06	6.75 ± 0.03	1.43	0.00	0.07	31.5

[a]Nova rate references: LMC (Capaccioli 1990); SMC (Graham 1979); M 33 (Della Valle et al. 1994), (Sharov 1993) ; M 101, M 51 (Shafter et al. 2000) ; M 100 (Ferrarese et al. 1996); M 31(Capaccioli et al. 1989); M81 (Moses & Shafter 1993); NGC 5128 (Ciardullo et al. 1990); NGC1316(Della Valle & Gilmozzi 2002); M87(Shafter et al. 2000); Virgo(Pritchet & van den Bergh 1987); M49(Ferrarese et al. 2003) ; NGC3982 (Ederoclite et al. 2004)

[b]from the NASA Extragalactic Database (NED)

[c]from K2MASS (with the exception of the Magellanic Clouds and the "Virgo Ellipticals", whose K-band magnitudes come from Shafter et al. (2000))

[d]Distance modulus references: LMC, SMC, M33, M101, M31, M81, and M100 are from Ferrarese et al. (2000), M51, NGC5128, NGC1316, M87, M49, and Virgo are from Tonry et al. (2001), NGC3982 is from Saha et al. (2001)

date	galaxy	Exposure Time (seconds)	seeing (pixels)
2005-04-13	NGC 4374	9×125,9×125,12×66	3.5 , 3.7 , 3.7
2005-04-13	NGC 4621	9×125,9×125,12×66	3.1,2.75,2.8
2005-04-14	NGC4373	9×125,9×125,12×66	3.4 , 3.4 , 2.9
2005-04-30	NGC 4374	9×125,9×125,12×66	4.7 , 4.3 , 3.2
2005-05-08	NGC 4621	9×125,9×125,12×66	...
2005-05-11	NGC 4621	9×125,9×125,12×66	3.1 , 3.2 , 2.8
2004-06-10	NGC 4374	9×125,9×125,12×66	3.5 , 3.5 , 4.0

Table 2.9: *Log of observations for NGC 4374 and NGC 4621. Scale of FORS2 CCD is 0.126arcsec/pixel*

2.2.3 The nova rate

I find 3 ± 1.7 novae in NGC 4374 and $2^{+1.4}_{-1.4}$ novae in NGC 4621. Adopting a control time of 23.67 days and 19 days for NGC 4374 and NGC 4621, respectively I find that the nova rate is 46 ± 27 novae yr^{-1} and 38 ± 27 novae yr^{-1} for NGC 4374 and NGC 4621, respectively.

Nova rates for other galaxies are available in literature (see Tab.2.8).

Given the K-band luminosity of the galaxies I find that the nova rates determined for NGC 4374 and NGC 4621 are in good agreement with the host galaxy mass – nova rate relation.

I also find no evidence of a clear overabundance of novae in the radio loud galaxy. Figure 2.8 shows that there is no clear indication of an enhanced normalized nova rate.

If there is no difference between the nova rate in radio loud and radio quiet galaxies, this means that the overproduction of SNeIa in radio loud galaxies can be explained by either production of SNIa via the "double-degenerate" scenario or assuming that CNe and SNeIa are produced by different stellar populations.

2.2.4 Summary

The nova rate for two elliptical galaxies whose nova rate were previously unknown are determined. I obtain 46 ± 27 novae yr^{-1} and 38 ± 27 novae yr^{-1}, for NGC 4374 and NGC 4621, respectively.

I compare these results with the previously known nova rates. My results confirm the

nova rate – galaxy mass relation and the possible existence of a universal normalized nova rate.

A universal normalized nova rate implies that there is no enhancement for radio-loud galaxies with respect to radio-quite ones, as observed for SNeIa. I propose that this is due to either different types of progenitors (i.e. "double–degenerate" systems for SNeIa) or to two different stellar populations having different mass–distributions of WDs.

2.3 The theoretical nova rate in ellipticals

I have followed Matteucci et al. (2003) to compute the nova rate in NGC 4374 and NGC 4621. I make use of a model that follows the chemical evolution of an elliptical galaxy of a given mass, effective radius and star formation efficiency. The use of such a code gives us the possibility of putting constraints on the number of binary system that can give rise to a CN explosion and/or the time between two explosions in a single system.

2.3.1 The model

The physical properties of elliptical galaxies cover an enormous range. Their absolute B magnitudes go from -8 to less than -23, their masses vary from as little as $10^7 M_\odot$ to nearly $10^{13} M_\odot$, and their diameters can be as small as a few tenths of a kiloparsec to as large as hundreds of kiloparsecs.

Elliptical galaxies apparently show a "fundamental plane" defined by central velocity dispersion σ_0, surface brightness and effective radius (or half–light radius) R_{eff}. The existence of the "fundamental plane" is still debated.

For the modeling of elliptical galaxies I make use of the model proposed by Matteucci et al. (1998), Here I focus on a model that takes into account a single zone interstellar medium with instantaneous mixing of gas.

The present model considers a monolithic collapse scenario. In this framework, ellipticals are assumed to have formed at high redshift as a result of a rapid collapse of a gas cloud. This gas is then rapidly converted into stars by means of a very strong burst, followed by a galactic wind powered by the energy injected into the interstellar medium (ISM) by supernovae and stellar winds. The wind carries out the residual gas from the galaxies, thus inhibiting further star formation.

A model which aims to describe the chemical evolution of a galaxy needs the following ingredients:

- initial conditions (gas content, metallicity)
- the stellar birthrate function
- stellar evolution and nucleosynthesis
- supplementary parameters such as infall of extragalactic gas, radial flows and galactic winds

The stellar birthrate of a stellar population is usually written as:

$$B(m,t) = \psi(t)\phi(m) \tag{2.1}$$

where $\psi(t)$ is the star formation rate and $\phi(m)$ is the initial mass function (IMF).

The IMF is usually considered constant in time and space. Various parametrizations are available for it. It is usually written in the form:

$$\phi(m) = am^{-(1+x)} \tag{2.2}$$

I used Salpeter's (1955) slope ($x = 1.35$). The normalization is obtained by

$$\int_{0.1}^{100} m\phi(m)dm = 1 \quad .$$

The fundamental equations of chemical evolution can be written as:

$$\begin{aligned}\frac{dG_i(t)}{dt} = &-\psi(t)X_i(t) + \int_{M_{\rm L}}^{M_{\rm Bm}} \psi(t-\tau_m)Q_{mi}(t-\tau_m)\phi(m)\mathrm{d}m \\ &+A\int_{M_{\rm Bm}}^{M_{\rm BM}} \phi(m)\left[\int_{\mu_{\min}}^{0.5} f(\mu)\psi(t-\tau_{m2})Q_{mi}(t-\tau_{m2})\mathrm{d}\mu\right]\mathrm{d}m \\ &+(1-A)\int_{M_{\rm Bm}}^{M_{\rm BM}} \psi(t-\tau_m)Q_{mi}(t-\tau_m)\phi(m)\mathrm{d}m \\ &+\int_{M_{\rm BM}}^{M_{\rm U}} \psi(t-\tau_m)Q_{mi}(t-\tau_m)\phi(m)\mathrm{d}m,\end{aligned} \tag{2.3}$$

where $G_i(t) = \rho_{\rm gas}(t)X_i(t)/\rho(0)$ is the volume gas density in the form of an element i normalized to the initial total volume gas density. The quantity $X_i(t)$ represents the abundance by mass of an element i and by definition the summation over all the elements present in the gas mixture is equal to unity.

The various integrals in equation 2.3 represent the rates at which SNe (I and II) as well as single low and intermediate mass stars and single massive stars restore their processed and unprocessed material into the ISM (for a detailed description of the integrals see Matteucci & Greggio 1986). I only remind here that the quantity Q_{mi} represents the fraction of a star of mass m which is restored in to the ISM in the form of an element i and therefore contains the nucleosynthesis prescriptions that I assume to be the same as in Matteucci & Greggio (1986).

The star formation rate $\psi(t)$ is given by:

$$\psi(t) = \nu\rho_{\rm gas}(t)/\rho(0). \tag{2.4}$$

i.e. normalized to the initial total volume density. $\psi(t)$ is assumed to drop to zero at the onset of the galactic wind. The quantity ν is expressed in units of $\rm Gyr^{-1}$ and represents the efficiency of star formation, namely the inverse of the time scale of star formation.

Therefore, the star formation rate in these galaxies can be considered as a strong burst which does not last more than 1 Gyr and is shorter in more massive systems. This is obtained by assuming that the star formation efficiency increases with galactic mass thus producing an " inverse wind" effect, as described in Matteucci (1994) As a consequence of this, the star formation period is longer in smaller systems thus allowing the SNe Ia to substantially pollute the ISM. This effect can explain the observed increase of the [α/Fe] ratio with galactic mass (Matteucci 1994, Worthey et al. 1992). The galactic wind develops as a consequence of the energy transfer from SNe into the ISM. In fact, when the thermal energy of the gas becomes larger than the binding energy of the gas, the wind starts (Arimoto & Yoshii 1987, Matteucci 1992, 1994, Matteucci & Tornambé 1987, Pipino et al. 2002). In order to compute the binding energy of the gas some assumptions have to be made about the galactic potential well. In particular, it is assumed that all ellipticals possess heavy but diffuse dark matter halos; a ratio between the half-light radius and the radius of the dark matter core $R_{luminous}/R_{dark}$=0.10 and a ratio dark to luminous mass of 10 are assumed.

The white-dwarf birthrate at a certain time is given by the deathrate at that time of stars with masses below $8M_{\odot}$ (and above $0.8M_{\odot}$ since these stars live as long as the Universe):

$$R_{WD}(t) = \int_{0.8}^{8.0} \psi(t-\tau_m)\phi(m)dm \tag{2.5}$$

where τ_m is the lifetime of a star of mass m. The hypothesis done by D'Antona & Matteucci (1991) is that a fraction α of white dwarfs are in binary systems such that a CN outburst

is possible. A CN outburst is possible only after matter is accreted onto the surface of the white dwarf. The time needed for this amount of matter to accrete is called Δt (a value of $\Delta t = 2$ Gyrs will be used in the following, as from Romano et al. 1999, 2001). With these assumptions, the CN rate is given by:

$$R_{\rm novae} = \alpha \int_{0.8}^{8.0} \psi(t - \tau_m - \Delta t)\phi(m)dm \tag{2.6}$$

The number of observed outbursts is related to the rate of formation of nova systems R_{novae} as $R_{\rm outbursts} = nR_{\rm novae}$, where n ($\sim 10^4$) is the average number of nova outbursts for a typical nova system (Bath & Shaviv 1976, Ford 1978, Shara et al. 1986). This number, which is just an average value, is inversely proportional to the recurrence time. The parameter α, which here is assumed to be constant in time and space, has been fixed in analogy with the same model for the Milky Way (Matteucci et al. 2003, Romano et al. 1999). It is clear from Equation 2.6, that parameters α and n cannot be studied independently.

Matteucci et al. (2003) noticed that, assuming $\alpha = 0.01$ and $n = 10^4$, the nova rates are about a factor 3–10 larger than it is derived from observations. If these values were realistic, the discrepancy could be partially due to an observational bias affecting the ground based nova surveys due to poor spatial resolution and bright limiting magnitude. An indication in this direction comes from the nova rate of M87 recently provided by Shara & Zurek (2002) on the basis of HST archive images, which is a factor 2–3 larger than previous ground-based estimates. Another possibility is that in early type galaxies the recurrence time between two consecutive nova explosions is considerably longer than in late spirals as a consequence of the different stellar population from which novae originate. This suggestion is supported both by observational and theoretical grounds. From one side Duerbeck (1990) and Della Valle et al. (1992, 1994) have demonstrated, on the basis of galactic and extragalactic nova observations, the existence of two populations of novae: fast and bright novae belonging to 'disk' stellar population and slow and faint novae which originate from a 'bulge' stellar population. In particular, the latter authors (see also DellaValle & Livio 1998) suggested that bulge novae could originate from relatively light WDs, likely in the range of masses of $\langle M_{WD}\rangle \leq 0.9 M_\odot$ while novae in the disk arise from massive WDs ($\langle M_{WD}\rangle \geq 1 M_\odot$). From the other side, Truran (1990, see also Ritter et al. 1991) has found that the mass of the WD and the recurrence time between the outbursts are inversely proportional. In order to match the 'theoretical' with 'empirical' rates, one needs to lower either α or n or both. For example for M87 the match between predicted and observed rates can be achieved by increasing the

recurrence time between two consecutive outbursts, to $T_r \sim 3 - 1 \cdot 10^5$ yr. This is about 10–3 times larger than assumed for novae in the 'disk' of the Galaxy. In this way, the prediction of models from Matteucci et al. (2003), for a luminous mass in the range 4-6 $\cdot 10^{11} M_\odot$ are in very good agreement with the preliminary new estimate from Shara & Zurek (2002) of the nova rate for M87. In fact, M87 can be modeled both as an elliptical galaxy with luminous mass $\sim 4 \cdot 10^{11}\ M_\odot$ and $R_{eff} \sim 6$ kpc or with luminous mass $\sim 6 \cdot 10^{11}\ M_\odot$ and $R_{eff} \sim 7$ kpc (Cohen & Ryzhov 1997). The predictions of these two models do not differ much and both of them can well represent M87. Another possibility is to adopt a fraction of binary systems giving rise to novae smaller than 0.01. Unfortunately, if from one side this value is justified for the Milky Way because this α gives both the observed present time Galactic rate and the correct yields of Lithium and CNO isotopes (see Romano & Matteucci 2003), on the other side, we completely lack this information for ellipticals.

2.3.2 Model results

Mass and luminosity

The mass of the galaxies has been estimated using the relation between the mass of the galaxy, its K-band luminosity and its $B - K$ color from Mannucci et al. (2005)

$$\log \frac{M/L_K}{M_\odot/L_{K,\odot}} = 0.212 \times (B - K) - 0.959 \quad , \tag{2.7}$$

therefore

$$M/M_\odot = L_K/L_{K,\odot} \times 10^{(0.212 \times (B-K) - 0.959)} \quad . \tag{2.8}$$

From the numbers in Table 2.8 I find masses of $8.28 \times 10^{10} M_\odot$ and $2.29 \times 10^{11} M_\odot$ for NGC 4621 and NGC 4374, respectively.

From the RC3 catalog (de Vaucouleurs et al. 1991), I find effective radii of 3.12 kpc and 5.19 kpc for NGC 4621 and NGC 4374, respectively.

Adopting the photometric code by Bruzual & Charlot (2003), I predicted K- and B-band luminosity. This is not a closed loop (deriving the mass from the K-band luminosity and the K-band luminosity from the mass) because the mass is derived as described above and the luminosities are derived from stellar population considerations. The code by Bruzual & Charlot (2003) convolves the spectra of single stellar population, with given metallicity and

parameter	NGC 4374	NGC 4621
Mass ($M_\odot$)	2.29E11	8.28E10
$R_{\rm eff}$ (kpc)	5.19E13	3.12E10
ν(Gyr^{-1})	13	10.5

Table 2.10: *Input parameters for the chemical evolution model*

parameter	NGC 4374 (model)	NGC 4374 (observations)	NGC 621 (model)	NGC 4621 (observations)
<Fe>	2.98	2.54 ± 0.11	3.25	3.17 ± 0.10
Mg_2	0.264	0.295 ± 0.004	0.293	0.360 ± 0.003
K-Luminosity ($10^{10}L_\odot$)	30.96	33.39	11.13	6.67
B-Luminosity ($10^{10}L_\odot$)	5.11	6.66	2.00	2.38
$B-K$	3.96	3.87	3.87	3.82
nova rate (yr−1)	57.9	46 ± 27	19.4	28 ± 27
norm. nova rate	1.79	1.4	1.5	4.20
SNeIa rate (0.01 yr^{-1})	0.744	–	0.326	–
SNu_K	0.024	–	0.028	–
SNu_M	0.037	–	0.016	–

Table 2.11: *Observables for the chemical evolution model*

IMF, and produces integrated broad band colors of galaxies. It can be seen from Table 2.11 that luminosities are in very good agreement with observations. The $B-K$ color is in very good agreement as well. In Figure 2.9, I show an attempt to follow the evolution of the K–luminosity and $B-K$ color of the modeled galaxies through their history.

The nova rate predicted by the model, assuming $n\alpha = 10$, is 57.9 novae yr^{-1} for NGC 4374 and 19.4 novae yr^{-1} for NGC 4621, respectively, leading to a normalized nova rate of 1.79 novae yr^{-1} $10^{-10}L_{K,\odot}^{-1}$ and 1.5 novae yr^{-1} $10^{-10}L_{K,\odot}^{-1}$. The predicted ν_K is in very good agreement both with observations and with the "universal value" (1.85±0.16 yr$^{-1}10^{-10}L_{K,\odot}$) suggested by several authors (Ferrarese et al. 2003). Upper panels of Figure 2.10 show the evolution of the CN rate through the history of the modeled galaxies. The Δt period during which no CN outburst occurs is clearly visible but the system is still accreting matter and a constant decrease in the last 8 Gyrs. The history of the normalized nova rate is shown in the lower panel of Figure 2.10. It is worth noting that the "universal value" of 1.5 novae yr$^{-1}10^{-10}L_{K,\odot}^{-1}$ has been achieved 5 Gyrs ago and does not seem to be constant in time.

The SN Ia rate per unit mass is 0.014 and 0.019 for NGC 4374 and NGC 4621, respectively. This is in good agreement with the estimates for elliptical galaxies and with galaxies with

$B-K$ colors of ∼3.5–4.5 mag reported by Mannucci et al. (2005). The history of the SN Ia rate is shown in the upper panels of Figure 2.11. Both galaxies show a peak soon after the formation of the galaxy. The evolution of the SN Ia rate in unit of K-luminosity is shown in the lower panels of Figure 2.11.

Metallicity and Lick indices

After two decades of observations with the Intermediate Dispersion Spectrograph (IDS) at Lick Observatory, Faber et al. (1985) and Burstein et al. (1986) defined and measured 11 absorption feature indices for 147 K-giant field and cluster stars. These indices constitute the "Lick/IDS" system.

Gorgas et al. (1993) adopted polynomial fitting functions to specify the behavior of the 11 Lick features as functions of $V-K$ color (the temperature indicator), $\log g$, and [Fe/H]. These fitting functions are easy to use to construct stellar population models of integrated stellar populations (Worthey 1992, 1994). These functions can be inverted and used, once one assumes to know the age and metallicity of a stellar population, to predict the Lick indices. Although these indices are widely used to derive ages and metallicities of galaxies, several criticisms have been expressed with regard to them. I decided to use these indices anyway; although they may not be 100% safe, they surely represent a good first order solution.

The need of using these indices arises from the fact that individual stars cannot be observed in distant galaxies and therefore one has to deal with the spectrum of the whole galaxy that is the convolution of all the spectra of stars of the galaxy. Uncertainties on the calibration of this system of indicators originate in the characteristics of spectra of individual stellar population.

Comparison between observations (Kuntschner et al. 2001) and this model are reported in Table 2.11 (the Lick indices <Fe> and Mg_2 are derived from a fit to Worthey 1994). A simple stellar population (see Pipino & Matteucci 2004) predicts average abundances on stellar populations [Fe/H] 0.159 and 0.04 for NGC 4621 and NGC 4374, respectively. [Mg/H] is 0.17 and 0.12 for NGC 4621 and NGC 4374, respectively. From an inspection of Table 2.11, it can be seen that the Mg_2 index is underestimated for NGC 4621. It is notable that I manage to reproduce pretty well these indicators of the chemistry, even though I do not attempt any fine–tuning of the parameters.

2.3.3 Comments

The theoretical modeling of the observed galaxies lead to a pretty good reproduction (without the fine-tuning of any of the three free parameters) of both the photometric and chemical properties of the observed galaxies as well as their SN Ia rates. In spite of this reproducing ability, one could ask if this modeling can put constraints on the αn product.

The nova rate is "tuned" by adopting a value for the αn combination. This can be done, as mentioned above, to either one of the parameters or both. The $n\alpha$ value that best fits the data is 10. This can be achieved by assuming $\alpha = 0.01$ (the same value as for the Milky Way, as mentioned above) and, therefore, $n = 10^3$. This would lead to $T_r \sim 10^5$yr. This result is in good agreement with the estimate (derived on the same grounds as this one) for M87 by Matteucci et al. (2003) and the hibernation scenario (derived on completely other grounds by Shara et al. 1986, see Section 1.6).

nova NGC 4374 # 1

B filter

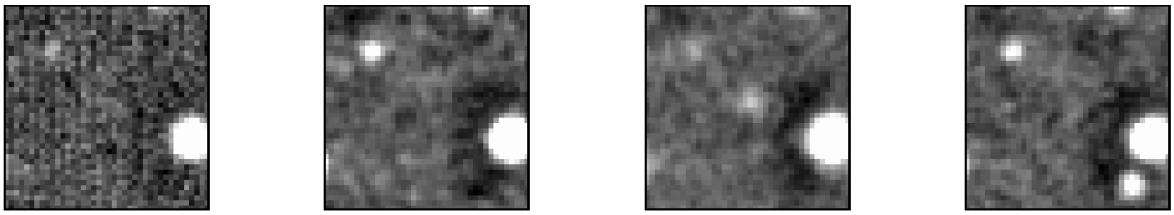

V filter

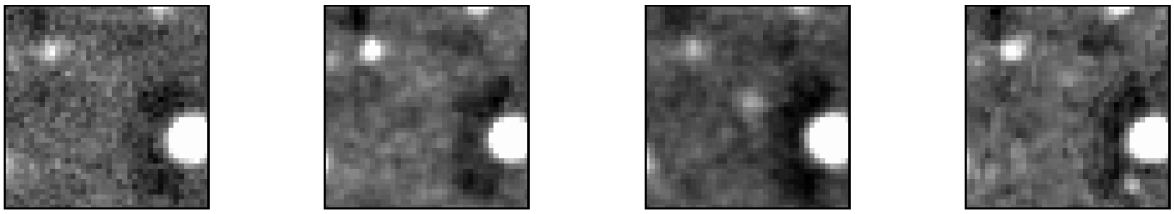

R filter

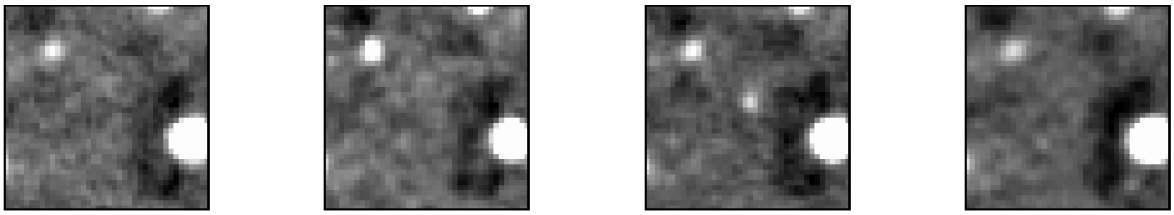

nova NGC4374 # 2

B filter

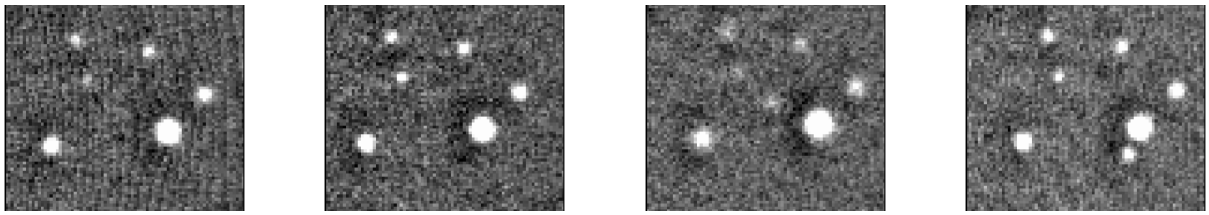

V filter

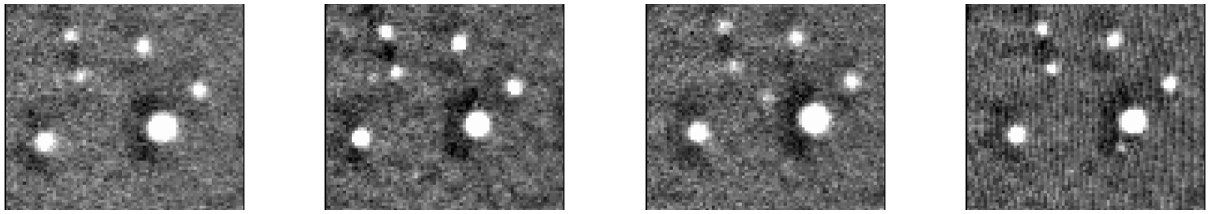

R filter

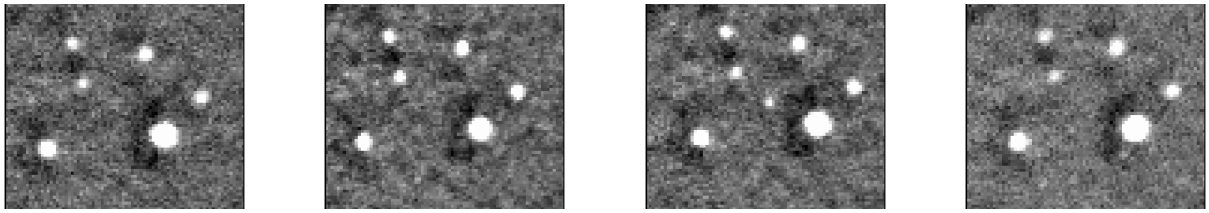

nova NGC 4374 # 3

B filter

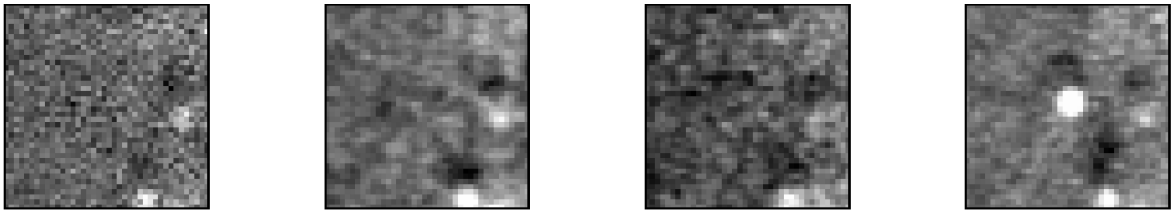

V filter

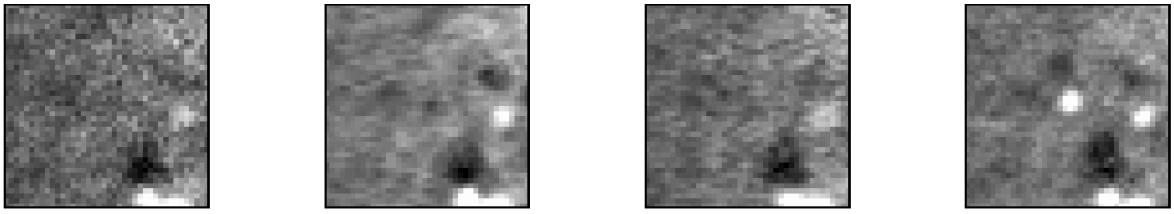

R filter

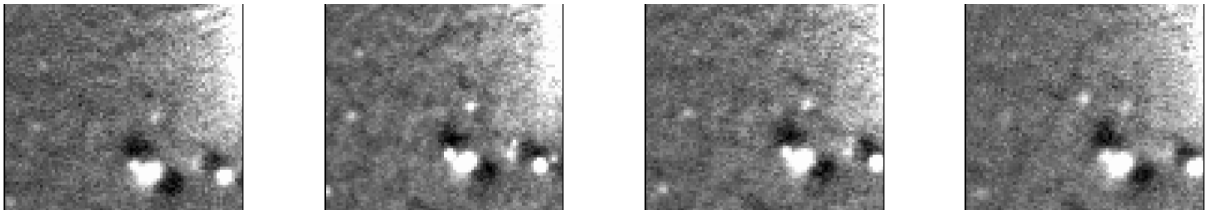

nova NGC 4621 # 1

B filter

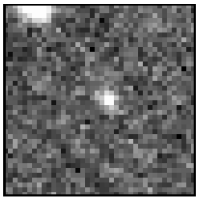
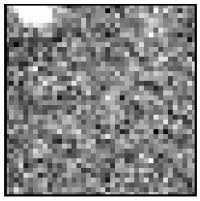

V filter

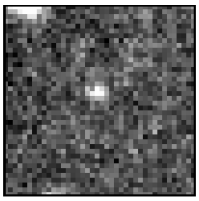
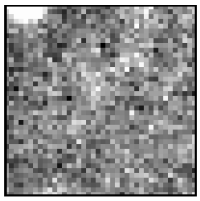

R filter

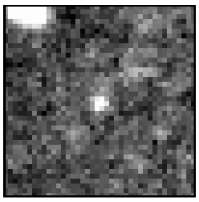
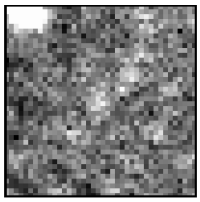

nova BGC4621 # 2

B filter

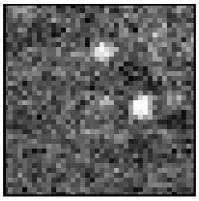
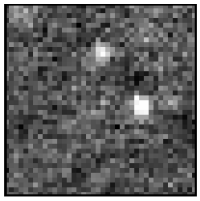

V filter

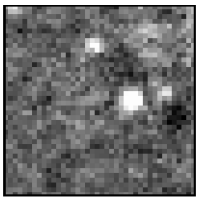
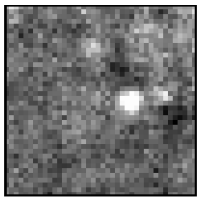

R filter

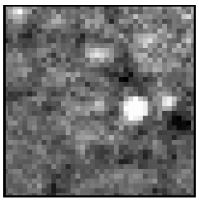
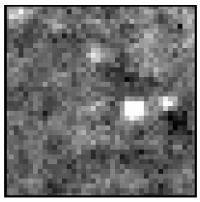

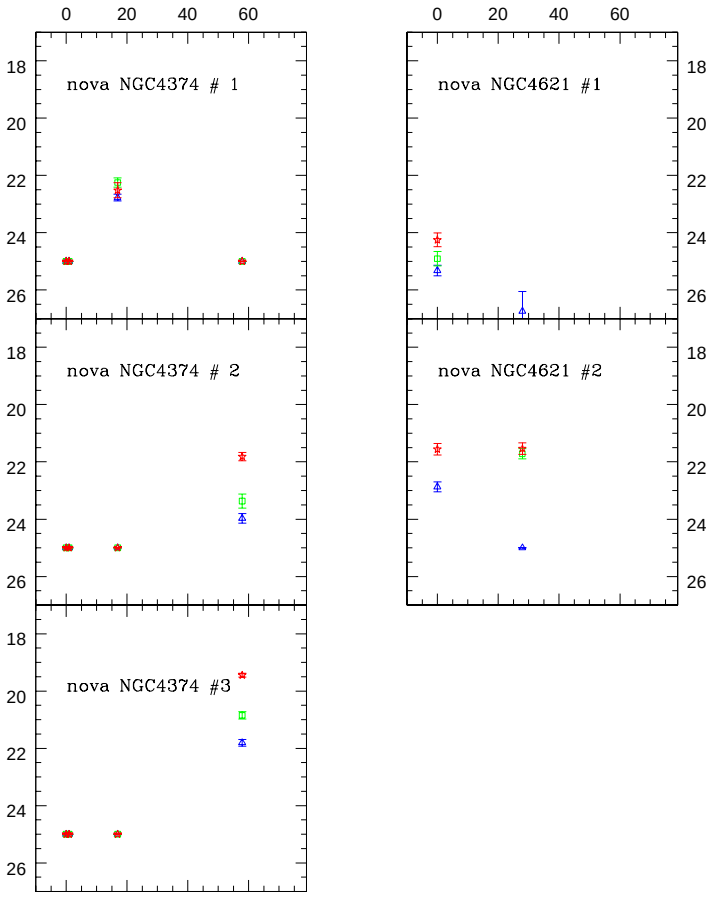

Figure 2.6: *Light curves of novae discovered in NGC 4374 and NGC 4621*

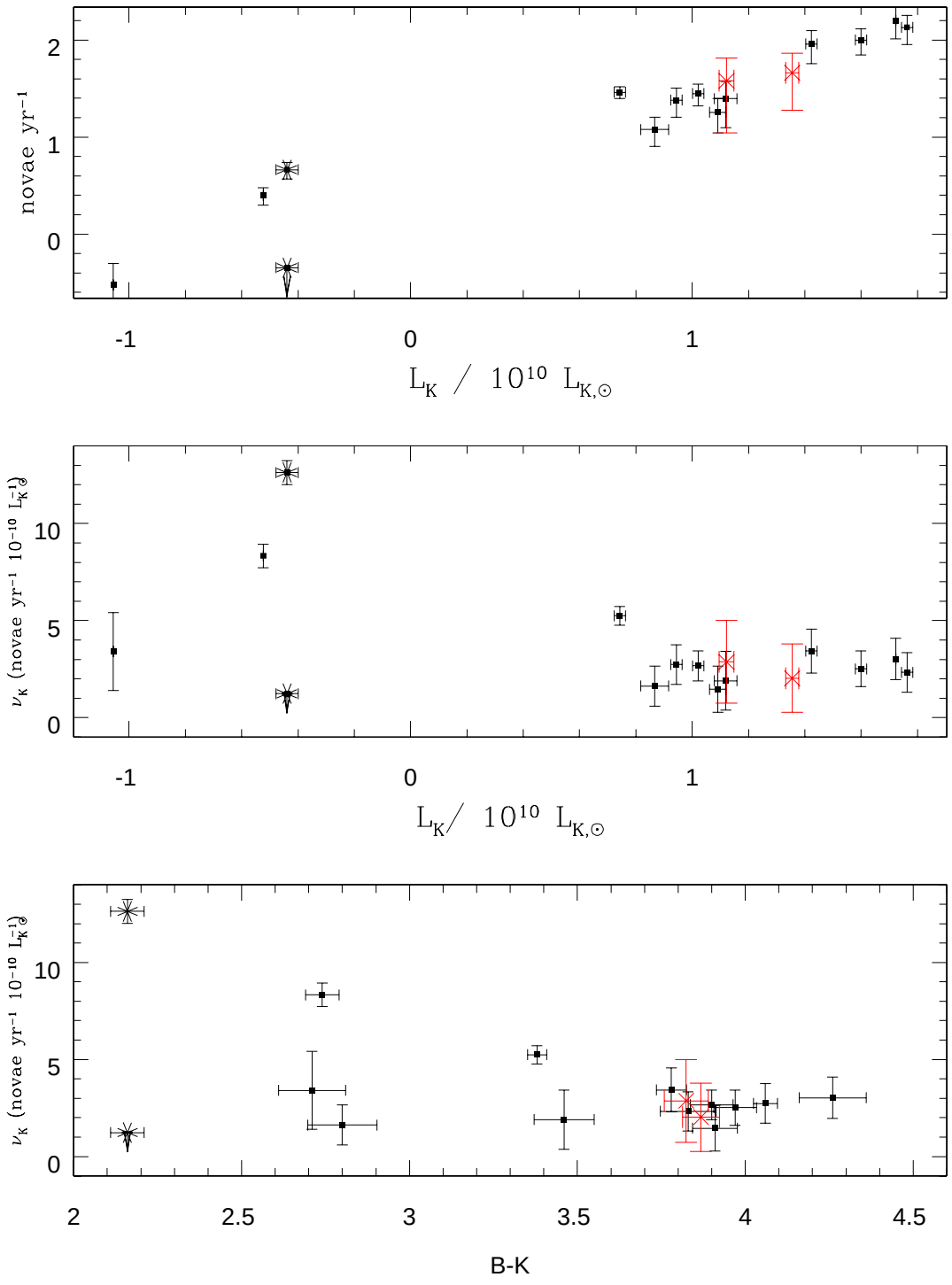

Figure 2.7: *Comparison of the properties of the nova rate of NGC 4374 and NGC 4621 (red crosses) with nova rates of other galaxies from the literature.* **Upper panel** *shows the nova rate vs the K-band luminosity of the galaxy.* **Middle panel** *shows the normalized nova rate vs the K-band luminosity of the galaxy.* **Lower panel** *shows the normalized nova rate vs the $B-K$ color of the galaxy.*

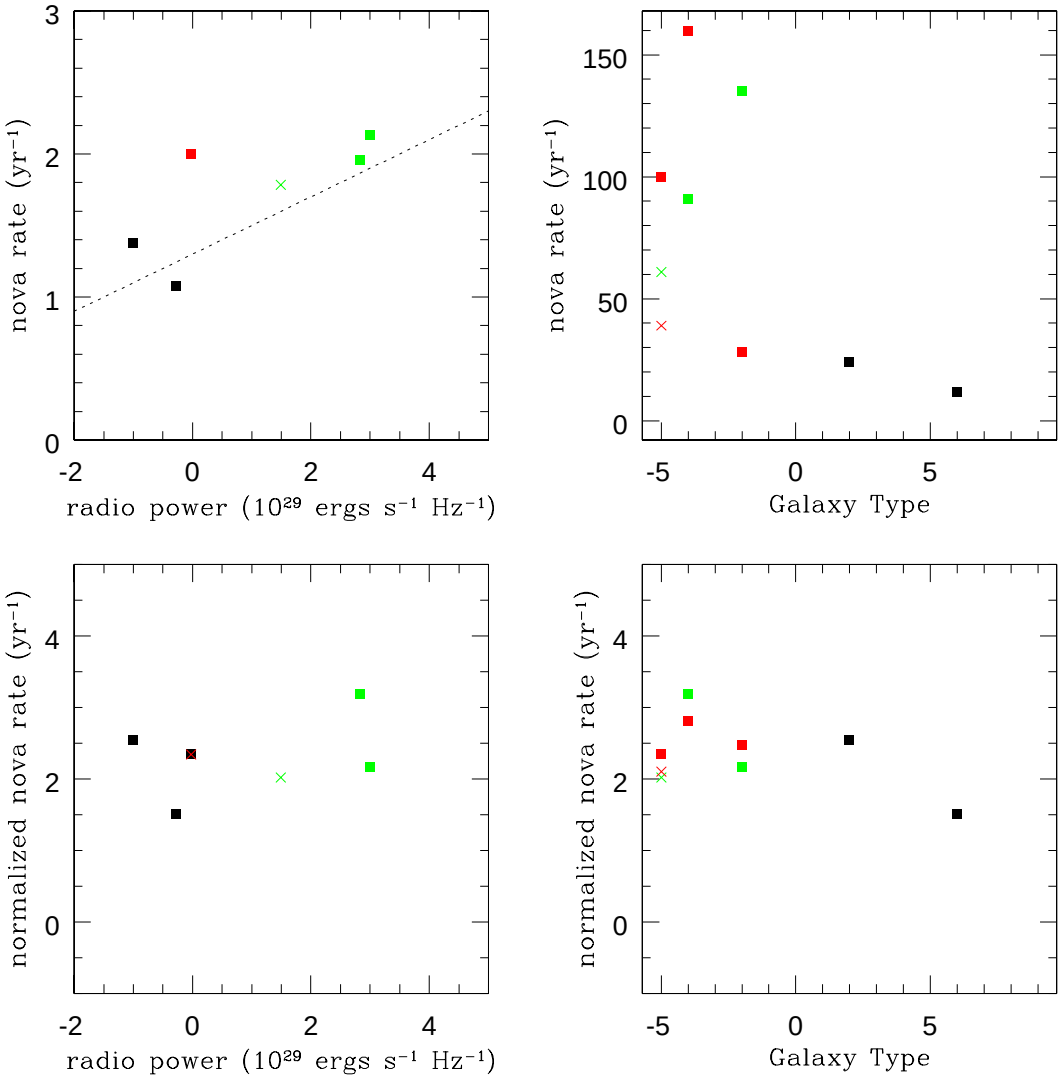

Figure 2.8: *Comparison of the properties of the nova rate of NGC 4374 and NGC 4621 (marked by the crosses) with other galaxies in the literature.* **Upper left corner** *shows the nova rate vs the Radio Power of the galaxy. The red dots refer to radio quite ellipticals and green dots to radio loud ones.* **Upper right corner** *shows the nova rate vs the galaxy type.* **Lower left corner** *shows the normalized nova rate vs the Radio Power of the galaxy.* **Lower right corner** *shows the normalized nova rate vs the Galaxy type.*

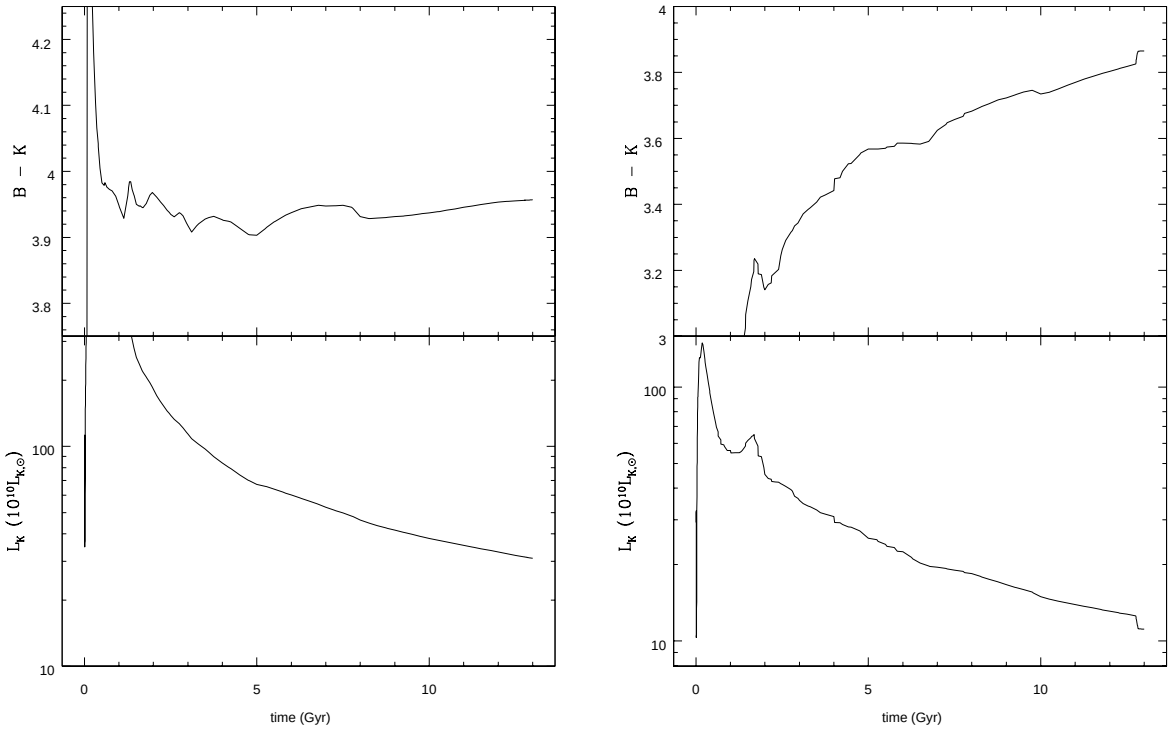

(a) NGC4374 (b) NGC4621

Figure 2.9: *Evolution of the $B-K$ color and K-band luminosity.*

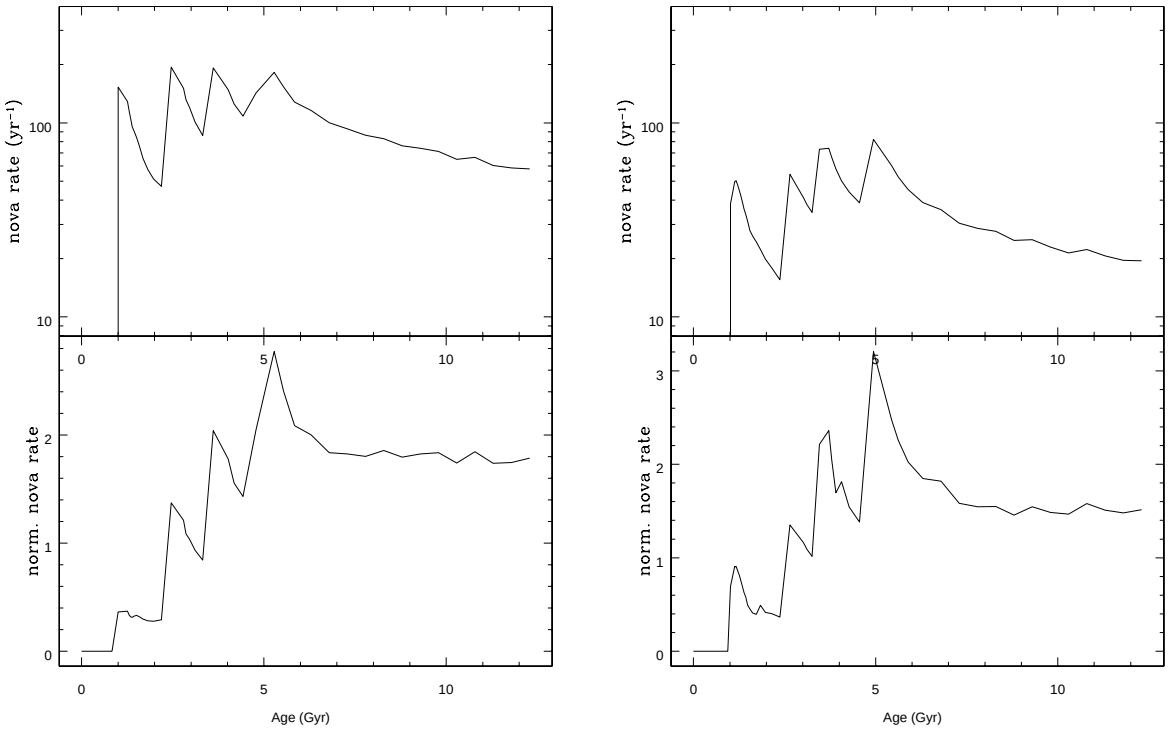

(a) NGC4374 (b) NGC4621

Figure 2.10: *Evolution of the nova rate and normalized nova rate.*

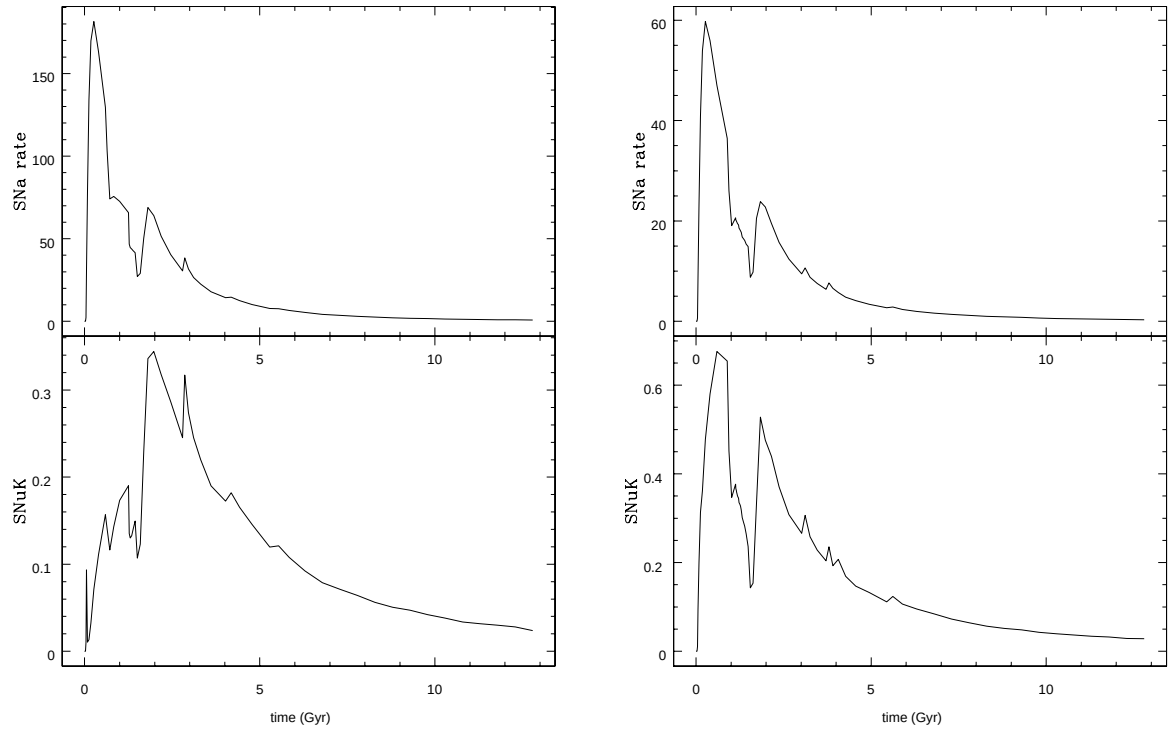

(a) NGC4374 (b) NGC4621

Figure 2.11: *Evolution of the rate of SNe Ia.*

Chapter 3

Galactic novae

3.1 Nova Sgr 2004: multi band observations

3.1.1 Introduction

Nova Sgr 2004 (= V5114 Sgr) was discovered by Nishimura et al. (2004). The same authors provided precise coordinates R.A. = $18^h19^m32^s.29$, Decl. = $-28°36'35".7$ (gal. coord. $l = 3°.9$ $b = -6.°.3$). Early spectroscopy on Mar 18.3 UT by Della Valle et al. (IAUC 8307) confirmed this object to be a classical nova. Here, I present photometric and spectroscopic observations taken at McDonald Observatory, Cerro Tololo Inter–American Observatory (CTIO), ESO-La Silla, and Lick Observatory. The spectra from ESO-LaSilla have been obtained as part of the Target of Opportunity campaign for the observation of Classical Novae in the Galaxy and in the Magellanic Clouds.

3.1.2 Observations and data reduction

Optical photometry has been carried out in 8 nights between March and April 2004 with the 0.8m telescope at McDonald Observatory. Another observing run has been carried out in 14 nights between June and July with the Small and Moderate Aperture Research Telescope System (SMARTS) 1.0m telescope at CTIO. Optical and infrared photometry has been also carried out with the ANDICAM dual-channel imager on the SMARTS 1.3m at CTIO during 25 nights between March and August. A log of photometric observations is given in Table 3.1.

Spectra at maximum and during the early decline have been obtained with FEROS

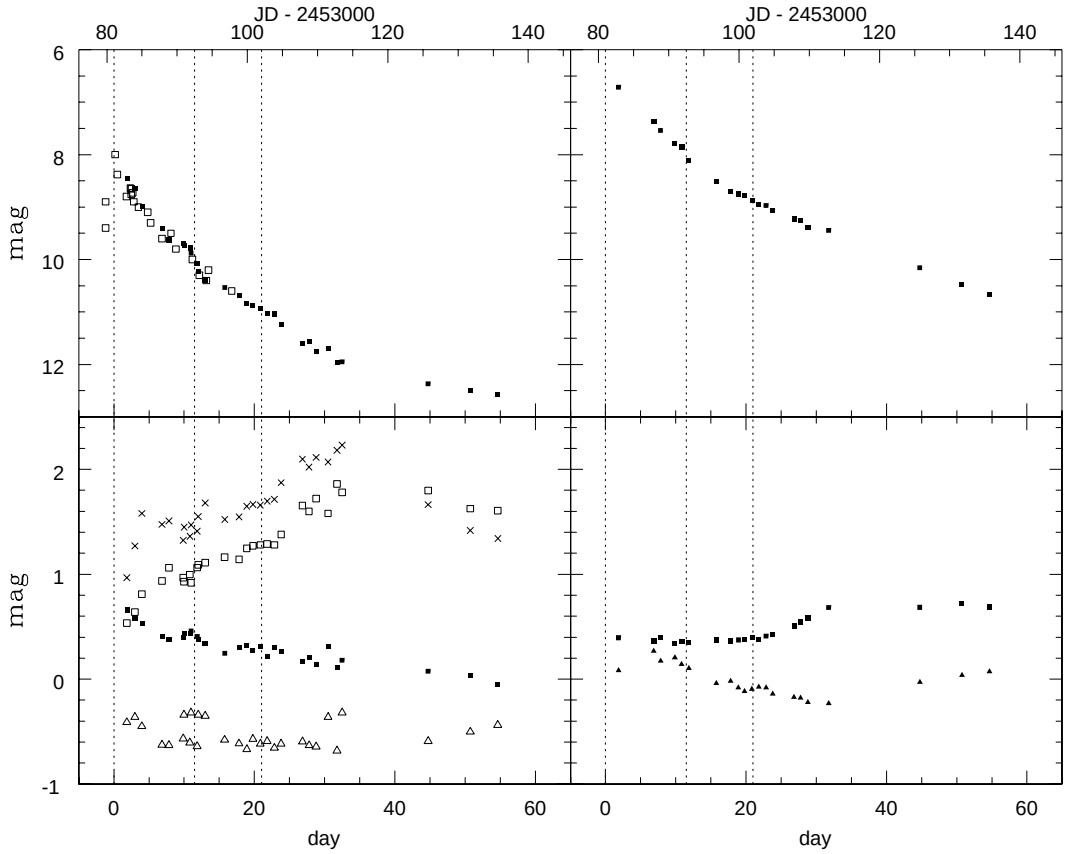

Figure 3.1: ***Upper left panel*** *V band light curve. Filled symbols represent my data points, empty symbols represent IAUC data. Vertical dotted lines represent maximum light, t_2, and t_3. Data points are affected by errors $\lesssim 0.04$ mag.* ***Lower left panel*** *Evolution of different colors: filled squares represent $B-V$, empty triangles $U-B$, crosses $V-I$ and empty squares $V-R$.* ***Upper right panel*** *J band light curve.* ***Lower right panel*** *Evolution of near infrared colors: triangles represent $J-H$ and squares $H-K$.*

(Kaufer et al. 1999) with a resolution R $\sim$ 48000 and spectral range 4000 – 9000 Å. Spectrophotometric standard stars have not been observed each night, and in this case the spectra have been corrected with an "average response curve". This procedure can introduce an uncertainty on the flux measurement up to 50%. Flux-determination is affected by undetermined uncertainty because FEROS is a fiber-fed spectrograph that was not equipped with an atmospheric dispersion corrector at the time of these observations. Indetermination is due to the fact that the observations are carried out guiding on the V-band image of the star that is differently displaced (due to atmospheric refraction) in the other bands. During my analysis, fluxes were corrected in order to match the observed magnitudes.

An independent spectroscopic follow up has been carried out with the RC spectrograph on the SMARTS 1.5m telescope at CTIO. A spectrophotometric standard star (either LTT 4364 or Feige 110) was observed each night to remove the instrumental signature. Due to seeing-related slit losses, absolute fluxes are considered affected by errors but relative intensities are supposed to be correct. Standard reduction has been carried out with an IDL routine written by the author.

An IR spectrum was taken June 22, 2004 at Lick Observatory using the Aerospace Corporation's Near-Infrared and Visible Imaging Spectrograph (NIRIS). The standard star used was HR 6836.

All spectra have been analyzed with the `onedspec` package in `IRAF`. Line fluxes have been measured by the integration of the line profile and not by gaussian fitting. Full width at half maximum (FWHM) of lines have been measured also via gaussian fitting but show no significant difference from direct measure. A complete log of my spectroscopic observations is given in Table 3.2.

3.1.3 Light curve

The optical and near-infrared light curves of Nova Sgr 2004 are shown in Figure 3.1. The light curves have been derived using both my photometric data and photometry available in the literature (IAUC 8306, 8307, 8310). The V light curve shows that Nova Sgr 2004 reached V=8.0 on Mar 17.17 UT (MJD = 53081.556). Nishimura et al. (2004) noted that nothing was detected in the same position in the red Digitized Sky Survey. After considering that the DSS limiting magnitude is $\sim$ 21, I can infer that the outburst amplitude was $\gtrsim$ 13 mag which is consistent with values observed for other novae with about the same rate of decline

JD	Telescope@Observatory	U	B	V	R	I	J	H	K
2453083.25	1.3m@CTIO	8.70	9.11	8.45	7.91	7.48	6.72	6.63	6.24
2453084.00	0.8m@McDonald	8.87	9.23	8.65	8.01	7.38	–	–	–
2453084.25	0.8m@McDonald	8.74	9.24	8.73	8.07	7.55	–	–	–
2453084.50	0.8m@McDonald	8.87	9.23	8.65	8.01	7.38	–	–	–
2453085.00	0.8m@McDonald	9.08	9.53	9.00	8.19	7.42	–	–	–
2453085.50	0.8m@McDonald	9.08	9.53	9.00	8.19	7.42	–	–	–
2453088.25	1.3m@CTIO	9.19	9.81	9.40	8.46	7.93	7.37	7.10	6.74
2453089.25	1.3m@CTIO	9.38	10.01	9.63	8.57	8.12	7.54	7.37	6.97
2453091.25	1.3m@CTIO	9.54	10.10	9.70	8.74	8.38	7.79	7.59	7.25
2453091.50	0.8m@McDonald	9.83	10.17	9.73	8.80	8.28	–	–	–
2453092.25	1.3m@CTIO	9.61	10.22	9.78	8.79	8.42	7.86	7.72	7.35
2453092.50	0.8m@McDonald	10.02	10.34	9.88	8.96	8.41	–	–	–
2453093.25	1.3m@CTIO	9.85	10.49	10.08	9.02	8.67	8.11	8.01	7.66
2453093.50	0.8m@McDonald	10.26	10.60	10.22	9.13	8.67	–	–	–
2453094.50	0.8m@McDonald	10.38	10.73	10.39	9.28	8.71	–	–	–
2453097.25	1.3m@CTIO	10.20	10.78	10.53	9.37	9.01	8.52	8.56	8.18
2453099.25	1.3m@CTIO	10.39	11.00	10.70	9.55	9.15	8.70	8.72	8.36
2453100.50	1.3m@CTIO	10.49	11.16	10.84	9.59	9.19	8.76	8.84	8.46
2453101.25	1.3m@CTIO	10.57	11.14	10.87	9.60	9.20	8.78	8.89	8.52
2453102.25	1.3m@CTIO	10.63	11.24	10.93	9.65	9.27	8.88	8.97	8.57
2453103.25	1.3m@CTIO	10.64	11.23	11.02	9.73	9.32	8.95	9.02	8.64
2453104.25	1.3m@CTIO	10.69	11.34	11.05	9.77	9.33	8.97	9.05	8.64
2453105.25	1.3m@CTIO	10.90	11.51	11.24	9.86	9.37	9.06	9.20	8.77
2453108.25	1.3m@CTIO	11.17	11.77	11.60	9.94	9.50	9.23	9.40	8.89
2453109.25	1.3m@CTIO	11.14	11.77	11.56	9.96	9.54	9.26	9.44	8.89
2453110.25	1.3m@CTIO	11.25	11.90	11.76	10.04	9.64	9.39	9.61	9.03
2453112.00	1.0m@CTIO	11.64	12.00	11.69	10.11	9.62	–	–	–
2453113.25	1.3m@CTIO	11.39	12.07	11.95	10.10	9.77	9.44	9.68	8.99
2453114.00	1.0m@CTIO	11.81	12.13	11.95	10.17	9.72	–	–	–
2453126.25	1.3m@CTIO	11.85	12.44	12.37	10.57	10.70	10.16	10.19	9.50
2453132.25	1.3m@CTIO	12.03	12.53	12.50	10.87	11.08	10.48	10.45	9.72
2453136.25	1.3m@CTIO	12.10	12.53	12.58	10.97	11.24	10.67	10.59	9.91
2453186.25	1.0m@CTIO	14.35	14.11	13.67	13.20	13.60	–	–	–
2453187.00	1.0m@CTIO	14.39	14.16	13.68	13.25	13.66	–	–	–
2453188.25	1.0m@CTIO	14.37	14.17	13.68	13.26	13.58	–	–	–
2453189.25	1.0m@CTIO	14.44	14.19	13.77	13.40	–	–	–	–
2453190.25	1.0m@CTIO	14.46	14.21	13.74	13.34	13.76	–	–	–
2453191.25	1.0m@CTIO	14.51	14.25	13.76	13.40	13.81	–	–	–
2453192.00	1.0m@CTIO	14.53	14.26	13.77	13.42	13.82	–	–	–
2453193.00	1.0m@CTIO	14.56	14.31	13.82	13.46	13.82	–	–	–
2453194.25	1.0m@CTIO	14.59	14.33	13.83	13.50	13.90	–	–	–
2453195.25	1.0m@CTIO	14.62	14.33	13.83	13.53	13.95	–	–	–
2453196.25	1.0m@CTIO	14.66	14.40	13.86	13.58	13.99	–	–	–
2453197.25	1.0m@CTIO	14.69	14.39	13.87	13.61	14.00	–	–	–
2453198.25	1.0m@CTIO	14.68	14.43	13.88	13.62	14.04	–	–	–
2453200.00	1.0m@CTIO	14.78	14.50	13.92	13.70	14.08	–	–	–

Table 3.1: *Log of the photometric observations for Nova Sgr 2004*

Date (UT)	Instrument	Exp.time (sec)	Wavelength range	Resolution (or scale)
Mar18.3	FEROS	240	4000-9000Å	48000
Mar19.3	FEROS	400	4000-9000Å	48000
Mar19.3	SMARTS	360	4000-5000Å	0.77
Mar19.3	SMARTS	360	4000-5000Å	0.77
Mar20.3	SMARTS	270	3500-5300Å	1.5
Mar21.4	SMARTS	120	4800-9500Å	5.6
Mar22.4	SMARTS	600	3900-4500Å	0.6
Mar26.4	FEROS	632	4000-9000Å	48000
Apr1.4	SMARTS	360	3500-5300Å	1.5
Apr2.3	SMARTS	360	4000-4900Å	0.77
Apr3.3	SMARTS	300	5900-7700Å	1.5
Apr5.3	SMARTS	360	3500-5300Å	1.5
Apr6.4	SMARTS	360	3900-4550Å	0.56
Apr9.4	FEROS	900	4000-9000Å	48000
Apr13.3	SMARTS	360	5600-7000Å	1.1
Apr13.4	SMARTS	360	3800-4550Å	0.56
Apr13.4	SMARTS	360	4050-4750Å	0.56
Apr15.4	SMARTS	540	4000-5000Å	0.77
Apr16.3	SMARTS	720	3500-5300Å	1.48
Apr17.3	SMARTS	360	3500-5300Å	1.48
Apr18.4	FEROS	900	4000-9000Å	48000
Apr18.4	SMARTS	300	4800-9500Å	5.6
Apr18.4	SMARTS	180	4800-9500Å	5.6
Apr19.4	SMARTS	480	3800-5600Å	1.48
Apr26.2	SMARTS	450	5600-6950Å	1.1
Apr26.4	SMARTS	540	3850-4550Å	0.56
Apr27.3	SMARTS	450	3870-4550Å	0.56
Apr28.2	SMARTS	600	3870-4550Å	0.56
Apr28.4	SMARTS	600	5650-7000Å	1.1
Apr29.2	SMARTS	600	3870-4550Å	0.56
Apr30.2	SMARTS	450	3870-4550Å	0.56
May1.2	SMARTS	450	3870-4550Å	0.56
May1.4	SMARTS	450	5600-7000Å	1.1
May2.2	SMARTS	360	3500-5300Å	1.48
May12.4	SMARTS	360	3500-5300Å	1.48
May13.3	FEROS	1500	4000-9000Å	48000
May13.4	SMARTS	360	3500-5300Å	1.48
May14.3	SMARTS	360	3500-5300Å	1.48
May15.1	SMARTS	450	5650-7000Å	1.1
May15.4	SMARTS	450	3900-4550Å	0.56
May25.3	SMARTS	720	3500-5300Å	1.48
May26.3	SMARTS	720	4000-5000Å	0.77
Jun6.2	SMARTS	720	4050-4750Å	0.56
Jun22	NIRIS	?	4500-25000Å	?
Jun22.2	SMARTS	360	3500-5300Å	1.48
Jun26.2	FEROS	3600	4000-9000Å	48000
Jun27.1	SMARTS	450	5650-7000Å	1.1
Jun27.4	SMARTS	720	3850-4550Å	0.56
Jun28.1	SMARTS	360	4800-9600Å	5.67
Jul15.1	SMARTS	600	3550-5300Å	1.48
Jul31.2	SMARTS	540	5650-7000Å	1.10
Aug14.2	SMARTS	600	3450-6900Å	2.88
Sep26.2	FEROS	7200	4000-9000Å	48000

Table 3.2: *Log of the spectroscopic observations for Nova Sgr 2004*

t_0	$JD = 2453081.556$
t_2	11 *days*
t_3	21 *days*
$m_{V,max}$	8.0 *mag*
$(B-V)_{max}$	0.66 *mag*
$(B-V)_{t_2}$	0.38 *mag*
$(B-V)_{15d}$	0.25 *mag*

Table 3.3: *Observed photometric properties for Nova Sgr 2004*

(see Warner 1995).

The nova decreased by two magnitudes from maximum in $t_2 = 11$ days and by three magnitudes in $t_3 = 21$ days. Adopting the maximum magnitude versus rate of decline (MMRD) relation by Della Valle & Livio (1995), Nova Sgr 2004 achieved an absolute V magnitude at maximum light of $M_V = -8.7 \pm 0.2$ mag. Photometric properties are summarized in Table. 3.3. The typical photometric errors are smaller than 0.04 mag in all bands but in U ~ 0.1 mag. $(J-H)$ color changes its slope after $\sim$ day 40. This could be in principle due to formation of dust in the ejecta but an inspection of the B and V light curves rules out "DQ Herculis" behaviour, therefore the reddened color is likely due to to variations in intensity of emission lines in the NIR.

The spectral energy distribution (SED) one day after maximum appears to be well fitted by a blackbody at T=9600K as shown in Figure 3.2. As the nova evolves, the SED is dominated by emission lines rather than continuum, therefore it cannot be fitted by a single blackbody.

3.1.4 Spectral evolution

Spectroscopic observations started immediately after discovery. Line identification for FEROS spectra (see Figure 3.3 and 3.4) is given in Table 3.4 while in Table 3.5 and 3.6 I show line identification for some of the spectra taken at CTIO.

The first spectrum (phase +1 day) was dominated by Balmer, Fe II and OI emission lines. This behaviour characterized the nova as a typical "FeII" type object, according to the Cerro Tololo classification (Williams et al. 1991, 1994). P-Cyg profiles were clearly visible in Balmer

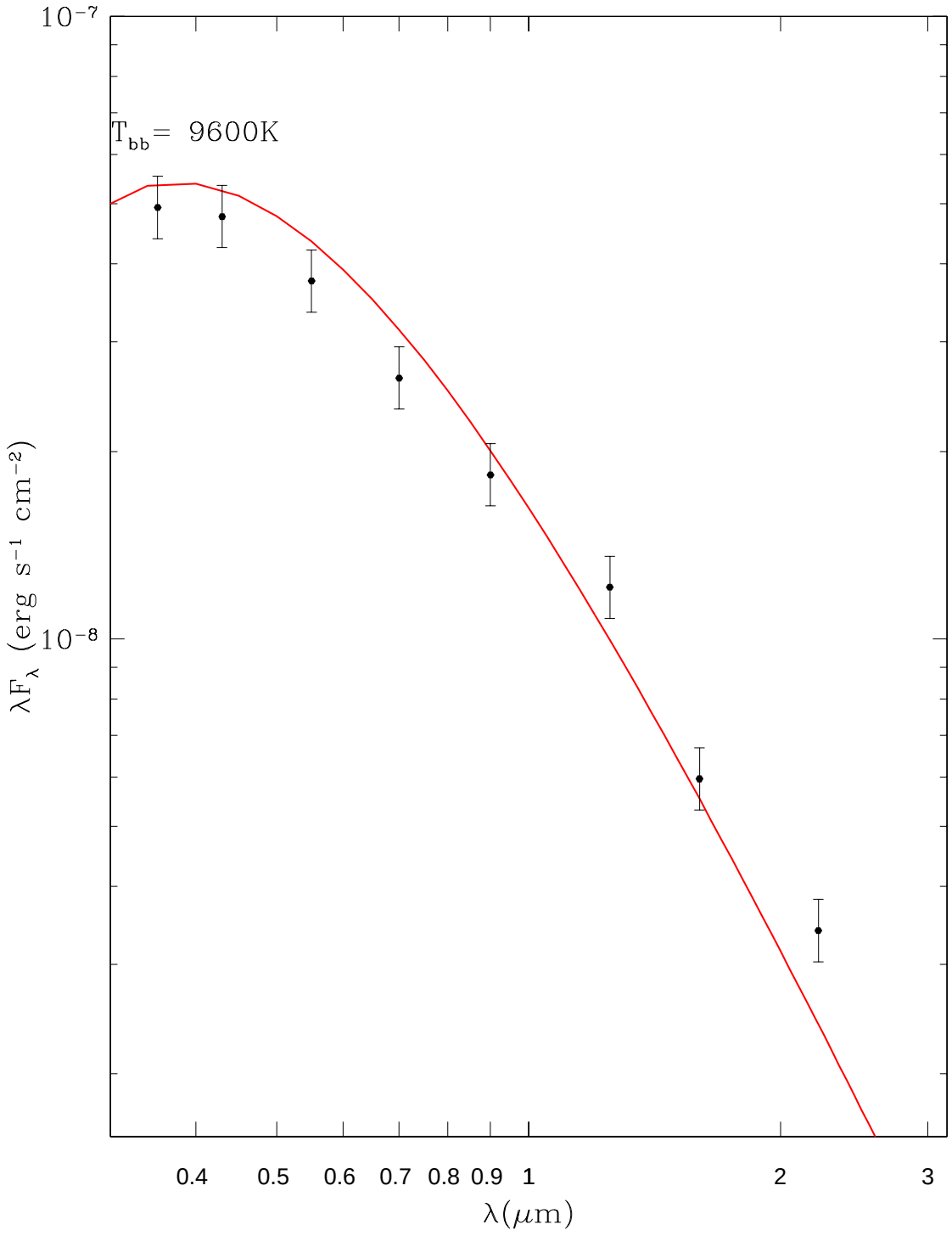

Figure 3.2: *Spectral energy distribution of Nova Sgr 2004 one day after maximum light.*

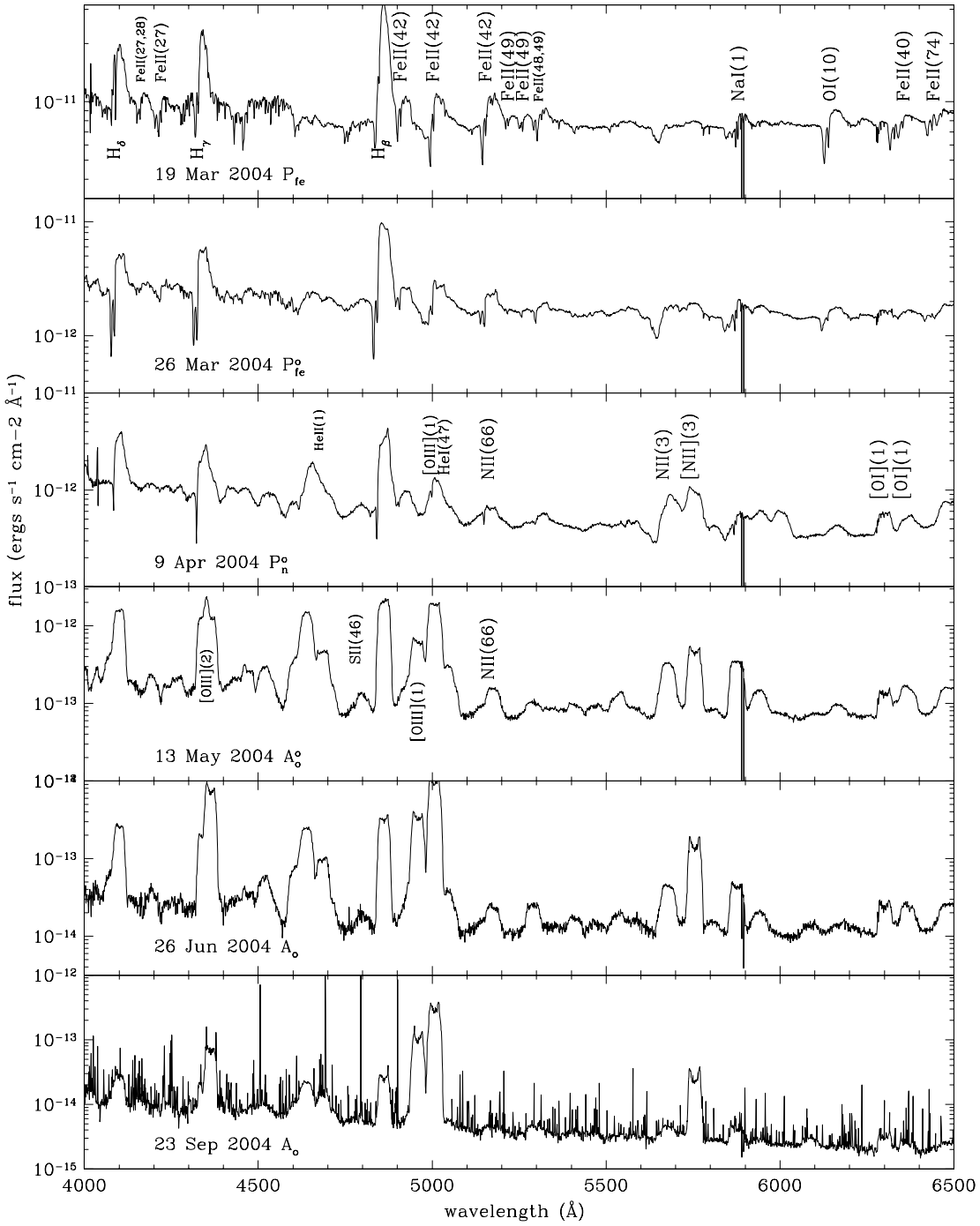

Figure 3.3: *Dereddened spectra ($E_{B-V} = 0.5$ mag) of the nova (blue part). Fluxes are in logarithmic scale to show the less intense lines.*

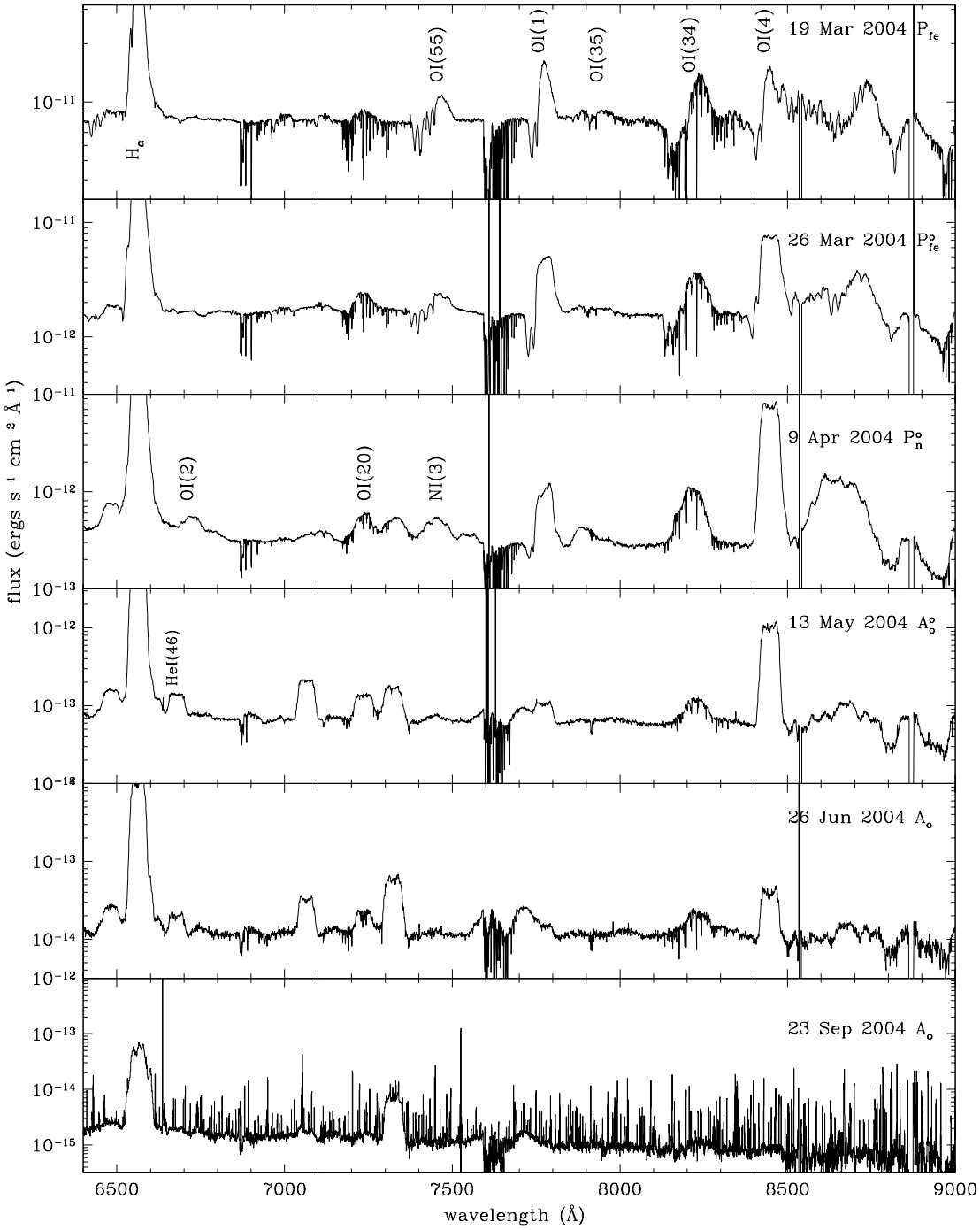

Figure 3.4: *Dereddened spectra ($E_{B-V} = 0.5$ mag) of the nova (red part). Fluxes are in logarithmic scale to show the less intense lines.*

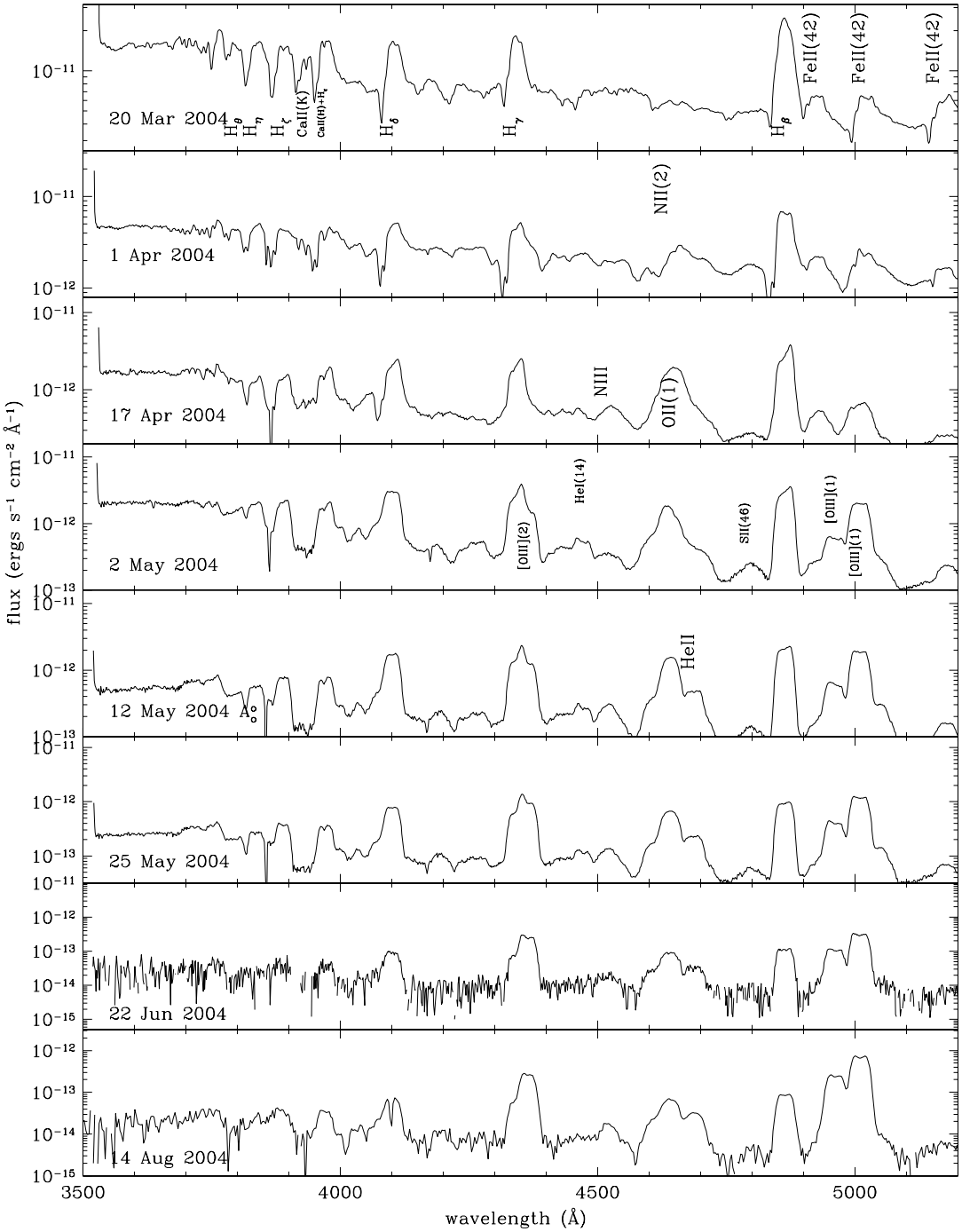

Figure 3.5: *Dereddened spectra ($E_{B-V} = 0.5$ mag) of Nova Sgr 2004 taken at CTIO and covering the region 3500–5200 Å.*

lines as well as in FeII, OI, and NaI lines. P-Cyg profiles were double thus suggesting the presence of two expansion systems with velocities (obtained by averaging of measurements of Balmer lines) of 1400 ± 50 km s^{-1}and 850 ± 30 km s^{-1}.

Eight days after maximum, the spectrum was still dominated by low ionization species. The double P-Cyg profiles were still clearly visible and the velocities (as derived from both the P-Cyg profiles and FWHM) were increasing. The emission lines started developing a flat topped profile.

On April 9 (phase +23 days), the 4640 Å emission band was observed together with NII and NIII, although FeII emission lines were still present. The OI λ8446 emission line was more intense than H_β and showed a flatter profile.

By April 18 (phase +34 days) P-Cyg profiles had disappeared and FeII emission lines were fading and forbidden and high excitation lines strengthened. The intensity of [O III]λ4363 indicated that Nova Sgr 2004 entered the auroral phase, described in Williams et al. (1991, 1994). Fluxes of Balmer lines, that had decreased very slowly until this moment, started to decrease faster (see Figure 3.7). The FWHM of Balmer lines reached a plateau (2000 ± 100 km s^{-1}).

The OI 8446 and HeI 5595 lines show flat topped profiles while the hydrogen lines have a clearly asymmetric profile (the red side being more prominent than the blue one). At this stage the OI λ8446 emission line reached its maximum intensity.

By May 13 (phase +57 days) the hydrogen lines turn to flat topped profiles (like oxygen) while nitrogen lines were still rounded. It has been noted in the past (see Payne-Gaposchkin 1957) that different line profiles observed at the same stage indicate that the emission lines originate in different layers of the ejecta. Flat topped profiles originate from optically thin spherical shells while rounded profiles are related with optically thick winds. The NIR part of the spectrum (observed only on Jun 22, see Figure 3.8, line identification given in Table 3.7) showed prominent Paschen and Brackett lines as well as oxygen and nitrogen lines. Common but unknown lines (1.10 , 1.19 , 1.55 and 2.10 μm) were present in this spectrum (see Venturini et al. 2004). Tentative identifications for these lines with van Hoof's line list[1] are given in Table 3.8. Wavelength of previously unidentified lines is not precisely known, therefore I accepted an uncertainty up to 10 Å.

In September the spectrum was dominated by [OIII] $\lambda\lambda$ 4959-5007 lines. All lines showed

[1]version 2.04 *http://www.pa.uky.edu/ ˜ peter/atomic/*

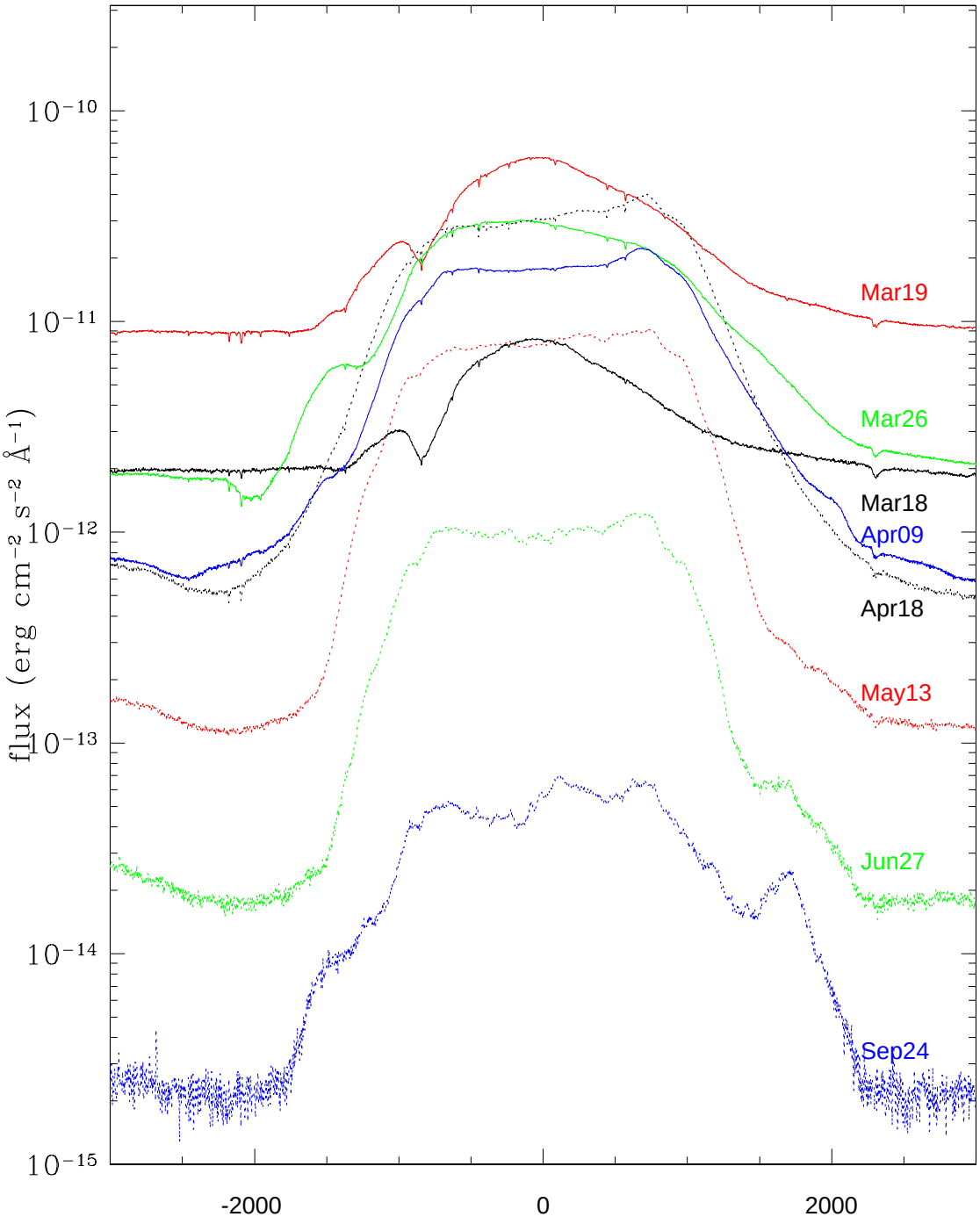

Figure 3.6: *Evolution of the profile of H_α emission line*

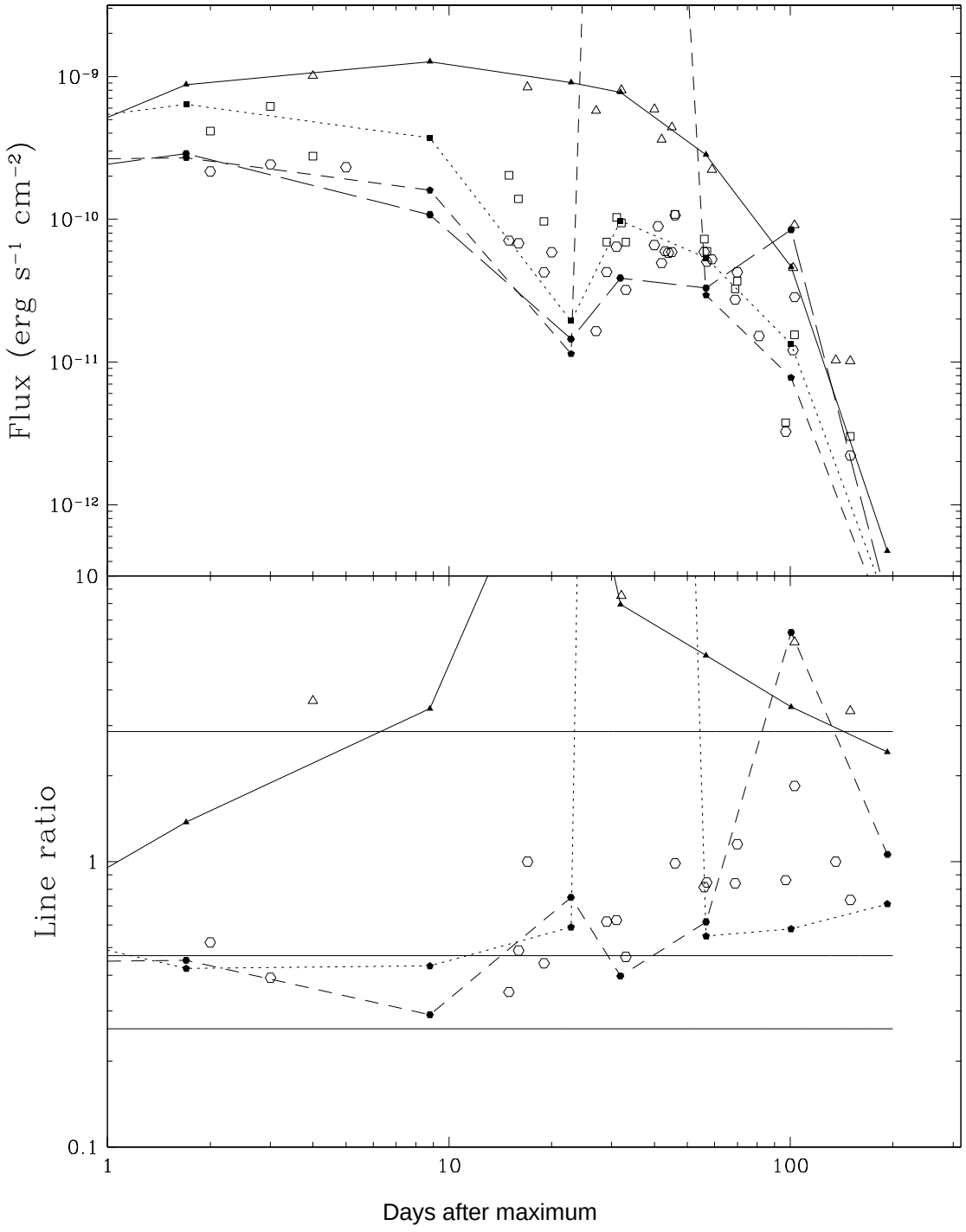

Figure 3.7: ***Upper panel:*** *Evolution of Balmer lines fluxes. Triangles represent H_α, squares H_β, pentagons H_γ and hexagons H_δ. Filled symbols represent data from FEROS, empty symbols from the RC spectrograph at the 1.5m telescope at CTIO. Lines connecting the FEROS symbols are meant to show the trend of the data.* ***Lower panel:*** *Evolution of Balmer lines divided by the H_β flux (symbols refer to the same lines as in the upper panel). Horizontal lines represent the Balmer lines ratios for case B at 10000K as from Osterbrock (1989) (from top to bottom H_α/H_β, H_γ/H_β and H_δ/H_β).*

Ident. wavelength	Mar18	Mar19	Mar26	Apr9	Apr18	May13	Jun26	Sep23
HeI 4026	–	–	–	–	–	2.051e-12	3.152e-13	2.185e-13
[SII] 4076	–	–	–	–	–	7.495e-12	1.965e-12	–
H_δ 4101	2.171e-10	2.882e-10	1.076e-10	1.449e-11	3.872e-11	3.294e-11	8.465e-11	2.083e-13
FeII(27 28	4.173e+03	3.720e-11	4.695e-11	1.691e-11	–	–	–	–
Fe27 4233	3.520e-11	2.466e-11	1.375e-11	7.940e-13	–	–	–	–
Fe27 4273	–	–	1.126e-11	5.570e-13	2.140e-12	2.365e-12	–	–
$H\gamma$ 4340	2.632e-10	2.694e-10	1.596e-10	1.140e-11	5.488e-01	2.937e-11	7.761e-12	1.395e-13
[OIII](2) 4363	–	–	–	–	–	2.702e-11	2.860e-11	4.880e-13
FeII(27) 4417	–	–	4.995e-12	5.595e-13	–	–	–	–
HeI(14) 4472	–	–	1.654e-11	2.748e-12	2.625e-12	3.239e-12	7.373e-13	–
NIII 4517	–	–	–	–	–	6.304e-12	1.839e-12	–
FeII(37) 4629	1.790e-11	1.205e-11	–	–	–	–	–	–
4640 4640	–	–	–	1.296e-11	8.805e-11	4.518e-11	1.276e-11	1.829e-13
FeII(37) 4665	1.486e-11	8.273e-12	6.870e-11	–	–	–	–	–
HeII(1) 4686	–	–	–	–	–	1.067e-11	3.827e-12	9.729e-14
SII(46) 4792	–	–	–	1.450e-12	1.880e-12	1.601e-12	–	–
H_β 4861	4.871e-10	6.381e-10	3.705e-10	1.936e-11	9.747e-11	5.355e-11	1.335e-11	1.964e-13
FeII(42) 4924	8.414e-11	8.568e-11	4.556e-11	2.492e-12	1.126e-11	–	–	–
[OIII](1) 4959	–	–	–	–	–	1.710e-11	1.294e-11	2.831e-12
[OIII](1) 5007	–	–	–	–	3.283e-11	5.583e-11	3.750e-11	8.450e-12
FeII(42) 5018	1.808e-10	1.238e-10	9.713e-11	3.347e-11	–	–	–	–
FeII(52) 5169	1.241e-10	9.705e-11	3.956e-11	1.465e-11	5.842e-12	2.942e-12	6.694e-13	–
FeII(49) 5234	3.090e-11	1.438e-11	2.107e-12	–	–	–	–	–
FeII(49) 5276	3.787e-11	1.684e-11	3.156e-12	2.463e-12	–	–	–	–
HeII(47) 5290	–	–	–	–	–	–	4.987e-13	–
FeII(49) 5317	–	–	–	9.873e-12	5.225e-12	–	–	–
FeII(48) 5337	5.188e-11	3.527e-11	1.583e-11	–	–	–	–	–
HeII(2) 5412	–	–	–	–	–	5.417e-13	2.009e-13	–
OI(1) 5577	–	–	1.446e-11	4.252e-12	2.452e-12	3.628e-13	1.930e-13	3.581e-14
NII(3) 5677	–	–	–	2.306e-11	1.340e-11	8.876e-12	1.471e-12	5.357e-14
NII(3) 5755	–	–	2.969e-11	2.999e-11	3.512e-11	1.291e-11	5.464e-12	6.916e-13
C IV 5809	–	–	–	–	3.713e-12	3.969e-13	1.537e-13	2.891e-14
HeI(11) 5876	–	–	–	–	1.127e-11	8.393e-12	1.277e-12	7.868e-14
NaI(1) 5890	7.322e-12	1.431e-11	2.145e-11	7.353e-12	–	–	–	–
NII(28) 5940	–	–	2.366e-11	1.155e-11	3.902e-12	2.875e-12	4.021e-13	4.919e-14
??? 6000	–	–	–	1.223e-11	7.460e-12	–	–	–
??? 6089	–	–	–	–	–	–	2.293e-13	1.478e-14
OI(10) 6159	1.556e-11	2.448e-11	1.474e-11	4.609e-12	2.354e-12	1.195e-12	1.661e-13	–
??? 6201	–	–	–	–	–	–	1.642e-13	–
FeII(74) 6247	6.565e-12	1.000e-11	3.567e-12	–	–	–	–	–
[OI](1) 6300	–	–	–	9.199e-12	5.728e-12	2.105e-12	5.970e-13	2.050e-14
[OI](1) 6364	–	–	–	2.338e-12	3.471e-12	1.884e-12	4.072e-13	1.477e-14
FeII(40) 6370	6.073e-12	1.220e-11	1.054e-11	4.148e-12	–	–	–	–
NII(8) 6482	–	–	–	1.520e-11	6.347e-12	2.140e-12	6.653e-13	1.256e-14
H_α 6563	3.628e-10	8.767e-10	1.271e-09	9.079e-10	7.751e-10	2.825e-10	4.651e-11	4.751e-13
[NII] 6583	–	–	–	–	–	–	–	1.971e-13
HeII(46) 6678	–	–	–	–	5.203e-12	2.868e-12	4.713e-13	8.073e-15
OI(2) 6726	5.716e-12	4.460e-12	5.613e-12	6.484e-12	5.550e-12	6.037e-13	–	–
OI(2) 7002	9.494e-12	8.721e-12	5.387e-12	9.134e-13	–	–	–	–
HeI(10) 7065	–	–	–	–	8.681e-12	5.411e-12	1.035e-12	9.033e-15
??? 7113	–	5.993e-12	–	–	3.033e-12	–	–	–
CII(3) 7231	–	3.098e-13	2.975e-11	1.306e-11	4.566e-12	3.080e-12	5.775e-13	–
[OII](2) 7330	–	–	–	1.289e-11	1.586e-11	4.612e-12	2.587e-12	8.054e-14
NI(3)+OI(55) 7468	3.051e-11	5.079e-11	4.119e-11	1.287e-11	5.884e-12	–	–	–
OI(1) 7774	5.961e-11	1.302e-10	1.667e-10	4.127e-11	1.602e-11	2.079e-12	2.236e-13	–
MGII(8) 7896	–	–	–	9.868e-12	4.794e-12	2.723e-13	–	–
??? 7958	–	–	–	–	1.636e-12	3.751e-13	–	–
OI(35) 7947	1.096e-11	2.555e-11	–	–	–	–	–	–
OI(34) 8223	5.741e-11	1.119e-10	1.174e-10	6.165e-11	2.252e-11	3.376e-12	7.275e-13	–
OI(4) 8446	5.722e-11	1.042e-10	3.898e-10	4.391e-10	2.938e-10	4.158e-11	1.701e-12	–
CaII 8498	1.953e-11	3.193e-11	–	–	–	–	–	–
CaII 8662	–	9.660e-12	–	–	–	–	–	–

Table 3.4: *Nova Sgr 2004 emission line fluxes (in ergs s^{-1} cm^{-2}) from dereddened ($E_{B-V} = 0.5$ mag) FEROS spectra.*

Ident. wavelength	Mar21	Apr18	Jun28	Aug14
H_ν 3968	–	–	5.264e-12	6.227e-13
H_δ 4101	–	–	1.290e-11	1.299e-12
H_γ+OIII 4340	–	–	7.880e-12	1.270e-12
[OIII] 4363	–	–	3.06e-11	5.946e-12
NIII 4517	–	–	9.485e-13	3.006e-13
4640 4640	–	–	9.680e-12	2.136e-12
HeII(1) 4686	–	–	2.112e-12	7.562e-13
H_β 4861	–	–	7.671e-12	2.226e-12
FeII(42) 4924	6.169e-11	1.497e-11	–	–
[OIII](1) 4958	–	–	1.110e-11	9.331e-12
[OIII](1) 5007	–	–	4.030e-11	2.706e-11
FeII(42) 5018	1.438e-10	4.881e-11	–	–
FeII(52) 5169	7.648e-11	6.986e-12	5.699e-13	1.909e-13
FeII(49) 5276	3.982e-12	–	–	–
He II(47) 5296	–	–	4.910e-13	2.915e-13
FeII(48) 5337	1.636e-11	4.421e-12	–	–
HeII(2) 5412	–	–	1.639e-13	7.069e-14
??? 5474	–	–	6.000e+00	5.475e-14
??? 5540	–	–	2.211e-13	3.051e-14
[OI](1) 5577	–	2.396e-12	1.108e-13	2.695e-14
NII(3) 5677	1.994e-11	1.768e-11	1.499e-12	3.686e-13
[NII](3) 5755	2.059e-11	4.741e-11	6.232e-12	3.409e-12
C IV 5819	–	5.698e-12	6.930e-14	3.116e-14
HeI(11) 5876	–	1.931e-11	1.507e-12	3.285e-13
NaI(1) 5890	1.205e-11	–	–	–
NII(28) 5940	7.182e-12	5.231e-12	4.379e-13	8.507e-14
??? 6004	–	8.955e-12	–	–
??? 6100	–	–	1.703e-13	7.221e-14
OI(10) 6159	2.356e-11	2.651e-12	–	–
??? 6188	–	–	2.100e-13	–
FeII(74) 6247	7.957e-12	–	–	–
[OI] 6300	2.292e-12	6.460e-12	5.537e-13	1.547e-13
[OI] 6364	1.033e-11	3.094e-12	4.883e-13	8.135e-14
NII(8) 6482	6.184e-12	4.263e-12	2.974e-13	8.719e-14
H_α 6563	1.034e-09	7.880e-10	4.517e-11	9.878e-12
HeI(46) 6678	2.665e-12	6.814e-12	3.705e-13	8.686e-14
OI(2) 6726	5.260e-12	7.093e-12	–	–
HeI(10) 7065	–	1.313e-11	9.149e-13	–
??? 7135	–	5.492e-12	–	–
CII(3) 7236	–	7.209e-12	4.428e-13	–
[OII](2) 7330	–	2.246e-11	2.202e-12	–
NI(3)+OI(55) 7470	4.606e-11	8.790e-12	–	–
??? 7586	–	–	1.702e-13	–
??? 7630	–	–	5.025e-14	–
??? 7731	–	–	7.604e-13	–
OI(1) 7775	1.939e-10	1.835e-11	–	–
MgII(8) 7896	6.723e-12	4.033e-12	–	–
OI(34) 8223	1.098e-10	2.561e-11	3.087e-13	–
??? 8350	1.657e-11	–	–	–
OI(4) 8446	2.841e-10	4.117e-10	7.923e-13	–
??? 8666	–	7.317e-11	–	–
??? 8704	–	–	5.306e-13	–
??? 8871	–	8.667e-12	1.558e-13	–
??? 9030	–	–	1.978e-13	–
??? 9042	–	1.652e-11	–	–
??? 9245	–	2.112e-11	7.588e-13	–
??? 9405	–	1.721e-11	–	–
??? 9556	–	–	2.032e-13	–

Table 3.5: *Nova Sgr 2004 emission line fluxes (in ergs s^{-1} cm^{-2}) from dereddened ($E_{B-V} = 0.5$ mag) CTIO spectra with wavelength range larger than 2000 Å and including the H_α region.*

Ident. wavelength	Mar20	Apr1	Apr17	May2	May12	May25	Jun22	Aug14
??? 3765	1.097e-10	2.864e-11	8.106e-12	3.515e-12	5.046e-12	6.655e-12	5.467e-12	6.279e-13
H_θ 3798	7.428e-11	1.958e-11	5.438e-12	4.038e-12	1.764e-12	1.917e-12	2.081e-12	2.742e-13
H_η 3835	1.509e-10	4.540e-11	1.549e-11	1.538e-11	6.803e-12	5.125e-12	1.922e-12	2.146e-13
H_ζ 3889	1.645e-10	6.452e-11	2.371e-11	2.068e-11	1.265e-11	9.422e-12	4.901e-12	6.375e-13
CaII(K) 3933	7.539e-11	–	–	–	–	–	–	–
?H_ν+CaII 3969	2.364e-10	7.904e-11	3.205e-11	2.223e-11	1.333e-11	1.572e-11	4.575e-12	5.804e-13
H_δ 4101	2.851e-10	8.203e-11	5.259e-11	6.788e-11	5.243e-11	3.943e-11	1.141e-11	1.370e-12
FeII(27 28	4.173e+03	4.041e-11	1.015e-11	–	2.046e-12	–	–	–
FeII(27) 4233	3.345e-11	–	–	–	–	–	–	–
H_γ+OIII 4343	3.107e-10	6.490e-11	5.900e-11	8.745e-11	7.625e-11	7.090e-11	3.868e-11	7.256e-12
NIII 4517	–	–	7.023e-12	–	4.903e-12	4.835e-12	1.751e-12	1.992e-13
4640 4640	–	9.484e-11	9.291e-11	6.486e-11	6.279e-11	4.104e-11	1.456e-11	2.141e-12
HeII(1) 4686	–	–	–	–	1.414e-11	1.107e-11	3.914e-12	7.596e-13
H_β 4861	6.065e-10	1.750e-10	9.914e-11	8.069e-11	7.291e-11	4.839e-11	1.499e-11	2.244e-12
FeII(42) 4924	5.939e-11	2.021e-11	9.535e-12	–	–	–	–	–
[OIII] 4959	–	–	–	1.440e-11	2.165e-11	2.226e-11	1.638e-11	6.948e-12
[OIII] 5007	–	–	2.060e-11	5.897e-11	7.465e-11	7.097e-11	4.729e-11	2.015e-11
FeII(42) 5018	1.151e-10	5.950e-11	–	–	–	–	–	–
FeII(52) 5169	7.531e-11	1.706e-11	5.993e-12	3.021e-12	3.994e-12	2.506e-12	–	–

Table 3.6: *Nova Sgr 2004 emission line fluxes (in ergs s^{-1} cm^{-2}) from dereddened ($E_{B-V} = 0.5$ mag) CTIO spectra shown in Figure 3.5.*

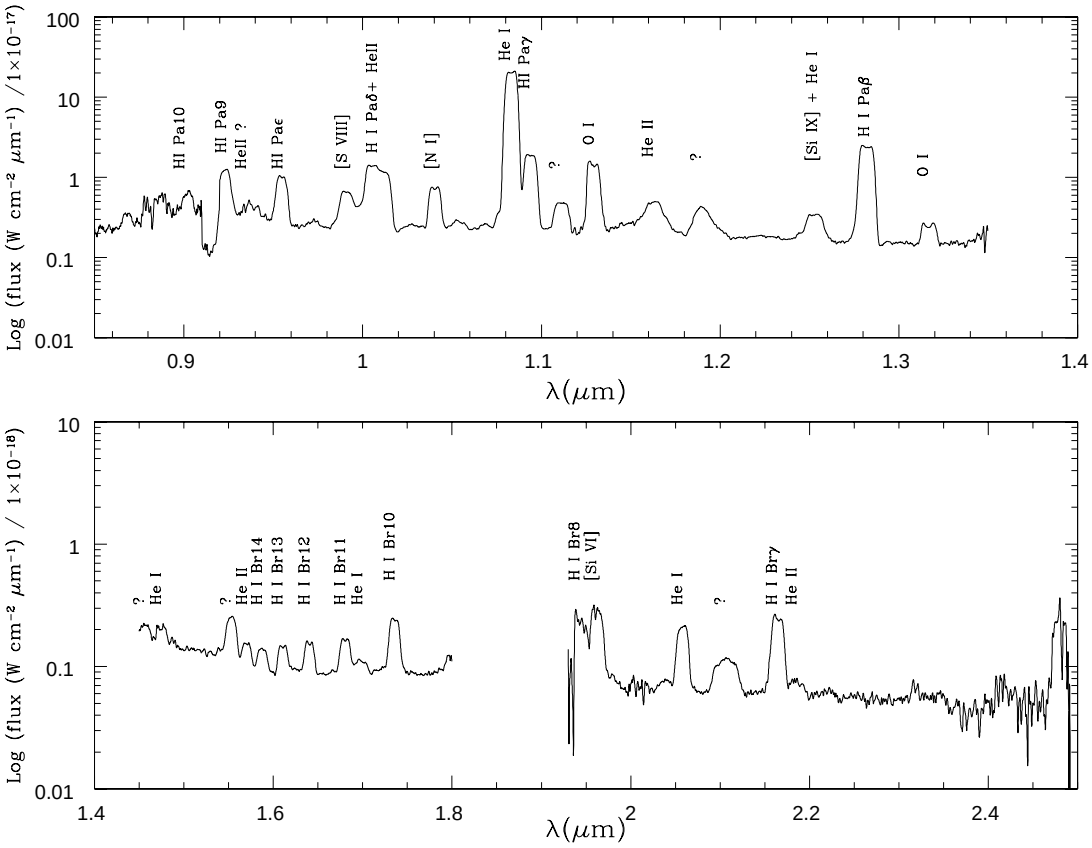

Figure 3.8: *Dereddened ($E_{B-V} = 0.5$ mag) IR spectrum of Nova Sgr 2004.*

saddle-shaped profiles. The OI λ8446 line had almost disappeared. H_α was clearly strongly blended with NII.

The overall evolution of expansion velocities measured from P-Cyg absorption is shown in Figure 3.9. Cassatella et al. (2004) have shown that the evolution of P-Cyg profiles as measured in the UV of Nova Cyg 1992 can be modeled with an exponential law $v(t) = v_\infty - (v_0 - v_\infty)e^{-t/\tau}$, where $v(t)$ is the velocity t days after maximum, v_0 is the expansion velocity at maximum light, v_∞ is the asymptotic velocity and τ is a timescale that I have found to be $\sim t_3$. I have fitted the data with a least-square algorithm (see Figure 3.9). I have derived $v_\infty = 2100 \pm 50$ km s^{-1} and 1500 ± 50 km s^{-1}, $v_0 = 1300 \pm 50$ km s^{-1} and 800 ± 50 km s^{-1} and $\tau = 18 \pm 1$ day. Both v_∞ and velocity measurements based on the FWHM of emission lines during the nebular stage are important quantities that should be considered in view of future observations aimed at determing the distance to Nova Sgr 2004, via nebular parallax.

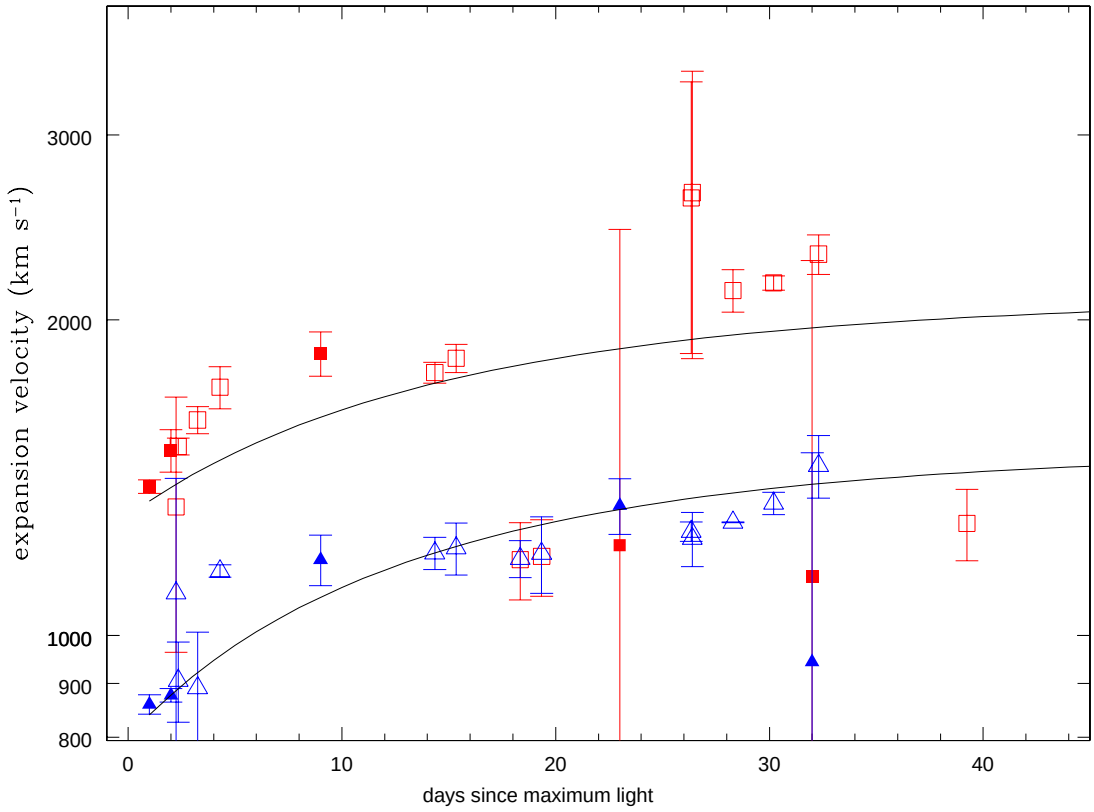

Figure 3.9: *Velocities of the ejecta. Measures are derived as average of p-Cyg profiles of Balmer lines. Squares refer to the faster absorption system and triangles to the slower one. Filled symbols refer to FEROS observations and empty sybols to CTIO observations. Continuous lines are exponential description of the evolution (see text).*

wavelength	ID	flux
0.4684	HeII (3 4)	2.779E-12
0.4858	Hbeta(4)	1.262E-11
0.4955	[OIII]	1.225E-11
0.5004	[OIII]	3.600E-11
0.5168	NII	6.216E-13
0.5293		6.491E-13
0.5409	HeII (4 7)	2.803E-13
0.5472		1.728E-13
0.5536		2.749E-13
0.5679	NII	1.525E-12
0.5756	[NII]	5.534E-12
0.5812	C IV	1.132E-12
0.5876	HeI	1.333E-13
0.5942	NII	3.706E-13
0.6087		2.299E-13
0.6180	?	3.069E-13
0.6304	[OI]	5.907E-13
0.6368	[OI]	3.859E-13
0.6484	NII	4.752E-13
0.6566	Hα(3)	4.284E-11
0.6680	HeI	3.318E-13
0.6894		9.923E-14
0.7068	HeI	5.756E-13
0.7243		2.690E-13
0.7328	[OII]	1.291E-12
0.8014		3.156E-14
0.8247	HeII (5 9)	1.766E-13
0.8454	OI	4.714E-13
0.8682	HIPa13	6.569E-14
0.8873	HIPa11	1.850E-13
0.9026	HIPa10	1.503E-13
0.9233	HIPa9	5.330E-12
0.9381		1.240E-13
0.9546	HIPaϵ	5.038E-13
0.9915	[SIII]	4.011E-13
1.0078	HIPaδ+HeII	1.633E-12
1.0405	[NI]	3.606E-13
1.0534		4.662E-14
1.0833	HeI	1.495E-11
1.0939	HIPaγ	1.287E-12
1.1114	?	2.253E-13
1.1291	OI	9.960E-13
1.1627	HeII ?	2.735E-13
1.1911	?	2.716E-13
1.2528	[SiIX]+HeI	2.090E-13
1.2819	HIPaβ	2.055E-12
1.3169	OI	1.007E-13
1.4567		7.252E-14
1.4750	HeII	5.533E-14
1.5528	?	1.592E-13
1.5704	HeII	4.362E-14
1.5881	HIBr14	4.872E-14
1.6114	HIBr13	6.479E-14
1.6402	HIBr12	7.323E-14
1.6806	HIBr11	9.966E-14
1.6983	HeI	2.913E-14
1.7354	HIBr10	2.099E-13
1.9440		2.201E-13
1.9621		3.010E-13
2.0383		1.746E-14
2.0582	HeI	2.041E-13
2.1068		1.443E-13
2.1642	HIBrγ	2.971E-13

Table 3.7: *Near infra red line dereddened ($E_{B-V} = 0.5$ mag) fluxes: $ergs^{-1}cm^{-2}$*

Observed wavelength (μ m)	Rest-frame wavelength	Element
1.1114	11119.98	C I
	11112.	N I
	11114.	N I
	11116.	N I
	11115.3	N II
	11120.10	N II
	11116.48	O II
1.1911	11905.516	He II
	11915.35	C I
	11905.6	C II
	11906.1	C IV
	11908.3	C IV
	11910.2	N I
1.4567	14564.9	C II
	14568.7	C II
	14560.7	C III
	14560.7	C III
1.5528	15514.13	He I
	15524.5	C I
	15531.3	C I
	15524.371	O I
2.0383	20373.28	He II
	20379.9	N I
	20389.	N I
	20387.63	O II
	20389.2	O II
2.1068	21067.	C III
	21067.	C III
	21068.	C III
	21068.	C III
	21061.	C IV
	21067.2	N I
	21067.6	N I
	21068.0	N I

Table 3.8: *Tentative identification of previously unidentified NIR lines*

3.1.5 Reddening and distance

I have used several methods to estimate the reddening of Nova Sgr 2004. This piece of information is crucial to measure the distance to the object. The results of my various estimates of the interstellar reddening are summarized in Table 3.9.

I could not use the commonly used NaD lines because they are saturated. Nevertheless it has been shown by Munari & Zwitter (1997) that alternatively to these lines, the KI λ7699 line can be used. The advantage to use this line is that it has a less steep curve of growth thus giving the opportunity to measure higher reddenings. After applying this method to Nova Sgr 2004, I found $E_{B-V} = 0.45$ mag. Colors at maximum are a widely used empirical indicator of interstellar reddening. van den Bergh & Younger (1987) showed that novae at maximum have an intrinsic $(B-V)$ of 0.23 ± 0.06 mag. The same authors showed also that novae, two magnitudes below maximum, have an intrinsic $(B-V) = -0.02 \pm 0.04$ mag. As from Table 3.3, Nova Sgr 2004 had $(B-V)_{max} = 0.66$ mag and $(B-V)_{t_2} = 0.25$ mag. This leads to $E_{B-V} = 0.43 \pm 0.06$ mag and $E_{B-V} = 0.40 \pm 0.04$ mag, respectively.

From Schlegel et al.'s (1998) dust maps of the Milky Way, I have derived $E_{B-V} = 0.58$ mag

.

Relations based on known emission-line ratios are considered the best ones (see Williams 1994). Williams (1994) shows that He lines are excellent diagnostics of reddening in novae. This is because He λ4686 and H_β have similar wavelengths, as do He II Pk-α (λ10124) and H I Pδ (λ10049). Williams (1994) defines $R = (f_{H_\beta}/f_{P\delta})/(f_{\lambda 4686}/f_{Pk-\alpha})$, which is independent of extinction, the He/H abundance, and level of ionization of the gas. Hummer & Storey (1987) have made extensive calculations of the recombination spectra of H I and He II over a wide range of temperatures and densities and Williams (1994) shows that recombination spectra are not sensitive to T_e or N_e and should produce a value of $R \sim 4$ over a wide range of conditions. In my case (only when the NIR spectrum has been observed, therefore on Jun22) $R \sim 3.8$.

Interstellar extinction is derived by the following argument. Define $X_\lambda = A_\lambda/E_{B-V}$ to be the ratio of the total absorption at wavelength λ to the color excess of an object. The observed flux f of an emission line is related to the reddening corrected flux f_i by

$$f = f_i \times 10^{-0.4 X_\lambda E_{B-V}}$$

therefore, if one has two lines, 1 and 2, with observed fluxes, f_1 and f_2, reddening corrected

method	reference	E(B-V)
$(B-V)_{max}$	van den Bergh & Younger (1987)	0.43
$(B-V)_{t_2}$	van den Bergh & Younger (1987)	0.40
K1 λ7699	Munari & Zwitter (1997)	0.45
Dust maps	Schlegel et al. (1998)	0.58
H–lines	Williams (1994)	0.65
He–lines	Williams (1994)	0.57
H–lines	Hummer & Storey (1987)	0.38

Table 3.9: *Measured values for the reddening of Nova Sgr 2004.*

fluxes f_{1i} and f_{2i}, the reddening has the value

$$E_{B-V} = \frac{2.5}{X_2 - X_1} \log\left(\frac{f_{2i}}{f_{1i}}\frac{f_1}{f_2}\right) \tag{3.1}$$

Williams (1994) derives, for the lines mentioned above,

$$E_{(B-V)_{HI}} = 1.08 \log(17 f_{P\delta}/f_{H_\delta})$$

and

$$E_{(B-V)_{HeII}} = 1.01 \log(4.1 f_{Pk-\alpha}/f_{\lambda 4686})$$

Using the optical–NIR spectrum observed on Jun 22, I obtain $E_{(B-V)_{HI}} = 0.65$ mag and $E_{(B-V)_{HeII}} = 0.57$ mag. Using Formula 3.1 shown above, I could extend the method to other H lines observed in the optical–NIR spectrum, deriving $E_{B-V} = 0.38$ mag.

In the following I adopt the average value $E_{B-V} = 0.5 \pm 0.1$ mag.

After assuming the maximum magnitude obtained in Section 3 with the MMRD ($M_V = -8.7 \pm 0.2$ mag) and the average absorption derived above, I derive a distance to Nova Sgr 2004 of 10 ± 1 kpc. A complementary estimate of the distance has been obtained using the Buscombe-DeVauculeurs relation (all novae show the same magnitude 15 days after maximum) as from Capaccioli et al. (1989). This second estimate leads to 7900 ± 800 pc. After taking the average weight, I get $d = 8700 \pm 600$ pc. For $l = 3°.9$ and $b = -6°.3$, I find the nova to be located 870 ± 60 pc above the galactic plane

3.1.6 Physical parameters

Analysis of dereddened line fluxes is the only way to derive physical parameters of nova ejecta (e.g. masses and temperatures). Since ejecta are still evolving toward the nebular stage, the line ratios are not the ones expected from atomic transition probabilities. For example looking at Figure 3.7, the H_α/H_β ratio converges toward the theoretical value only after phase ~ 100.

A different explanation (also at later stages) is invoked for the case of [OI] $\lambda\lambda$6300,6364. This is a well known example of lines that does not respect the theoretical ratio $\sim$ 3:1. Williams (1994) interpreted this as due to large optical depth in the 6300Å line. He computes the hydrogen column density for an expanding shell mass of $1 \times 10^{-4} M_\odot$ and finds

$$N_H R = \frac{3M_{sh}}{4\pi m_H R^2} = \frac{3 \times 10^{52}}{R^2} cm^{-2}$$

If one assumes an oxygen abundance of O/H $= 5 \times 10^{-2}$ (Gehrz et al. 1993), λ6300 will be optically thick only when $R < 7 \times 10^{13}$ cm, which is satisfied for only the first week after the outburst, even if the ejecta were to be largely neutral. Since [O I] is usually observed for months after the outburst, it is virtually certain that the ambient density shell cannot provide the required column density, and thus the optically thick [O I] lines cannot realistically be produced in a homogeneous shell. Williams (1994) showed that the optical depth of that line can be derived from

$$\frac{j_{6300}}{j_{6364}} = \frac{1 - e^{-\tau}}{1 - e^{-\tau/3}} \tag{3.2}$$

Following this argument, I find τ_{6300} to be in the exrange 1.7 - 6.4, in good agreement with the values exhibited by other novae.

The fact that the [O I] lines are formed in the high–density limit in novae ejecta causes the intensity of the [O I] λ5577 to be comparable to that of λ6300 for realistic temperatures and therefore more easily detectable for use as a temperature discriminant (Filippenko & Halpern 1984, Osterbrock 1989). The critical densities for the $^1D_2$ and $^1S_0$ levels of O I are $N_e = 10^{6.5}$ cm^3 and 10^8 cm^{-3}, respectively, and for electron densities exceeding these values the volume emission coefficient of either forbidden line can be written

$$j_{21} = \frac{g_2}{g_1} N_{OI} A_{21} \frac{h\nu_{21}}{4\pi} \exp\Big(-\frac{\chi_{12}}{kT_e}\Big) \quad ,$$

where χ_{12} is the excitation potential of the excited state. Taking into account the finite

Date	j_{6300}/j_{6363}	τ	T_e(K)	$M_{\rm O\ I}$($M_\odot$)	$\frac{j_{4959}+j_{5007}}{j_{4363}}$	N_e(cm^{-3})
Jun 26	1.47	3.18	4234	5.03E-6	1.76	1.50E9
Jun 28	1.13	6.37	3570	2.447E-5	1.68	6.14E9
Aug 14	1.90	1.67	4139	9.145E-7	6.12	5.11E8
Sep 26	1.39	3.63	5707	4.81E-8	23.12	1.77E7

Table 3.10: *Physical parameters for Nova Sgr 2004:* O I $\lambda\lambda$6300/6363 *line ratios, optical depth in* λ6300 *(*τ_{6300}*), electron temperature,* O I *mass,* [O III] *line ratios and electron densities.*

optical depth of λ6300, the intensity ratio of the [O I] lines is then

$$\begin{aligned}\frac{f_{\lambda6300}}{f_{\lambda5577}} &= \frac{g(^1D_2)}{g(^1S_0)}\frac{A_{\lambda6300}}{A_{\lambda5577}}\frac{5577}{6300}\frac{1-e^{-\tau}}{\tau}\exp\Big(\frac{25000}{T_e}\Big)\\ &= 0.023\frac{1-e^{-\tau}}{\tau}\exp\Big(\frac{25800}{T_e}\Big).\end{aligned}$$

Solving for the temperature gives

$$T_e = \frac{11200}{\log[43\tau/(1-e^{-\tau})\times F_{\lambda6300}/F_{\lambda5577}]} \quad . \tag{3.3}$$

I find T_e to be between 3600 K and 5700 K.

The knowledge of the optical depth and electron temperature allow us to estimate the mass of oxygen in the ejecta using the 6300 Å line:

$$M_{OI} = 152 d_{kpc}^2 \exp\frac{22850}{T_e}\times 10^{1.05E(B-V)}\frac{\tau}{1-e^{-\tau}}F_{\lambda6300}M_\odot \quad . \tag{3.4}$$

This follows from the fact that the emission coefficient for the λ6300 line can be written as

$$j_{\lambda6300} = \frac{5}{9}N_{\rm O\ I}A_{\lambda6300}\frac{h\nu}{4\pi}\exp\Big(-\frac{22850}{T_e}\Big)$$

with T_e the electron temperature of the neutral gas. The mass of O I emitting gas is

$$M_{OI} = m_0\int_{\rm Vol} N_{\rm O\ I}dV \quad ,$$

and therefore the neutral oxygen mass can be related to the observed flux through relation 3.4, leading, in the case of Nova Sgr 2004 to $M_{\rm O\ I} = 2.4\times10^{-5} - 4.8\times10^{-8}M_\odot$.

Electron densities can be determined adopting the temperatures computed above and [OIII] line ratios as in Osterbrock (1989)

$$\frac{j_{4959}+j_{5007}}{j_{4363}} = 7.73\frac{e^{3.29\times10^{-4}/T_e}}{1+4.510^{-4}\frac{N_e}{T_e^{1/2}}} \tag{3.5}$$

Date	v_{ther}/v_{exp}	ϵ	M_H ($M_\odot$)
Jun 26	0.22	7.17E-2	3.00E-5
Jun 28	0.20	7.15E-2	4.07E-5
Aug 14	0.21	4.59E-3	6.37E-6
Sep 26	0.24	3.10E-4	5.72E-7

Table 3.11: *Physical parameters for Nova Sgr 2004: v_{ther}/v_{exp}, ϵ and the hydrogen mass.*

The use of the electron temperature derived for O I is justified since there is no observational evidence of ion (or element) stratification in nova ejecta (see Shara et al. 1997). The values I obtain are in the range 10^7 – 10^9 cm^{-3}, close to the upper limit of the critical densities to give rise to nebular and auroral lines. This is an indication that these lines likely arise from regions characterized by a relatively high density.

Hydrogen mass can be derived following Mustel & Boyarchuk (1970). The H_α line is given by

$$j_{H_\alpha} = g_\alpha \times n_e^2 \times \epsilon \times V \tag{3.6}$$

where g_α is the emission coefficient, n_e is the electron density, ϵ is the so-called "filling factor" (a measure of the clumpiness of the ejecta) and V is the volume that can be expressed as

$$V = 4\pi \times R^2 \times \delta \tag{3.7}$$

where the radius R can be obtained by simple expansion $v_{exp} \times \Delta t$ and $\delta = R\ v_{ther}/v_{exp}$ is assumed to be representative of the thickness of the shell. Deriving v_{exp} from the Full Width at Half Maximum (FWHM) of Balmer lines ($\sim$ 2000 Km s^{-1}) and $v_{ther} = \sqrt{3kT/m_e}$ ($\sim$ 400 Km s^{-1}) it follows that $\delta \sim 0.2 \times R$ (see, e.g. $\delta = 0.5 \times R$ for the slow nova FH Ser 1970, Della Valle et al. 1997). Solving Equation 3.6 for ϵ,

$$\epsilon = \frac{j_{H_\alpha} d^2}{g_\alpha n_e^2 V} \tag{3.8}$$

I find that the filling factor spans a range of 7.2×10^{-2} – 3.1×10^{-4}. Finally, I can determine from

$$M_H = n_e m_H 4\pi R^3 \epsilon \frac{v_{ther}}{v_{exp}} \tag{3.9}$$

values of M_H to be $\sim 4.1 \times 10^{-5} - 5.7 \times 10^{-7} M_\odot$.

The derived physical parameters are summarized in Tables 3.10 and 3.11.

3.2 Summary and conclusions

Nova Sgr 2004 is an FeII nova that occurred in the bulge of the Milky Way. The rate of decline characterizes Nova Sgr 2004 as a borderline object between the fast ($t_2 < 12$days) and slow ($t_2 > 12$ days) classes (DellaValle & Livio 1998). These authors have shown that He/N and FeIIb (i.e. Fe II broad) novae belong to the fast class and are preferentially concentrated towards the galactic disc, i.e. at small z above the galactic plane ($z < 200$ pc), while FeII novae belong to both slow and fast classes and they are observed both in the disk and in the bulge, extending up to $\sim 1kpc$. Nova Sgr 2004 located at about 0.9 kpc above the galactic plane in the direction of the galactic bulge is an Fe II nova which does not represent an exception to this scenario (Della Valle et al. 1992).

Spectroscopic observations show a dramatic change in the overall appearance of the spectrum of the nova at about 30 days after maximum light (in coincidence with the entrance in the "auroral phase"): permitted lines start fading at a different rate, P-Cyg profiles disappear, velocities reach a "plateau" phase, and $U - V$ and $J - K$ colors increase. The lack of detection of [Ne III] line points at a "standard" evolution of the nebular spectrum (see Williams et al. 1994).

The rather high values of optical depth in the OIλ6300 suggest very high densities for the zones of the ejecta where these lines are formed. I have derived the filling factor in the range $\sim 7.2 \times 10^{-2}$ to 3.1×10^{-4}. Comparing these values with other values reported in the literature (see Table 3.12), two facts emerge: a) the filling factors in nova ejecta are definitely smaller than 1, likely close to 0.1, during the early stages; b) these values decrease by 1–3 orders of magnitude with time. This fact indicates that the volume of the expanding shell (computed with 3.7) is increasing with time more rapidly than the volume actually occupied by most of the ejected material. In other words, the decreasing trend exhibited by the filling factor suggests that the ejected matter tends to remain clumped in sub–structures having higher density than the average density characterizing the expanding shell.

Computed oxygen and hydrogen masses are in the ranges $2.4 \times 10^{-5} - 4.8 \times 10^{-8} M_{\odot}$ and $4.1 \times 10^{-5} - 5.7 \times 10^{-7} M_{\odot}$. This high mass ratio is close to the upper limit for Classical Novae shown in Warner (1995).

Nova	Filling factor value	Reference
T Pyx	10^{-2}–10^{-5}	Shara et al. (1997)
Nova Vel 1999	0.1	Della Valle et al. (2002)
Nova SMC 2001	$0.1 - 10^{-3}$	Mason et al. (2005)
Nova LMC 2002	$10^{-2} - 10^{-4}$	Mason et al. (2005)
Nova Sgr 2004	$7.2 \times 10^{-2} - 3.1 \times 10^{-4}$	***this work***

Table 3.12: *Comparison between filling factors in literature*

3.3 RR Pic: an old nova

3.3.1 Introduction

RR Pic is an old nova which erupted in 1925 (Spencer Jones 1931) and hence is well in its quiescence state by now. The binary is partly eclipsing and its orbital period of 0.145025 days places it just above the gap of the period distribution of cataclysmic variables. Recent time-resolved spectroscopy taken with the B&C at the 1.52 ESO telescope on La Silla has confirmed the presence of an additional emission source on the leading side of the disc (Schmidtobreick et al. 2003b). They also found high velocity line wings moving with the orbital period but shifted by 0.4 phases. However, there is an offset of $\Delta\phi = 0.53$ between the zero-phase measured from radial velocities and the extrapolated eclipse phase from 1970 and 1984. A later analysis (Schmidtobreick et al. 2005) revealed that this offset is varying in time, which could hint at a change of the orbital period. However, since the radial velocities are most likely influenced by the isolated emission sources in the disc, also a variable emission structure in the disc of RR Pic might explain these variations.

3.3.2 The light curves

Time-resolved V-photometry was done using the 1m-telescope at CTIO-Chile. The data presented here were taken in 2005 between Feb 07 and Apr 10 and cover about 18 cycles with a time resolution of 40 s. The details of the observations are given in Table 3.13. The reduction was done with IRAF and included the usual steps of bias subtraction and division by skyflats.

Aperture photometry for all stars on the CCD field was computed using the stand–alone version of DAOPHOT and DAOMASTER (Stetson 1992). Differential light curves were

Date	UT	$\#_{\mathrm{exp}}$	t_{exp} [s]	cycles	ID
2005-02-08	00:45:44	483	20	2.03	1
2005-02-09	01:17:57	533	20	1.76	1
2005-02-10	01:17:23	495	20	1.63	1
2005-02-11	01:13:37	530	20	1.74	1
2005-02-12	01:09:17	540	20	1.77	1
2005-02-13	01:07:03	499	20	1.79	1
2005-02-14	01:06:42	534	20	1.76	1
2005-03-18	01:36:23	240	20	0.80	1
2005-03-20	01:03:17	320	20	1.08	1
2005-03-25	02:31:58	80	20	0.26	2
2005-03-26	00:24:42	320	20	1.06	2
2005-03-26	23:58:29	329	20	1.15	2
2005-03-31	00:38:39	241	20	0.92	2
2005-03-31	03:52:05	56	20	0.18	1
2005-04-09	23:29:27	318	20	1.06	2

Table 3.13: *Summary of observational details: Date & UT at the start of the first exposure, the number of exposures, the individual exposure time, the covered orbital cycles and the acquisition ID are given.*

established with respect to an average light curve of those comparison stars, which were present on all frames and checked to be non–variable. While the original idea was to use the same comparison stars for all epochs, we had to settle for two sets of comparison stars, as some of the later data were taken with a different acquisition. The first set included five, the second set six comparison stars (see Table 3.13). The difference in magnitude between the two sets were established from three common stars as 0.31. The magnitudes of the second set were shifted accordingly.

Apart from the hump-like variability, they show the strong flickering and random variation typical for RR Pic. We do not find any convincing evidence for an eclipse in any of the lightcurves. The average light curve is plotted in Figure 3.12. The extrapolated eclipse phase coincides with a broad minimum, but comparing the overall shape of the light curve suggests that the eclipse should actually be located around phase 0.2, where a small minimum is presentin the average curve. This phase offset points towards a change in the orbital period. The Scargle periodogram (Scargle 1982), yields an orbital period $P = 0.1449(5)$ d, which is not yet precise enough to measure the small change of 10^{-4} needed to explain the phase shift. Some data taken later in the year will help to increase the accuracy to decide if a change of orbital period took place in RR Pic during the last decades (Schmidtobreick et al. 2006).

To search for superhumps, we have subtracted the average light curve from the individual data points. A clear signal is present in the Scargle periodogram of the resulting differential light curve at a period of $P = 1.577(6)$ d. Interpreted as a beat period between orbital and precession period, it yields a precession period of 1.8 d which is also present in the periodogram. The differential light curve averaged over the 0.1577 d period shows a clear hump, shich we thus interpret as a superhump. Using the empirical formula $\epsilon = 0.22 \times q$ with $\epsilon = \frac{P_{SH} - P_{orb}}{P_{orb}} = 0.0862$ we find a mass ratio $q = 0.4$. Although this value is rather high, it is not unlikely for a high transfer novalike.

3.3.3 Doppler tomography

Time resolved spectroscopy was obtained with EMMI on the NTT at ESO/La Silla on Jan 31 – Feb 02 2004. The echelle mode with grating #9 centered on 5200Å, yielded a resolution of 0.7Å and allowed to use the strong emission lines H_α,H_β, and HeII (4686 Å) for Doppler tomography techniques. We here use the code of Spruit (1998) with a MIDAS interface replacing the original IDL routines (Tappert et al. 2003).

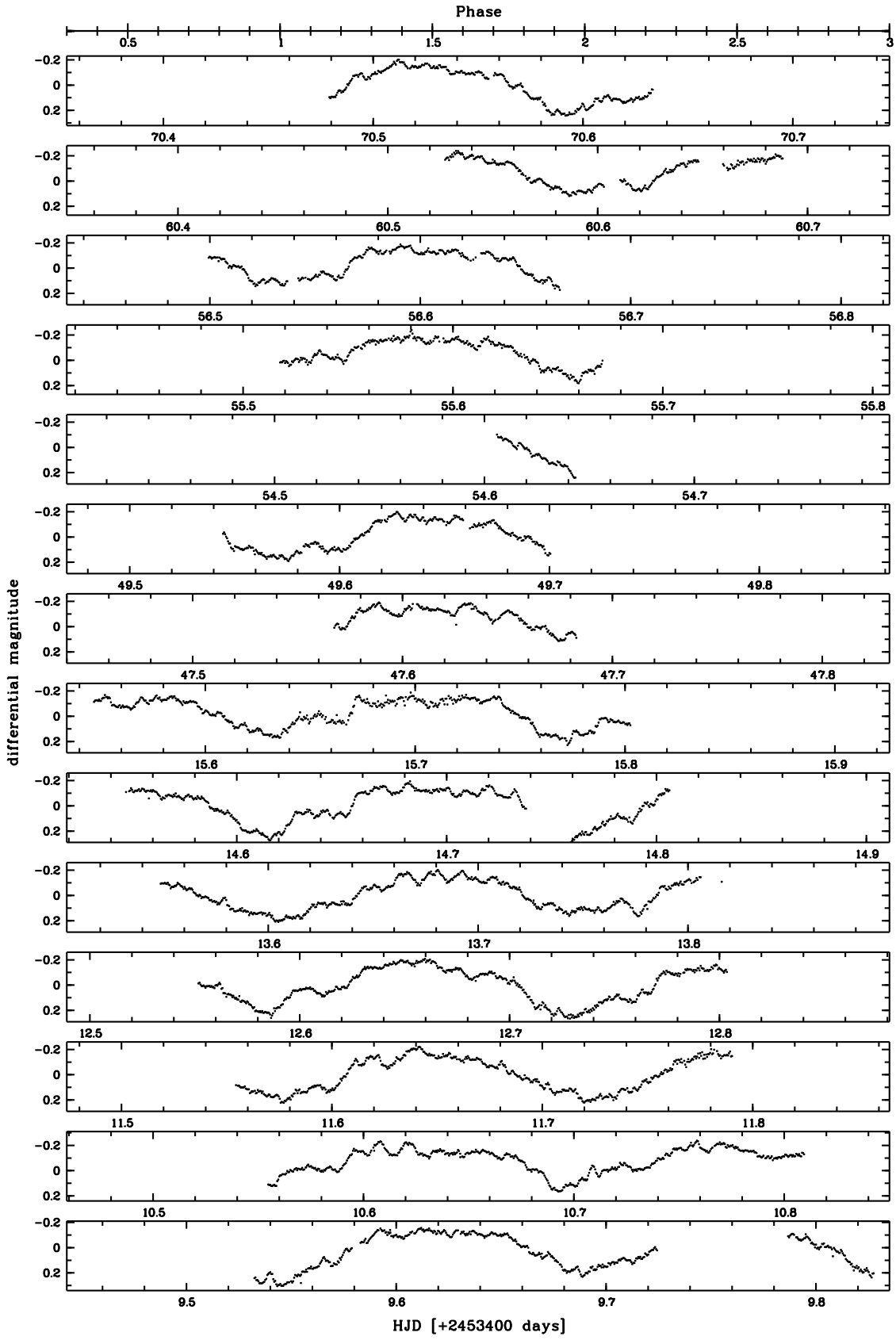

Figure 3.10: *The lightcurves of RR Pic. The phase refers to the orbital period of* $P = 0.145025\,d$*,* $\phi = 0$ *corresponds to the eclipse–ephemeris as defined by Schmidtobreick et al. (2005).*

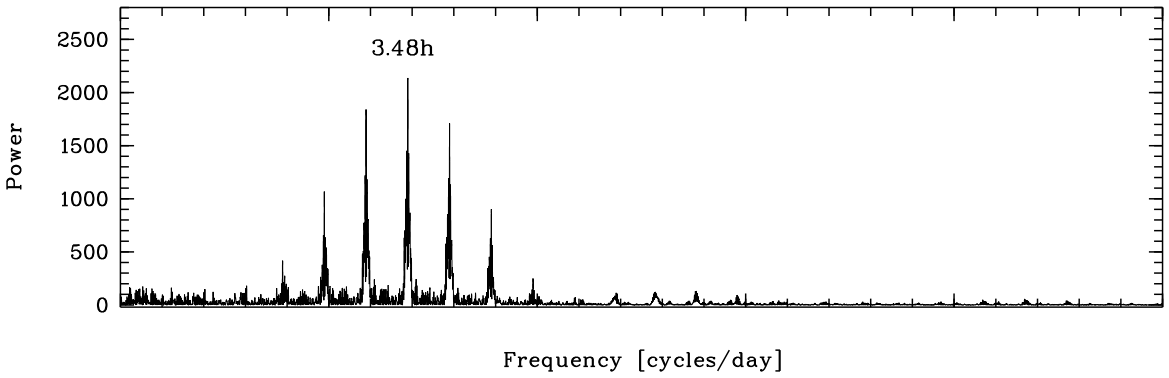

Figure 3.11: *The Scargle–diagram for the data. The period of 3.48 h is clearly indicated by the maximum peak.*

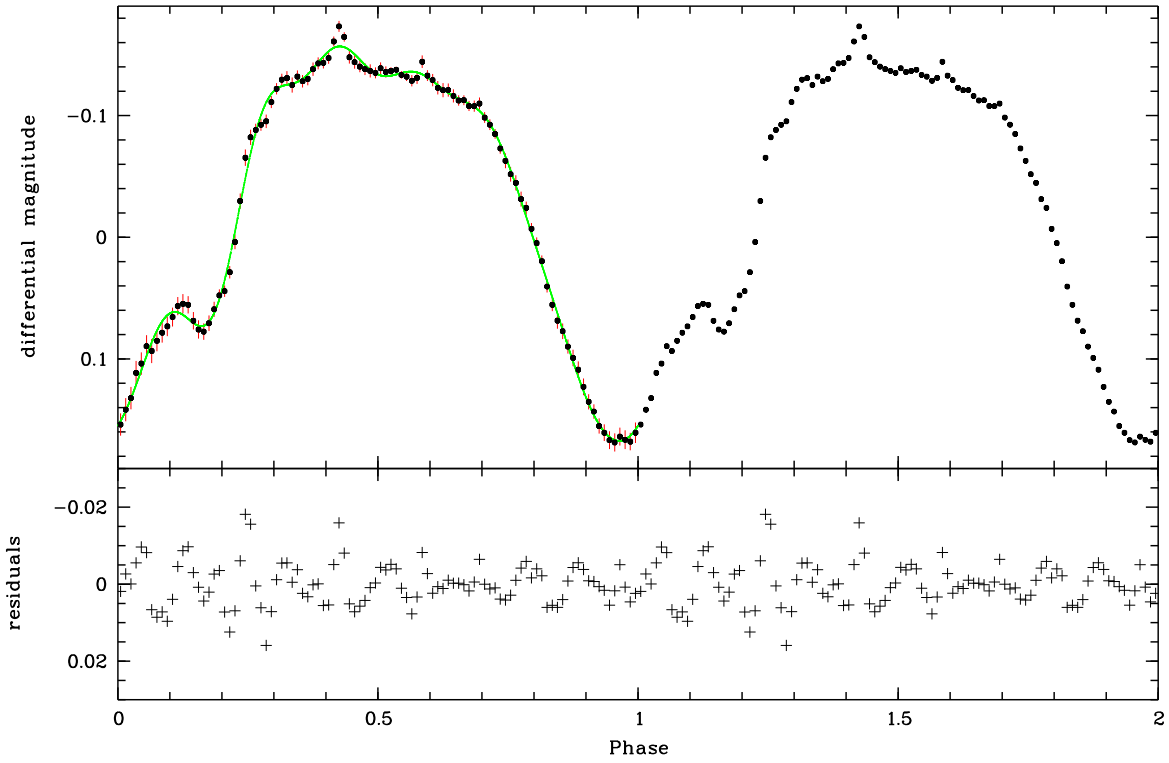

Figure 3.12: *The average differential V–magnitude of RR Pic is plotted against the phase using the period $P = 0.1450$ d. The zero-phase was chosen to correspond to the eclipse–ephemeris as defined by Schmidtobreick et al. (2005). On the first half, the errorbars are over–plotted, and the fit using the orbital period and its harmonics (see text for details) is given as a line. Below, the residuals of fit and average lightcurve are plotted.*

The Doppler maps $I(v_x, v_y)$ are given in Figure 3.15. They display the flux emitted by gas moving with the velocity (v_x, v_y) and thus show the emission distribution in velocity

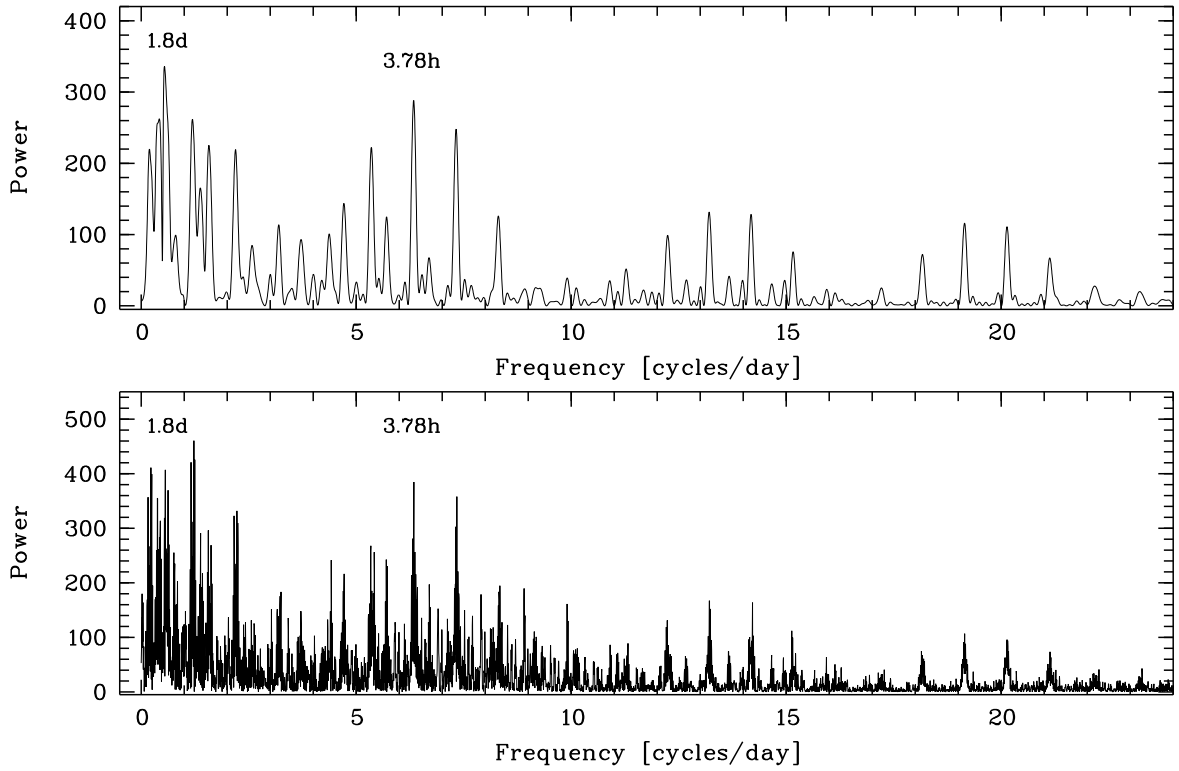

Figure 3.13: *The Scargle–diagram for the data minus the average lightcurve. A new peak becomes visible indicating a period of 3.78 h in the data.*

coordinates with the center of mass at (0,0).

In general, we note that the emission distribution is rather unstable. The maps in H_α show a ringlike feature with is commonly interpreted as emission from the accretion disc. However, the ring is patchy. Apart from the always present emission source around phase 0.9, which we attribute to a hot spot, additional emission sources appear around 0.75 and 0.5. The map of the old data (Schmidtobreick et al. 2003b) resembles the emission distribution on Feb 01. The maps in H_β more or less follow the behaviour in H_α but are more noisy due to the weaker emission line. The He II maps instead show a different structure. They are clearly dominated by an elongated emission close to zero velocity which points towards a weak emission region at phase $\phi_r \sim 0.5$, the latter coinciding with the emission source present in H_α. The hot spot emission is only marginally present in He II. We do not find any evidence for disc emission in this line.

It is therefore well possible that this variation of the emission distribution distorts the line profile in such a manner that the phase offset between radial velocities and photometry varies in the order of $\delta\phi \sim 0.3$. Although other effects cannot be excluded, this could already

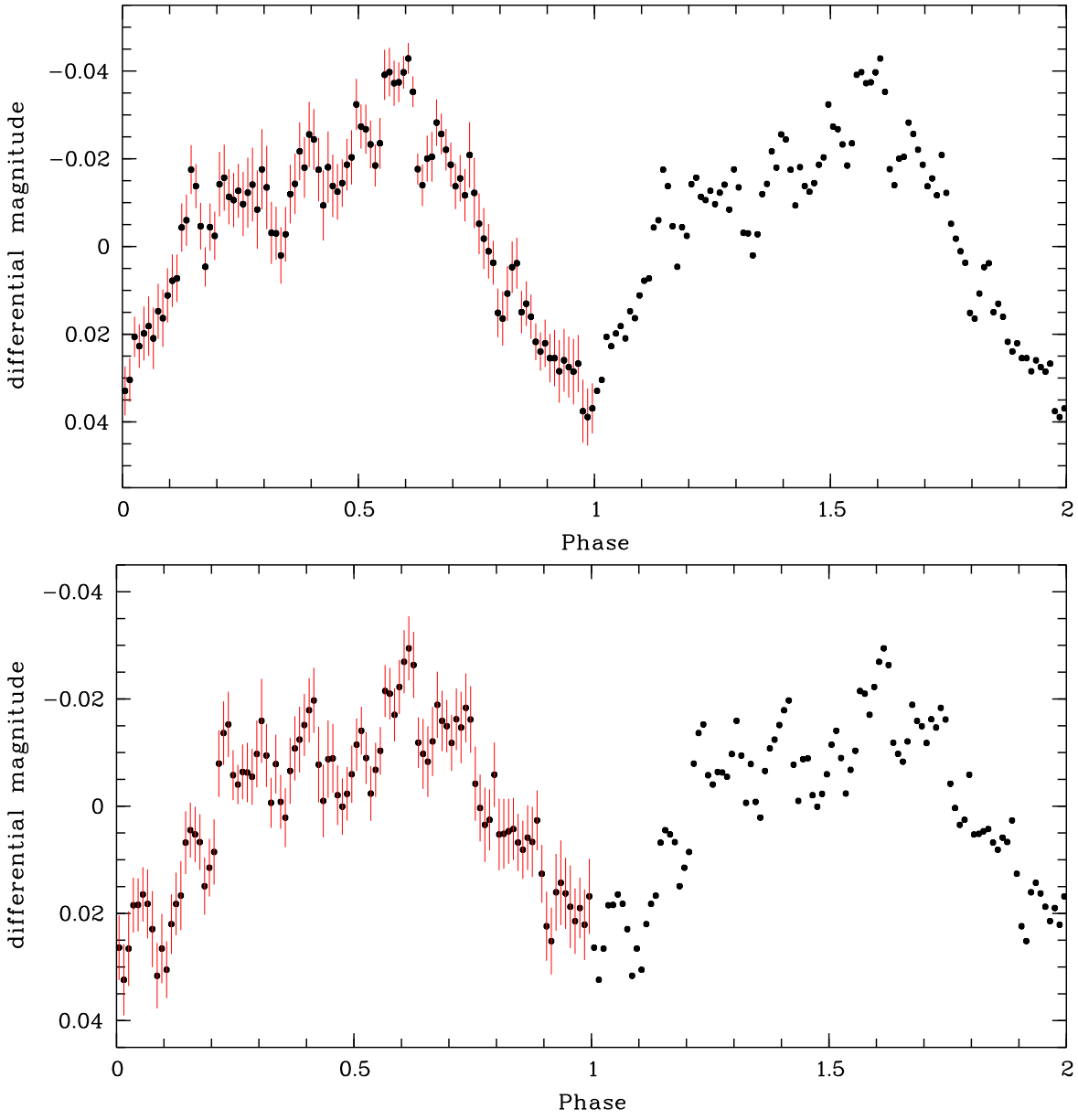

Figure 3.14: *The average differential V–magnitudes of RR Pic, of which the average orbital variation were subtracted, are plotted against the phase using the period* $P = 0.1577\,d$.

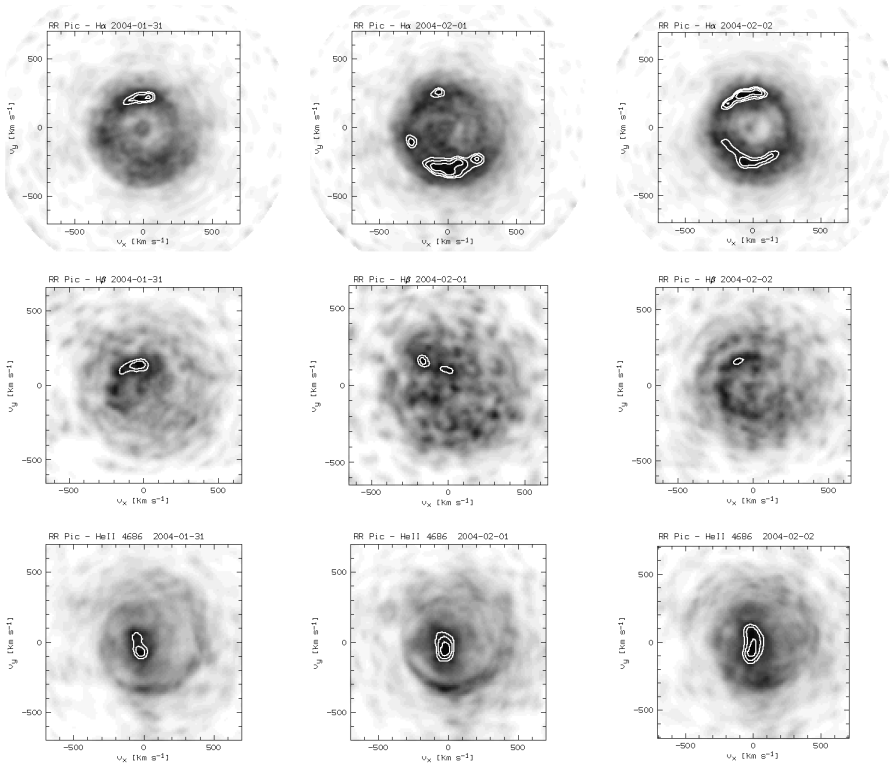

Figure 3.15: *The Doppler maps in Hα (upper row), Hβ (middle row) and HeII (lower row) on three consecutive nights (from left to right). The contours plotted refer to 90%, 85% and 80% of the maximum value, which has been normalised for all maps.*

cause the observed mismatch.

3.4 Attempt of photometric recovery of four Old Novae

A lot of studies have been carried out on CNe during outburst but still a lot of work has to be done on CN progenitors. In this work we attempt the recovery for four old novae and we give tentative identifications for 2 of them.

3.4.1 Introduction

Light from CVs is basically due to three components. The white dwarf mainly contributes in the UV, the secondary star in the red and infra-red while the optical range is dominated by the accretion disk (see Section 1.1). Due to this composition, CVs are usually extremely blue objects with respect to main sequence stars. Therefore, following Schmidtobreick et al. (2003a), one can plot color-color diagrams of regions were old novae are supposed to be

found.

3.4.2 Observations and data analysis

Four fields have been observed in three nights with the New Technology Telescope (NTT) at La Silla (Chile) with the SUperb Seeing Imager 2 (SUSI2) under very poor weather conditions.

Standard reduction has been carried out with `IRAF`[2]. PSF-photometry has been carried out with the `DAOPHOT` package in `IRAF`. U-band observations proved to be not long enough in order to reach the magnitudes where the old novae were supposed to be found.

3.4.3 Discussion

3.4.4 LZ Mus

LZ Mus was discovered by Liller (1998). Maximum light was observed by Farrell et al. (1999). They found V=9.4 mag on Jan 1.12,1999 UT. Not enough photometry is available to derive a rate of decline and colours at maximum are unknown. Therefore, there is no way to derive the distance to this object. This means that we cannot make assumptions on the luminosity of this object today.

Color-color diagrams (shown in Figure 3.17) have been obtained selecting all those objects with photometric errors < 0.05 mag. No object noticeably bluer than the others is clearly visible.

3.4.5 EL Aql

EL Aql was discovered by Wolf (1927). Maximum observed magnitude was 6.4 on 1927 Jun15 (Duerbeck 1987). Duerbeck (1987) reports $t_3 = 25$ days. We can use the relations from Capaccioli (1990) to convert t_3 into t_2: $t_2 = (t_3 - 1.9)/1.68$ (if $t_3 < 80$ days) and $t_2 = (t_3 - 2.3)/1.68$ (if $t_3 > 80$ days). Therefore $t_2 \simeq 14$ days. Applying the Maximum Magnitude vs. Rate of Decline relationship from Della Valle & Livio (1995) we find a maximum magnitude at maximum $V \sim -8.44$. This leads to a distance of $d = 10^{0.2(m-M+5-A)}$. Assuming an $E_{B-V} = 1.231$ (from Schlegel et al. 1998), we find $A_V = 4.080$ mag and therefore $d \sim 1.42$ kpc.

[2]IRAF (Image Reduction Analysis Facility) is distributed by the National Optical Astronomy Observatories, which are operated by the Association of Universities for Research in Astronomy, Inc., under cooperative agreement with the National Science Foundation.

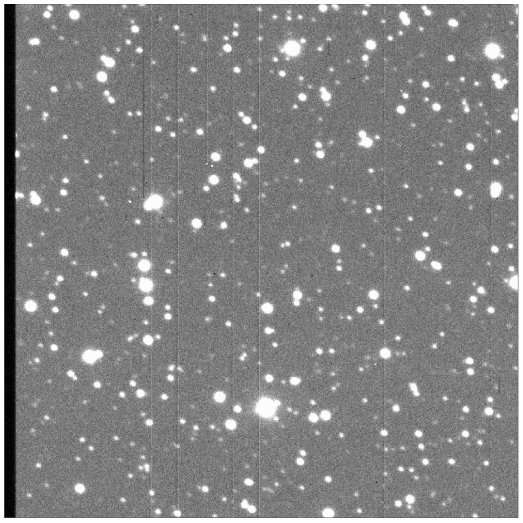

Figure 3.16: *The field ($1' \times 1'$) centered on the position of LZ Mus reported by Farrell et al. (1999)*

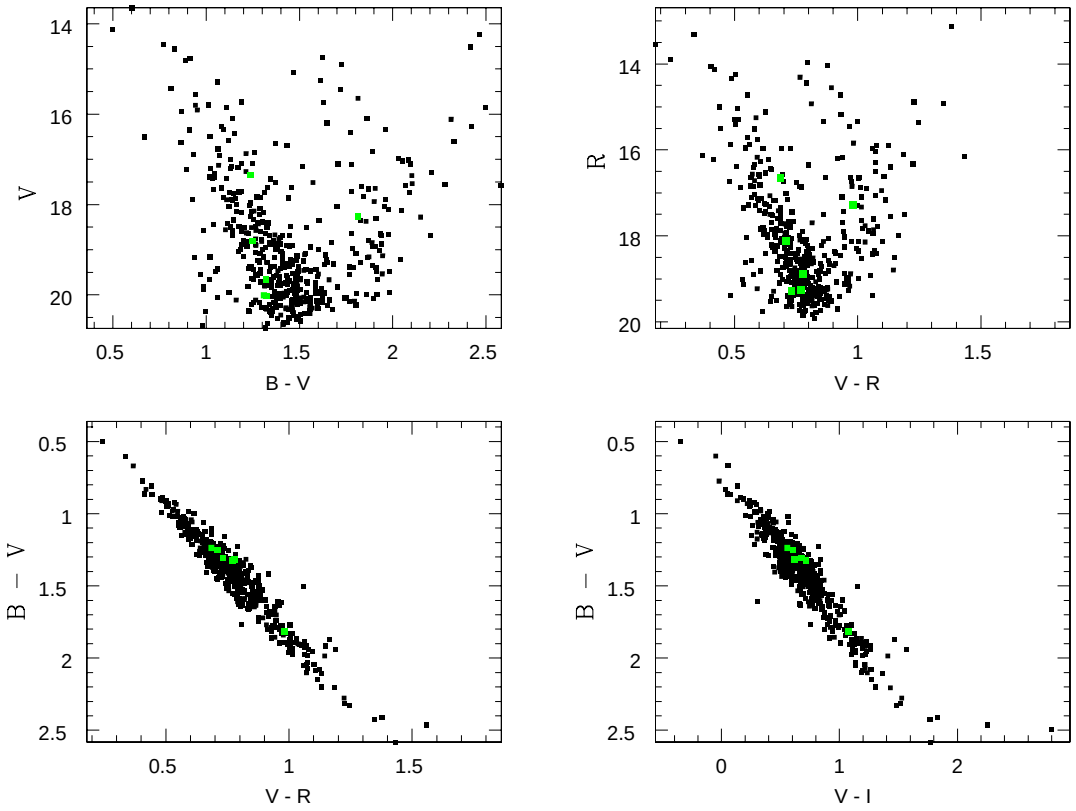

Figure 3.17: *Color-color diagram for the region of LZ Mus. In green are shown the stars that are in a $1' \times 1'$ box centered on the expected position.*

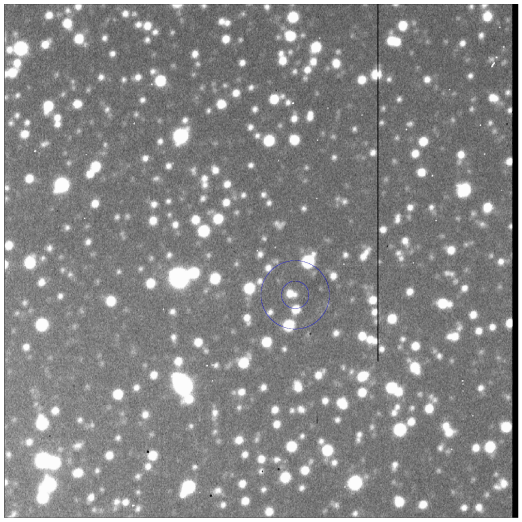

Figure 3.18: *The field ($1' \times 1'$) centered on the position of EL Aql reported by Farrell et al. (1999)*

Since old novae are observed to have absolute magnitudes at minimum light 3.4 – 4.4 (Warner 1995 his Table 4.6), assuming the distance computed above, EL Aql could have a magnitude of 18.24 – 19.24.

Color-color diagrams (shown in Figure 3.19) have been obtained selecting all those objects with photometric errors < 0.03 mag.

Three objects have been found to lie above the main sequence and still be inside a $1' \times 1'$ box. The one which is closest to the expected position is shown in Figure 3.18.

3.4.6 MU Ser

MU Ser has been discovered by M.Wakuda on 1983 Feb23 (Wakuda 1983). The progenitor is not seen on Palomar plates, therefore it must be fainter than $B \sim 20$ mag. Schlegel et al. (1985) note that the maximum magnitude must have been at least ~ 7.8 mag. They also give values for $t_2(5.3 \pm 1.6$ days) and $M_V(\sim 9.9 \pm 0.5$, even if -9.9 sounds more reasonable). Distance is shown to be $18.2^{+6.5}_{5.4}$ kpc.

From their distance, a rough estimate for the magnitude of the progenitor is 21.1 – 22.1.

Color-color diagrams (shown in Figure 3.21) have been obtained selecting all those objects with photometric errors < 0.05 mag.

One object is observed to be out of the main sequence (see Figure 3.21), therefore that is our candidate (finding chart in Figure 3.20).

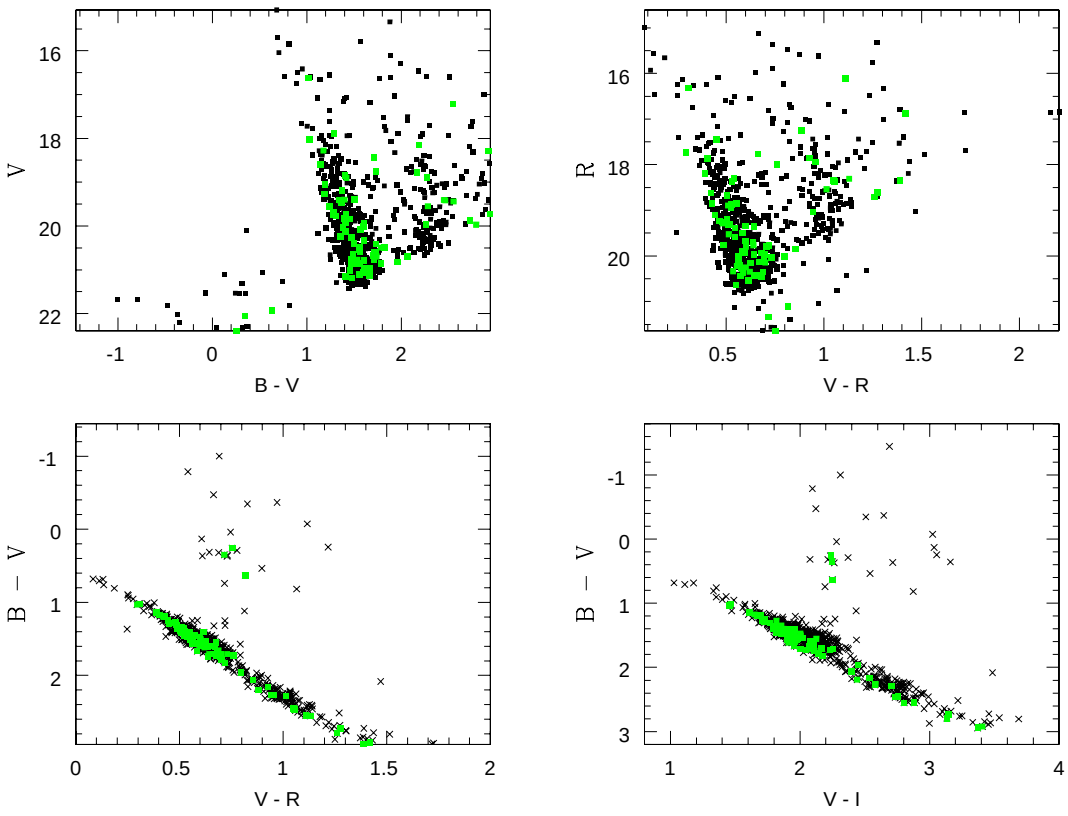

Figure 3.19: *Color-color diagram for the region of EL Aql. In green are shown the stars that are in a* $1' \times 1'$ *box centered on the expected position.*

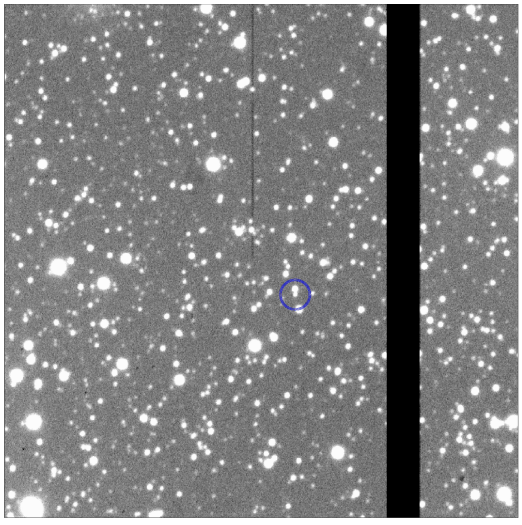

Figure 3.20: *The field* $(1' \times 1')$ *centered on the position of MU Ser reported by Duerbeck (1987)*

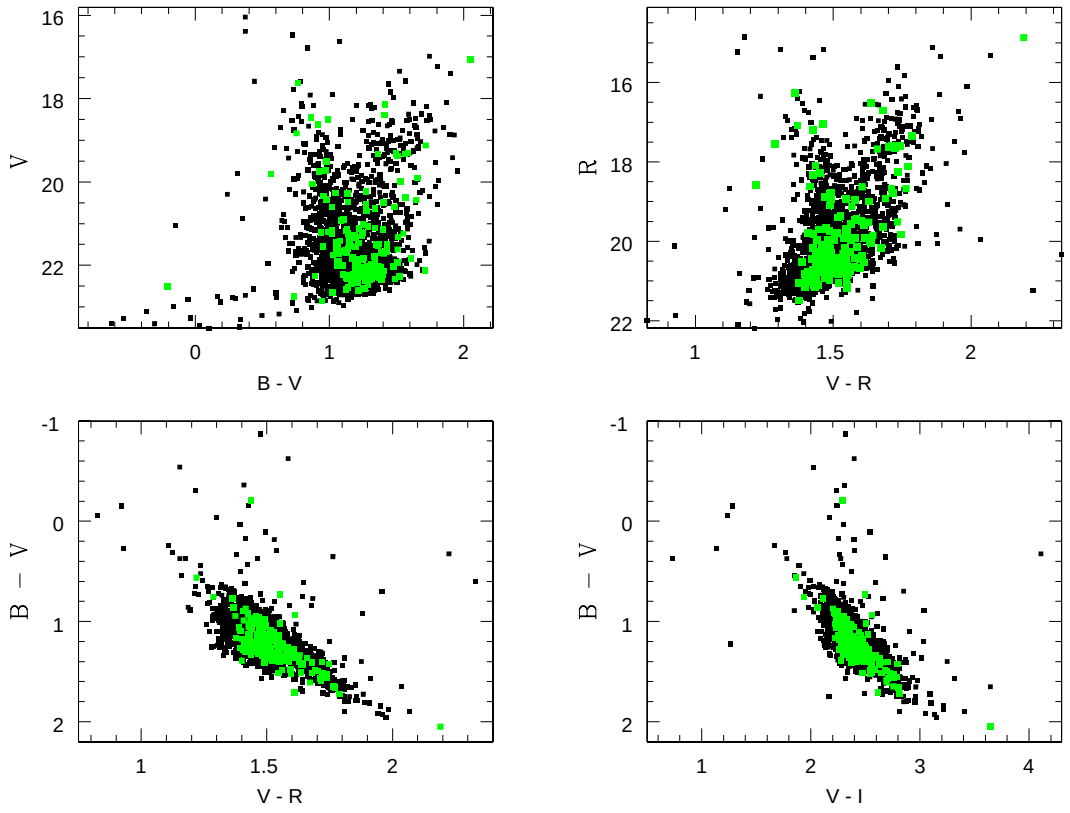

Figure 3.21: *Color-color diagram for the region of MU Ser. In green are shown the stars that are in a* $1' \times 1'$ *box centered on the expected position.*

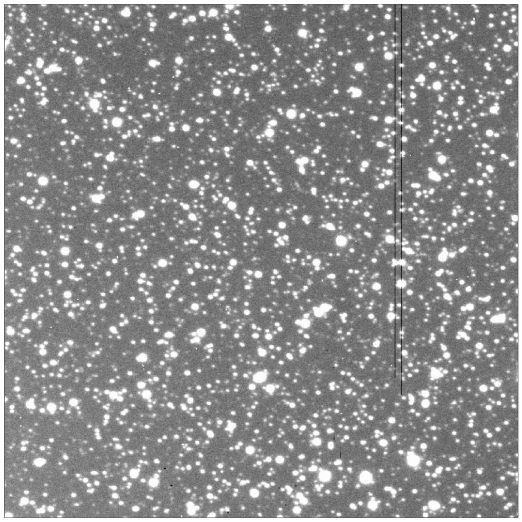

Figure 3.22: *The field ($1' \times 1'$) centered on the position of V2264 Oph reported by McNaught (1991)*

3.4.7 V2264 Oph

V2264 Oph was discovered by Bateson et al. (1991). These authors proposed this object to be either a classical nova or a dwarf nova in outburst. Wagner et al. (1991) reported this object to be a Mira variable. This chance was ruled out by McNaught (1991) who noted that no object brighter than 21 mag was observed on the SERC J,I and R ESO B and R and Palomar B and R surveys. The same author also provided good coordinates. The spectrum, according to Wagner et al. (1991), showed Balmer emission lines as well as other permitted lines. FWHM of H_α is about 2300 km/s.

As for LZ Mus, not enough photometry is available to derive a rate of decline and colours at maximum are unknown. Therefore there is no way to derive the distance from this object. This means that we cannot make assumptions on the luminosity of this object today. Even if, having been $\sim$10 mag at maximum, it is unlikely to be brighter than 23 mag now.

Color-color diagrams (shown in Figure 3.23) have been obtained selecting all those objects with photometric errors < 0.1 mag. No object clearly stands out of the main sequence.

3.4.8 Summary and conclusion

We tried to mimic the same successful technique used by Schmidtobreick et al. (2003a). We managed to give tentative identification for 2 out of 4 old novae.

We are not confident with magnitudes in an "absolute" sense but differential magnitudes

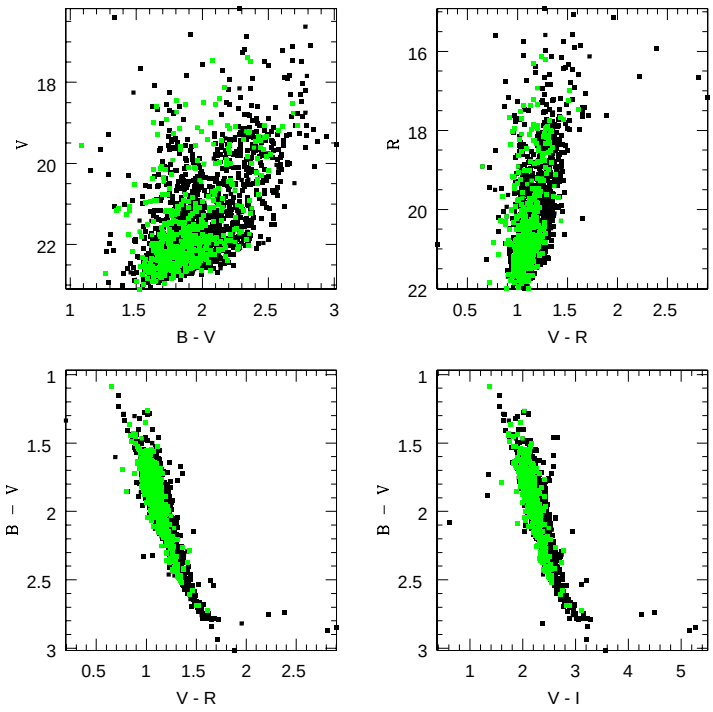

Figure 3.23: *The field ($1' \times 1'$) centered on the position of V2264 Oph reported by McNaught (1991)*

are supposed to be correct.

We do not provide spectroscopic confirmation for the recovered objects. Spectroscopic observations will follow.

Chapter 4

Summary, conclusions and perspectives

4.1 Summary and conclusions

In this thesis, I have investigated a wide range of observational properties of both galactic and extragalactic novae. In particular I have carried out a survey to discover new nova systems in galaxies: ellipticals and spirals.

I have analyzed six spiral galaxies (NGC 3627, NGC 3982, NGC 4496, NGC 4527, NGC 4536, NGC 4639) from the HST archive and I have observed two early type galaxies (NGC 4621 and NGC 4374) with the Very Large Telescope (VLT, European Southern Observatory, Cerro Paranal, Chile).

Our main results relative to this survey can be summarized as follows:

- I did not find any nova in the spiral galaxies. This is in good agreement with the low number of novae expected in this kind of galaxy.

- I found 3 novae in the radio-loud galaxy NGC 4374 and 2 in the radio-quite galaxy NGC 4621.

- By analyzing the nova rate in these two galaxies plus the nova rate already observed in other systems, I concluded that early type galaxies do **NOT** show a relation between radio emission and normalized nova rate. This is at variance with what happens for Type Ia supernovae, which instead do show such a correlation. As a consequence of this, two conclusions may arise: either part of the type Ia supernovae is produced in double-degenerate systems rather than in single-degenerate ones, which are the progenitors of

novae, or classical novae and supernovae arise from the same progenitor model but from white-dwarfs with different masses.

- A theoretical modelling of the elliptical galaxies NGC 4374 and NGC 4621 has been able to reproduce successfully the photometric and chemical properties reported in the literature. To reproduce the nova rate I had to put constrains on the αn product (where α is the ratio of binary systems that can undergo a CN outburst and n is the number of outbursts during the lifetime of a CN system). If α is the same as in the Milky Way, $n \sim 10^3$ thus supporting long time between two outbursts in the same CN system as predicted by the "hibernation scenario"

I also studied in detail the properties of two specific nova systems (Nova Sgr 2004 and RR Pic):

- Nova Sgr 2004 was the brightest nova of 2004. I collected a large amount of data. The nova showed to be a rather normal FeII with an intermediate rate of decline. It also showed a very low filling factor like other novae in the literature, thus suggesting that ejected material is clumped in substructures characterized by higher density than the average ρ of the shell.

- Observations of the very old nova (RR Pic) show that this system may have changed its period over the last few decades. Hints of a superhump are also observed. It has also been shown that hydrogen and helium, as expected, arise from different parts of the accretion disc.

Finally, by means of the New Technology Telescope (NTT) at Cerro La Silla, Chile, I observed four stellar fields in the Milky Way where four novae already exploded . Our aim was to test the "hibernation scenario". I managed to recover photometrically 2 out of four of the studied systems which do not allow to draw firm conclusions.

4.2 Perspectives

New determinations of nova rates are still required.

Nova Sgr 2004 data were obtained during the La Silla Target of Opportunity campaign. During the last two years, this campaign has monitored (from maximum light to nebular stage) a dozen of novae.

The hunt for old nova systems is supposed to shed light on the evolution of the nova system between two outbursts. Most importantly, this is supposed to put constraints on the possibility of CNe to become SNeIa and on the "hibernation scenario".

Modelling of the nova phenomenon via the Monte-Carlo approach is only beginning. Several density and velocity laws are to be tested. Data from the Cerro Tololo Nova Survey and from the La Silla Target of Opportunity campaign are already available. This will give us the unique opportunity to derive abundances in CNe as it has never been possible so far.

Bibliography

Arimoto, N., & Yoshii, Y., 1987, A&A, 173, 23

Baade, W. 1944, ApJ, 100, 137

Baade, W. 1957, Obs., 77, 165

Baade, W. 1958, Ric. Astr. Specola Vaticana, 5, 165

Bateson, F. M., Gilmore, A. C., Camilleri, P., Kilmartin, P. M., Wagner, M., Hunter, P. M., Seargent, D. A. J., Jones, A., Lester, D., Williams, P. 1991, IAUC 5238, 2

Bath, G. T. & Shaviv, G. 1976, MNRAS, 1975, 305

Bath, G. T. & Shaviv, G. 1978, MNRAS, 183, 515

Bianchini,A., Tappert,C., Osborne,H., Canterna,R., Tamburini,F. 2001

Biretta, J. et al. 2001, WFPC2 Instrument Handbook, ver. 6.0 (Baltimore: STScI)

Bruzual, G. & Charlot, S. 2003, MNRAS, 344, 1000

Buscombe, W. & de Vaucouleurs, G. 1955, Obs., 75, 170

Burstein, D., Faber, S. M., Gaskell, C. M., Krumm, N. 1984, ApJ, 287, 586

Calura, F., Matteucci, F., Vladilo, G. 2003, MNRAS, 340, 59

Capaccioli, M., Della Valle, M., Rosino, L., D'Onofrio, M. 1989, AJ, 97, 1622

Capaccioli, M. 1990, ApJ, 360, 63

Cassatella, A. , Lamers, H. ,Rossi, C. , Altamore, A. , González-Riestra, R. 2004, A&A, 420, 571

Cecchini, G. & Gratton, L. 1942, Le Stelle Nuove, ed. U. Hoepli, Milano

Chiappini, C., Matteucci, F., Romano, D. 2001, ApJ, 554, 1044

Ciardullo, R., Shaefer, A. W., Ford, H. C., Neill, J. D., Shara, M. M., Tomaney, A. B. 1990, ApJ, 292, 90

Cohen, J. G. 1985, ApJ, 292, 90

Darnley,M.J. 2006 MNRAS *in press*

D'Antona, F.& Matteucci, F. 1991, A&A, 248, 62

Della Valle, M. 1991, A&A, 252, 9

Della Valle,M. 2002, AIPC, 637, 443

Della Valle, M., Bianchini, A., Livio, M., Orio, M. 1992, A&A, 266, 232

Della Valle, M., Duerbeck, H. 1993, A&A, 271, 175

Della Valle, M., Rosino, L., Bianchini, A., Livio, M. 1994, A&A, 287, 403

Della Valle, M., Livio, M. 1995, ApJ, 452, 704

Della Valle, M. & Livio, M. 1998, ApJ, 506, 818

Della Valle, M., Ederoclite, A., Schmidtobreick, L., Germany, L., Dall, T., Saviane, I. 2004, IAUC, 8307

Della Valle, M., Gilmozzi, R. 2002, Science, 296, 1275

Della Valle, M., Gilmozzi, R., Bianchini, A., Esenoglu, H. 1997, A&A, 325, 1151

Della Valle, M., Panagia, N., Padovani, P., Cappellaro, P., Mannucci, F., Turatto, M. 2005, ApJ, 629, 750

DellaValle, M., Pasquini, L., Daou, D., Williams, R. E. 2002, A&A, 390, 155

de Vaucouleurs, G., de Vaucouleurs, A., Corwin, H. G., Buta, R. J., Paturel, G., Fouqué,P. 1991, *Third reference catalog of bright galaxies (RC3)*, Springer-Verlag, New York

Downes,R.A., Duerbeck,H.W. 2000, AJ, 120, 2007

Downes, R. A., Webbink, R. F., Shara, M. M., et al. 2001, PASP, 113, 764

Duerbeck, H. W. 1981, PASP, 93, 165

Duerbeck, H. W. 1987, SSRv, 45, 1

Duerbeck, H. W. 1990, IAU Coll. 122, Physics of Classical Novae, eds. Cassatella & Viotti (Springer Berlin), p.34

Ederoclite et al., A&A, *submitted*

Ederoclite, A., Mason, E., Della Valle, M., Gilmozzi, R., Williams, R. E. 2005, ASPC, 330, 435

Faber, S. M., Friel, E. D., Burstein, D., Gaskell, C. M. 1985, ApJS, 57, 711

Farrell, F., Holvorcem, P., Garradd, G. 1999, IAUC 7080, 1

Ferrarese, L. et al., 1996, ApJ, 464, 568

Ferrarese, L., Livio, M., Freedman, W., Saha, A., Stetson, P. B., Ford, H. C., Hill, R. J., Madore,B . F. 1996, ApJ, 468, L95

Ferrarese, L. et al. 2000, ApJ, 529, 745

Ferrarese, L. , Côté, P. , Jordán, A. 2003, ApJ, 599, 1302

Filippenko, A. V., Halpern, J. P. 1984, ApJ, 285, 458

Freedman, W. L. et al. 1994, ApJ, 427, 628

Ford, H. C. 1978, ApJ, 219, 595

Gallagher, J. S. & Starrfield, S. 1978, ARA&A, 16, 171

Gehrz, R. D., Truran, J. W., Williams, R. E. 1993, in Protostars and Planets III, ed. E.H.Levy & J.I.Lunine (Tucson:Univ.Arizona Press),75

Gorgas, J., Faber, S. M., Burnstein, D., Gonzáles, J. J., Courteau, S., Prosser, C. 1993, ApJS, 86, 153

Graham, J. A. 1979, in IAU Colloq. 46, Changing trends in Variable Star Research, ed.F.M.Bateson, J.Smak, & I.H.Urch (Hamilton: Univ. Waikato), 96

Greenstein, J. L. 1960, in *Stellar Atmospheres*, ed. J.L. Greenstein, Univ. Chicago Press, Chicago, p.676

Hachisu, I. 2003, ASP Conf. series, 303, 261

Hauschildt, P. H., Starrfield, S., Shore, S. N., Allard, F., Baron, E. 1995, ApJ, 447, 829

Hauschildt, P. H., Baron, E., Starrfield, S., Allard, F. 1996, ApJ, 462, 386

Hauschildt, P. H., Shore, S. N., Schwarz, G. J., Baron, E., Starrfield, S., Allard, F. 1997, ApJ, 490, 803

Hernanz, M. 2005, ASPC, 330, 265

Holtzman, J. A., et al. 1995a, PASP, 107, 156

Holtzman, J.A. 1995b, PASP, 107, 1065

Howell,S. 2005, ASPC, 330, 67

Hubble, E. P. 1929, ApJ, 69, 103

Humason, M. L. 1938, ApJ, 88, 228

Hummer, D. & Storey, P. 1987, MNRAS, 224, 801

Iben, I. Jr. & Tutukov, A. V. 1984, ApJS, 54, 335

Iwanowska, W., Burnicki, A. 1962, Bull. Acad. Pol. Sci. Math. Astron. Pys. 10, 537

Jacobi, G. H. et al. 1992 PASP, 107, 1065

José, J. & Hernanz, M. 1998, ApJ, 494, 680

Kaufer, A., Stahl, O., Tubbesing, S., Norregaard, P., Avila, G., Francois, P., Pasquini, L., Pizzella, A. 1999, Messenger, 95, 8

Kelson, D. D. et al. 1996, ApJ, 463, 26

Kenyon, S. J., Hartmann, L., Gomez, M., Carr, J. S., Tokunaga, A. 1993, AJ, 105, 1505

Kopylov, I. M. 1955, Izv. Krymsk. Astrofiz. Obs. 13, 23

Kraft, R. P. 1959, ApJ, 130, 110

Kraft, R. P. 1962, Ap.J., 135, 408

Kraft, R. P 1964, ApJ, 139, 457

Kubiak, M. 1984, Acta Astron., 34, 331

Kuntschner, H., Lucey, J. R., Smith, R. J., Hudson, M. J., Davies, R. L. 2001, MNRAS, 323, 615

Kukarkin, B.V. 1949, in The Investigation of Structure and Evolution of Stellar Systems on the basis of Variable Stars Study

Larson, R. B. 1974, MNRAS, 169, 229

La Dous, C. 1989, A&A, 211, 131

Liller, W. 1998, IAUC 7079, 1

Livio, M. 1993, *22nd Saas Fee Advanced Course., Interacting Binaries*, eds. H.Nussbaumer & A.Orr, Springer-Verlag, Berlin, p.135

MacDonald, J. 1980, ApJ, 267, 732

McNaught, R. H.1991, IAUC, 5241

Mannucci, F., Della Valle, M., Panagia, N., Cappellaro, E., Cresci, G., Maiolino, R., Petrosian, A., Turatto, M. 2005, A&A, 433, 807

Mason, E., DellaValle, M., Gilmozzi, R., LoCurto, G., Williams, R. E. 2005, A&A, 435, 1031

Matteucci, F., 1992, ApJ, 397, 32

Matteucci, F. 1994 A&A, 288, 57

Matteucci, F. & Greggio, L. 1986, A&A, 154, 279

Matteucci,F., Ponzone, R., Gibson, B. K. 1998, A&A, 335, 855

Matteucci, F., Renda, A., Pipino, A., Della Valle, M. 2003, A&A, 405, 23

Matteucci, F., & Tornambé, A., 1987, A&A, 185, 51

McLaughlin, D. B. 1939, Pop.Astr., 47, 410, 481, 538

McLaughlin, D. B. 1941, Pop.Astr., 49, 292

McLaughlin, D. B. 1943, Pub. Astr. Obs. Univ, Michigan, 8, 149

McLaughlin,D.B. 1960, in *Stellar Atmospheres*, ed. J.L.Greenstein, Univ.Chicago Press, Chicago, p.585

McLaughlin, D. B. 1960, ApJ 131, 739

Mestel, L. 1952, MNRAS, 112, 598

Minkowski, R. 1948, ApJ, 107, 106

Minkowski, R. 1950, Publ. Mich. Obs., 10, 25

Moses, R. N., Shafter, A. W. 1993, BAAS, 25, 1248

Munari, U., Zwitter, T. 1997, A&A, 318, 269

Mustel, E. R. & Boyarchuk, A. A. 1970, Ap&SS, 6, 183

Munari,U. & Renzini,A. 1992, ApJ, 397, 87L

Neill,J.D. & Shara,M.M. 2003,AJ

Nishimura,H., Nakano, S., Liller,W., West,D., Waagen,E., Royer,R., Bedient,J., Pearce,A. 2004, IAUC, 8306

Osterbrock, D. E. 1989 *Astrophysics of gaseous nebulae and active galactic nuclei*, (University Science Books, Mill Valley, CA)

Patterson, J. 1984, ApJS, 54, 443

Payne-Gaposchkin, C. 1957 The Galactic Novae (North-Holland Publishing Company, Amsterdam)

Perlmutter, S. et al. 1997, ApJ, 483, 565

Pfau, W. 1976, A&A, 50, 113

Phillips, M. M. 1993, ApJ, 413, 105

Phillips, M. M., Lira, P., Sumtzeff, N. B., Schommer, R. A., Hamuy, M., Maza, J. 1999, AJ, 118, 1766

Pipino, A., Matteucci, F., Borgani, S., & Biviano, A., 2002, NewA., 7, 227

Pipino, A. & Matteucci, F. 2004, MNRAS, 347, 968

Plaut, L. 1965, in Stars and Stellar Systems V, A. Blaauw & M. Schmidt (eds.), University of Chicago Press, p. 311

Prialnik, D. & Kovetz, A. 1995, ApJ, 445, 789

Pringle, J. E. 1985 in *Interacting Binaries*, eds. J.E.Pringle & R.A.Wade, Cambridge University Press, Cambridge, p.1

Pritchet, C., van den Bergh, S. 1985, ApJ, 288, L41

Pritchet, C., van den Bergh, S. 1987, ApJ, 318, 507

Riess, A. G. et al. 1998, AJ, 116, 1009

Ritter, H. & Kolb, U. 2003, A&A, 404, 301

Ritter, H., Politano, M., Livio, M., & Webbink, R., 1991, ApJ, 376, 177

Romano, D. & Matteucci, F. 2003 MNRAS,342, 185

Romano, D., Matteucci, F., Molaro, P., Bonifacio, P. 1999,A&A 352, 117

Romano, D., Matteucci, F., Ventura, P., D'Antona, F. 2001,A&A, 374, 646

Rosino, L. 1964, AnAp, 27, 498

Rosino, L. 1973, A&AS, 9, 347

Rosino, L. & Bianchini, A. 1973, A&A, 22, 461

Rudy, R., Erwin, P., Rossano, G. S., Puetter, R. C. 1991, ApJ, 383, 344

Saha, A., Sandage, A., Labhardt, L., Tammann, G. A., Macchetto, F. D., Panagia, N. 1996, ApJ, 466, 55

Saha, A., Sandage, A., Labhardt, L., Tammann, G. A., Macchetto, F. D., Panagia, N. 1996, ApJS, 107, 693

Saha, A., Sandage, A., Tammann, G. A., Labhardt, L., Macchetto, F. D., Panagia, N. 1999, ApJ, 486, 1

Saha, A., Sandage, A., Tammann, G. A., Labhardt, L., Macchetto, F. D., Panagia, N. 1999, ApJ, 522, 802

Saha, A., Sandage, A., Thim, F., Labhardt, L., Tammann, G. A., Christensen, J., Panagia, N., Macchetto, F. D. 2001, ApJ, 551, 973

Saha, A., Sandage, A., Tammann, G. A., Dolphin, A. E., Christensen, J., Panagia, N., Macchetto, F. D. 2001, ApJ, 562, 314

Salpeter, E. E. 1955, ApJ, 121, 161

Sarna, J. M., Ergma, E., Gerskevits, J. 2005, Act.Astr., 56, 65

Scargle, J. D. 1982, ApJ, 263, 835

Schlegel, E. M., Honeycutt, R. K., Kaitchuck, R. H. 1985, PASP, 97, 107

Schlegel, D. J., Finkbeiner, D. P., Davis, M. 1998, ApJ, 500, 525

Schmidt, T. 1957, Z. Astrophys., 41, 182

Schmidtobreick, L., Tappert, C., Bianchini, A., Mennickent, R. E. 2003, A& A, 410, 943

Schmidtobreick, L., Tappert, C., Saviane, I. 2003, MNRAS, 342, 145

Schmidtobreick, L., Galli, L., Saviane, I., Tappert, C., Whiting, A. 2005a, ASP Conf. Ser. 335, 333

Schmidtobreick, L., Tappert, C., Ederoclite, A., Mason, E. 2006 *in preparation*

Shafter, A. W. 1997, ApJ, 487, 226

Shafter, A. W., Ciardullo, R., Pritchet, C. J. 2000, ApJ, 530, 193

Shakura, N. I. & Sunyaev, R. 1973, A&A, 24, 337

Shara, M. M. 1981, APJ, 243, 926

Shara, M. M., Prialnik, D., Shaviv, G. 1980, ApJ, 239, 586

Shara, M. M. 1989, PASP, 101, 5

Shara, M. M., Livio, M., Moffat, A. F. J., Orio, M. 1986, ApJ, 311, 163

Shara, M. M., Zurek, D. R., Williams, R. E., Prialnik, D., Gilmozzi, R., Moffat, A. F. J. 1997, AJ, 114, 258

Shara, M. M., & Zurek, D.R. 2002, in "Classical Nova Explosions", ed. M. Hernanz & J. Josè, A.I.P. Conference Proceed., p.457

Sharov, A. S. 1993, Astron. Lett., 19, 147

Silbermann, N. A. et al. 1996, ApJ, 470, 1

Spencer Jones, H. 1931, Cape Obs. Ann., 10, Part 9

Spite, F. & Spite, M. 1982, A&A, 141, 56

Spruit, H. 1998, preprint, astro-ph/9806141

Starrfield, S., Truran, J. W., Sparks, W. M., Kutter, G. S. 1972, ApJ, 176, 169

Starrfield, S., Sparks, W. M., Truran, J. W. 1985, ApJ, 291, 136

Stetson, P. B., 1992, in Worrall et al., eds, Astronomical Data Analysis Software and Systems I, ASP Conf. Ser. 25, 291

Stetson. P. B et al. 1998, 508, 491

Tappert, C., Mennickent, R., Arenas, J., Matsumoto, K., Hanuschik, R. 2003, A& A, 408, 651

Tomaney, A. B., Shafter, A. W. 1992, ApJS, 81, 683

Tonry, J. L., Dressler, A., Blakeslee, J. P., Ajhar, E. A., Fletcher, A. B., Luppino, G. A., Metzger, M. R., Moore, C. B. 2001, ApJ, 546, 681

Truran, J. W. 1982, in Essays in Nuclear Astrophysics, ed.C.A.Barnes, D.D.Clayton, and D.Schramm (Cambridge: Cambridge University Press), p.467

Truran, J. W., 1990, I.A.U. Coll.122, eds. A. Cassatella & R. Viotti, Springer-Verlag: Berlin, p.373

Turatto, M. 2003, in "Supernovae and Gamma-Ray Bursters", ed. K.Weiler, Lecture Notes in Physics, 598, 21

van den Bergh, S. & Younger, P. F. 1987, A&AS, 70, 125

Venturini, C. C., Rudy, R. J., Lynch, D. K., Mazuk, S., Puetter, R. C. 2004, AJ, 128, 405

Vogt, N. 1989, in *Classical Novae*, eds. M.F.Bode & A.Evans, Wiley, Chichester, p.225

Wagner, R. M., Gilmore, A. C., Kilmartin, P. M. 1991, IAUC 5240, 1

Wagner, R. M., Starrfield, S. G., Gilmore, A. C. 1991, IAUC 5243, 1

Walker, M. F. 1954, PASP, 66, 230

Kosai, H., Wakuda, M. 1983, IAUC 3777, 1

Warner, B. 1986, MNRAS, 219, 751

Warner, B. 1995, Cataclysmic variable stars , Cambridge University Press

Warner,B. 2002, AIPC, 637, 3

West,D. 2004, IAUC, 8306, 3

Whelan, J. & Iben, I. Jr. 1973, ApJ, 186, 1007

Wiescher, M., Gorres, J., Thielemann, F. K., Ritter, H. 1986, A&A 160, 56

Williams, R. E. 1992, AJ, 104, 725

Williams, R. E. 1994 ApJ, 426, 279

Williams, R. E., Hamuy, M., Phillips, M. M., Heathcote, S. R., Wells, L., Navarrete, M. 1991, ApJ, 376, 721W

Williams, R. E., Phillips, M. M., Hamuy, M. 1994, ApJS, 90, 297

Wolf, M. 1927 AN, 230, 421

Wood, J., Horne, K., Berriman, G., Wade, R., O'Donoghue, D., Warner, B. 1986, MNRAS, 219, 62

Worthey, G. 1992, Ph.D. thesis, Univ. California, Santa Cruz

Worthey, G., Faber, S. M., Gonzalez, J. J. 1992, ApJ, 398, 69

Worthey, G 1994, ApJS, 95, 107

Yaron, O., Prialnik, D., Shara, M. M., Kovetz, A., 2005, ApJ 623, 398

Yungelson, L. 2003, IAUJD, 5E, 13

Yungelson, L, Livio, M., Tutukov, A. 1997, ApJ, 481, 127

Zangrilli, L, Tout, C. A., Bianchini, A. 1997, MNRAS, 289, 59

Zwicky, F. 1936, PASP, 48, 191

Zwicky, F. 1942, ApJ, 96, 28

Acknowledgements

The scientific work included in this thesis took advantage of the collaboration of several people.

I am grateful to my advisor, Paolo Mazzali, and co-advisor, Francesca Matteucci. They gave me the chance to join the nova field which I now find so exciting!

I must also thank Massimo Della Valle who advertized this field so strongly during my first week in Trieste and has been an incredible source of advices during these three years.

Lot of thanks to Roberto Gilmozzi, who accepted this unknown student as his student at ESO/Chile.

Thanks to Bob Williams for all his suggestions, discussions and data.

Thanks to John Danziger and Angelo Cassatella for interesting discussions about spectroscopy.

Thanks to Elena Mason, Claus Tappert and Linda Schmidtobreick: the "Cataclysmic Community" I found in Chile.

Thanks to Thomas H. Dall for giving me the chance to join LaSilla SciOps for two "turnos".

Thanks to the referee, Pierluigi Selvelli, for his suggestions and his support.

Thanks to Chris Sterken and Hilmar Duerbeck, for having read and corrected (once more!) this manuscript.

I wouldn't have been able to make a thesis without the support of my family and all my friends, so:

I am sure my father supported me somehow: *Grazie*.

I would like to thank my mum who always supported me.

I need to thank my grandfather for his "break a leg" 's.

Many thanks to nonna Flora, Antonella, Rosaria, Daniela, Paola, Dino, Emilio, Vanda and two newcomers: Elena and Sofia. Thanks to Luciano, Claudia, Giorgia and little Irene (born just one month after I left for Chile).

I want to thank Francesca for her patience.

The greatest rock'n'roll band in the world had to stop rehearsing for a while. I thank the XOut: Simone, Paola and Flora.

Thanks to Laura, Daphne, Tahira, Silvia and Sonia.

A lot of people made my stay in Chile a unique experience: so thanks to Alberto, Anaelle, Aurelie, Benoit, Carla, Carol, Celine, Christian, Christophe, Farhid, Franck, Gianluca, Hannes, Irina, Lorenzo, Luca, Luca, Mike, Nadia, Nicole, Pascale, Pasquier, Silvia,Silvia, Theresa,Ulysses, Xavier.

Thanks to the Trieste PhD students (and former ones): Alex, Amata, Andrea, Antonio, Chiara, David, Dunja, Edoardo, Elisabetta, Eros, Fabio, Francesco, Francesco, Guido, Italo, Luca, Luca , Luigi, Sdrjan, Silvia Kuna and Silvia.

Thanks also to Marco and Paola for helping me in Trieste and Munich.

Thanks to the Roman Amateurs of Astronomy association.

Last but not least, thanks to Radio Rock and Radio Rock Italia for being a musical lighthouse also from Chile.

Last, but not least, thanks to all the people I didn't thank.